Sirt6-dependent gene regulation of oncofetal gene loci in hepatocytes

Dissertation

Zur Erlangung des Grades

Doktor der Naturwissenschaften

Am Fachbereich Biologie

Der Johannes Gutenberg-Universität Mainz

Shengyun Ma

Geboren am 24.06.1988 in Shandong, China

Mainz, 2015

Declaration

This Ph.D. thesis entitled “Sirt6-dependent gene regulation of oncofetal gene loci in hepatocytes” was carried out by me for the degree of Doctor rerum naturalium (Dr.rer.nat.). I hereby declare that I wrote the dissertation submitted without any unauthorized external assistance and used only sources acknowledged in the work. All textual passages which are appropriated verbatim or paraphrased from published and unpublished texts as well as all information obtained from oral sources are duly indicated and listed in accordance with bibliographical rules. In carrying out this research, I complied with the rules of standard scientific practice as formulated in the statutes of Johannes Gutenberg-University Mainz to insure standard scientific practice.

Summary

Hepatocellular carcinoma (HCC), the primary malignant tumor of liver, represents the third leading cause of cancer-related deaths globally due to the lack of effective treatment options. Accumulating studies have revealed that SIRT6, a NAD^+-dependent histone deacetylase, plays pivotal roles in liver-related disease and liver tumor formation. Genetic deletion of Sirt6 in mice develops a pro-oncogenic phenotype in the liver with dramatic elevation of oncofetal genes typical for HCC, such as *Igf2*, *H19* and α-Fetoprotein (*Afp)*. However, the underlying mechanisms regulating these genes remain unknown. For delineating the role of Sirt6 in the tumor-related phenotype, Sirt6 knockout mice model together with primary human hepatocytes and human hepatoma cells (Hep3B) were used in this study.

The present study shows that Sirt6 suppresses the expression of these oncofetal genes. Functional analysis of the *Igf2/H19* gene locus as a model showed that loss of Sirt6 causes nucleosome remodeling, altered chromatin loop, enhancer switch from the poised (enriched with H3K27me3 and H3K4me1) to active (enriched with H3K27ac and H3K4me1) by recruiting pioneer factors Foxa1 and Foxa2. Interestingly, these alterations establish a super-enhancer to drive *H19* and *Igf2* transcription. Moreover, Sirt6 deletion causes cytoplasmic translocation of Suz12, a core component of the Polycomb repressive complex 2 (PRC2), and weakens PRC2-mediated repression at the *Igf2/H19* gene locus. Further analysis of Hep3B cells in relation to primary human hepatocytes indicated that this regulatory mechanism is relevant for human cancer development.

Besides, this study also suggests the role of Sirt6 in hepatic differentiation. Sirt6 knockout leads to the increased expression of embryonic hepatoblast markers and the reduced transcription of adult hepatocytes markers. Correspondingly, this trend reversed when SIRT6 was overexpressed in Hep3B cells. Functional analysis of this regulatory mechanism at the *Alb/Afp* gene locus as a model showed that Sirt6 deletion causes epigenetic and genetic alterations, which induces Foxa2 switch from enhancer of *Alb* (hepatocytes marker) to *Afp* (hepatoblast marker). However, PRC2-mediated repression is not evident at these temporal enhancers.

Altogether, in hepatocytes, loss of Sirt6 induces disruption of enhancer activity through genetic and epigenetic alterations, resulting in activation of a tumorigenic phenotype.

Zusammenfassung

Das Hepatozelluläre Karzinom (Hepatocellular carcinoma, HCC), der häufigste bösartige Tumor der Leber, ist aufgrund eines Mangels an effektiven Behandlungsoptionen die weltweit dritthäufigste krebsbedingte Todesursache. Aktuelle Untersuchungen zeigen, dass SIRT6, eine NAD^+-abhängige Histon-Deacetylase, eine zentrale Rolle bei Lebererkrankungen und der Entstehung von Lebertumoren spielt. Mäuse mit einer genetischen Deletion von Sirt6 entwickeln in der Leber einen pro-onkogenen Phänotyp mit einer drastischen Erhöhung onkofetaler Gene wie Igf2, H19 and α-Fetoprotein (AFP), welche für das HCC kennzeichnend ist. Dennoch verbleiben die zugrunde liegenden Mechanismen, wie diese Gene reguliert werden, unbekannt. Um die Rolle von Sirt6 im tumor-assoziierten Phänotyp zu charakterisieren, wurden in dieser Arbeit Hepatozyten aus Sirt6-defizienten Mäusen, primäre humane Hepatozyten und humane Hepatomzellen (Hep3B) verwendet.

Die vorliegende Arbeit zeigt, dass Sirt6 die Expression onkofetaler Gene supprimiert. Die funktionellen Untersuchungen des Igf2/H19 Genlokus zeigen, dass der Verlust von Sirt6 durch die Rekrutierung der Pionierfaktoren Foxa1 und Foxa2 zu einer Umordnung von Nukleosomen mit veränderten Chromatinschleifen und einem „*Enhancer switch“* einer H3K27me3 und H3K4me1 Anreicherung zur Akkumulation der Aktivierungsmarker (H3K27ac und H3K4me1) führt. Diese Veränderungen führen interessanterweise zur Etablierung eines *Super-Enhancers*, welcher die Transkription von H19 und Igf2 vorantreibt. Die Sirt6-Deletion führt darüber hinaus zu einer zytoplasmatischen Translokation von Suz12, einer Kernkomponente des PRC2-Komplexes (Polycomb repressive complex 2), und schwächt damit die PRC2-vermittelte Repression am Igf2/H19 Genlokus. Weitere Untersuchungen von Hep3B Zellen im Vergleich zu primären humanen Hepatozyten deuten darauf hin, dass dieser regulatorische Mechanismus für die humane Krebsentwicklung von Bedeutung ist. Zudem legt diese Arbeit auch eine Rolle von Sirt6

bei der hepatischen Differenzierung nahe.

Der Sirt6-knockout führt zu einer erhöhten Expression embryonaler Hepatoblasten-Marker und einer reduzierten Transkription von Markern adulter Hepatozyten. Übereinstimmend damit zeigt sich ein umgekehrter Trend bei der Überexpression von SIRT6 in Hep3B Zellen. Funktionelle Untersuchungen dieses regulatorischen Mechanismus am Albumin/α-Fetoprotein Genlokus als Modell zeigen, dass die Sirt6-Deletion hier in epigenetischen und genetischen Veränderungen resultieren, welche Foxa2 dazu veranlassen vom Albumin- (Hepatozyten Marker) zum α-Fetoprotein-*Enhancer* (Hepatoblasten Marker) zu wechseln. Allerdings ist eine PRC2-vermittelte Repression an diesen *temporalen Enhancern* nicht erkennbar.

Insgesamt führt der Verlust von Sirt6 in Hepatozyten durch genetische und epigenetische Veränderungen zu einer gestörten Enhanceraktivität, was in einem tumorigenen Phänotyp resultiert.

Table of Contents

1 Introduction

1.1 Hepatocellular carcinoma (HCC)

1.1.1 Epidemiology and etiologic associations of HCC

HCC is the fifth most common diagnosed cancer globally but, owing to the lack of effective treatment options, represents the third most frequent cause of neoplasm-related mortality and the second leading cause of cancer death in men (Franceschi and Raza, 2009; Sachdeva et al., 2015; Singal and El-Serag, 2015). Its incidence is increasing worldwide. For example, in the United States, HCC patients have more than doubled over the past 20 years and are anticipated to continue increasing over the next 2 decades. HCC is most prevalent in Asian nations like China, where it has a high mortality rate within weeks or months after detection (Sachdeva et al., 2015).

HCC is a kind of primary malignant tumor of the liver which begins in hepatocytes (the main cells of the liver) and most frequently occurs in those persons who have chronic liver disease and scarring called cirrhosis (Clark et al., 2015; Pellicoro et al., 2014) (Figure 1.1). Epidemiologic and clinical studies have identified many factors that affect risk for HCC such as the dissemination of hepatitis B and C virus infection, alcohol intake, toxins consumption, nonalcoholic steatohepatitis and hereditary hemochromatosis (Clark et al., 2015; Singal and El-Serag, 2015). Considerable efforts to improve the treatments for HCC have been made in recent decades, like surgical resection or liver transplantation. However, resection is indicated among patients who have one tumor and well-preserved liver function, while the applicability of liver transplantation is greatly limited by donor shortage (Llovet et al., 2003). Consequently, most patients present with advanced disease are not candidates for surgery. In addition, systemic chemotherapeutic treatment is ineffective against HCC (Llovet et al., 2003), and no single drug or drug combination so far prolongs survival (Zender et al., 2006).

Therefore, it is particularly important to afford an effective early detection and diagnosis confirmation, subsequently allowing effective therapy, because liver transplantation and resection are only effective therapeutic options at early stages. The well-established HCC

associated genes like alpha-fetoprotein (*Afp*), *H19*, insulin-like growth factor 2 (*Igf2*), and glypican-3 (*Gpc3*) are therefore critical points not only for HCC detection, but have been shown to play a role in HCC progression. Thus, regulations of these genes that play pivotal roles in liver tumor development are important to investigate.

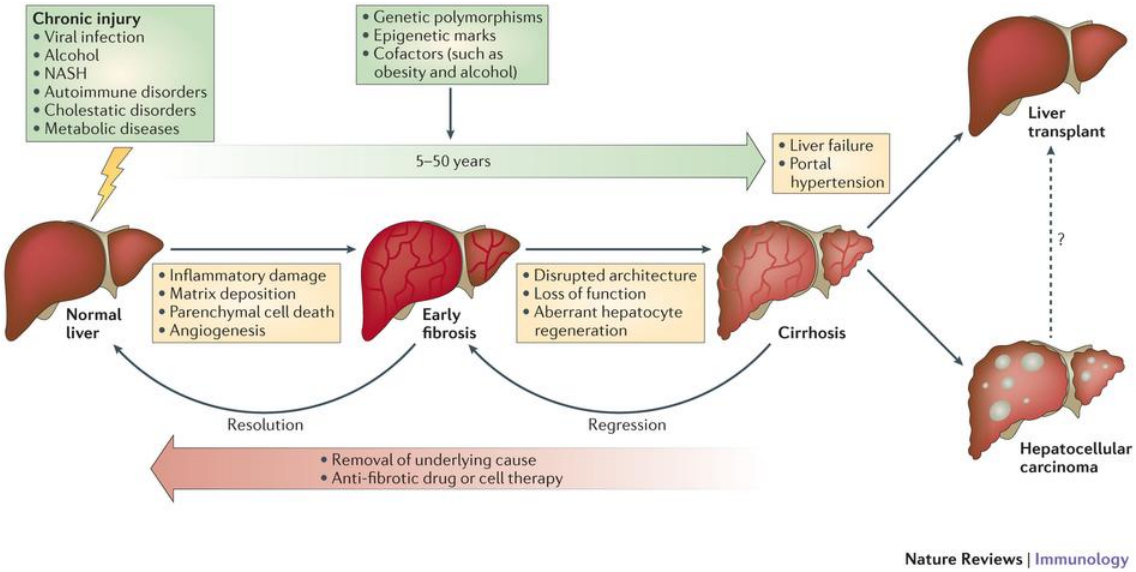

Figure 1.1 Natural history of chronic liver disease (Pellicoro et al., 2014). Hepatic fibrosis is the wound-healing response of the liver to many causes of chronic injury, of which viral infection, alcohol and non-alcoholic steatohepatitis (NASH) are the most common. Regardless of the underlying cause, iterative injury causes inflammatory damage, matrix deposition, parenchymal cell death and angiogenesis leading to progressive fibrosis. The scar matrix typically accumulates very slowly (the median time to cirrhosis in chronic hepatitis C is 30 years) but once cirrhosis is established the potential for reversing this process is decreased and complications develop. Genetic polymorphisms, epigenetic marks and cofactors (such as obesity and alcohol) can modulate the risk of fibrosis progression. If the cause of fibrosis is eliminated, resolution (that is, complete reversal to near-normal liver architecture) of early hepatic fibrosis can occur. In cirrhosis, although resolution is not possible, regression (that is, improvement but not reversal) of fibrosis improves clinical outcomes. Anti-fibrotic therapies are emerging that can slow, halt or reverse fibrosis progression. Currently, liver transplantation is the only available treatment for liver failure or for some cases of primary liver cancer. Hepatocellular carcinoma is rising in incidence worldwide and is a major cause of liver-related death in patients with cirrhosis. Figure is taken from Pellicoro, A., Ramachandran, P., Iredale, J.P., and Fallowfield, J.A. (2014). Liver fibrosis and repair: immune regulation of wound healing in a solid organ. Nature reviews Immunology *14*, 181-194.

1.1.2 Dedifferentiation and oncofetal gene expression

For decades the widely studied model of preneoplastic nodules in the liver during experimental induction of HCCs by chemicals was interpreted to support the hypothesis that HCC arose by dedifferentiation of mature liver cells (Sell and Leffert, 2008).

Previously, some studies indicate that oncofetal genes have been proposed as a marker of embryonal dedifferentiation of adult tissues (Stuhlmuller et al., 2003). Oncofetal genes are characterized as abundantly expressed in the fetal period, becoming inactive within postnatal stages and reappear in association with tumors (Adinolfi and Lessof, 1985). Due to their ability of renewed synthesis of various fetal proteins in a variety of cancer, oncofetal genes are used for diagnostic and prognostic purposes. Until now, several oncofetal genes have been identified in hepatocellular carcinoma, like H19, *IGF2, AFP, GPC3*, and *SALL4*.

1.1.2.1 The imprinted IGF2/H19 gene locus

As an oncofetal gene, *H19* is predominantly expressed in embryogenesis and placental development. For example, prominent expression of *H19* in liver can be observed in the embryo at 35 days post conception and reappears later in gestation during the second trimester of pregnancy (Ariel et al., 1997). In addition to that, *H19* is either highly expressed and/or manifests an aberrant allelic pattern of expression in many human cancers (Matouk et al., 2013; Ohlsson, 2004). In recent years, it has become increasingly clear that it is essential for development and human tumor growth and supposed to be a tumor biomarker (LeRoith and Roberts, 2003; Matouk et al., 2007), though *H19* was first described as a tumor suppressor (Yoshimizu et al., 2008). In cirrhosis liver and HCC, *H19* expresses excessively, even more than the widely used HCC marker AFP (Ariel et al., 1998; Matouk et al., 2007). Knockdown *H19* in HCC tumors exhibits significant inhibition of tumor growth or in certain cases even a complete inhibition of tumor formation, while ectopic *H19* expression enhances tumorigenic potential of carcinoma cells in vivo (Matouk et al., 2007). In addition, *H19* exerts a tumor suppressor to control the timing of appearance of SV40-induced HCC using in vivo murine models of tumorigenesis (Yoshimizu et al., 2008). Apart from promoting HCC tumor growth, *H19* is also found to up-regulate the miR-200 family, and subsequently suppress the rate of tumor metastasis in advanced stages of HCC (Zhang et al., 2013).

IGF2 is one of the growth factors produced by liver cells, which are highly active in physiological fetal liver growth. HCC patients show an abnormal secretion and activation of IGF2 in blood serum (Morace et al., 2012). Rather than acting as an oncofetal gene, IGF2 is known to be involved in liver carcinogenesis in humans and animal models. IGF2 overexpression has been associated with hepatocytes proliferation, terminal stages of malignant transformation and rapidly growing tumors or parts of a tumor (Ariel et al., 1998; Li et al., 1997).

Despite these, *IGF2* and *H19* are two imprinted genes locate adjacent to each other at chromosome 11p15.5 in humans and chromosome 7 in mice. Both genes are reciprocally imprinted, with expression of the maternal *H19* and paternal *IGF2* alleles, and are normally characterized by monoallelic expression (Kim and Lee, 1997). The imbalance in expression levels of *IGF2* and *H19* transcripts is closely linked to progression of HCC (Iizuka et al., 2004). For example, the two genes are coordinately overexpressed in 37% of HCC (Sohda et al., 1998). Because the frequent biallelic expression of *H19* and *IGF2* in hepatocellular carcinoma plays a causal role in the epigenetic mechanism involved in tumor development and/or process (Kim and Lee, 1997). However, it remains unclear that by what pathways the levels of *IGF2* and *H1*9 are altered in the progression of HCC correspondingly.

Regional coordination of gene expression and repression is highly associated with the genomic structure (Figure 1.2), such as the promoters of *IGF2*, the imprinting control region (ICR) and the enhancers region. The expression of *H19* and *IGF2* is controlled by the shared endodermal enhancers that are located at 5–7 kb downstream of *H19* (Leighton et al., 1995). There is evidence that the endodermal enhancers are crucial for activation of the *IGF2* and *H19* genes upon induction of liver carcinogenesis (Vernucci et al., 2000). In HCC, the *IGF2-H19* hepatic control region also overlaps with so called “stretch enhancers”, a kind of enhancer which is important for cell-specific regulation and human disease (Parker et al., 2013). Apart from the endodermal tissue specific enhancers, some studies also find several segments function as enhancers in specific mesodermal and/or ectodermal tissues (Ishihara et al., 2000). For example, CS9

mesodermal enhancer is important for diaphragm formation activity (Borensztein et al., 2013), while both CS6 and CS9 are in regulation of myotome and the rib primordial (Ishihara et al., 2000). Another well-known region is the imprinting control region (ICR), also named differentially methylated region (DMR), which is located 2-kb upstream of *H19* (Elson and Bartolomei, 1997). CTCF binds to the unmethylated ICR and the *Igf2* promoters on the maternal allele and forms a long-distance intrachromosomal loop, resulting in preventing the *IGF2* gene from accessing endodermal enhancers downstream of the *H19* gene (Li et al., 2008). Furthermore, a number of additional regulatory regions have been described surrounding these loci. At the 5' end of *IGF2*, there are two differentially methylated regions (DMRs). The DMR1 serves as an *Igf2* silencer, involved in imprinting on the maternal allele and postnatal repression on the paternal allele, whereas the intragenic DMR2 stimulates *Igf2* transcription on the paternal allele (Court et al., 2011). It has also been demonstrated that *IGF2* imprint is promoter-specific, in that expression from the P1 promoter is biallelic, whereas that from the P2–P4 promoters is monoallelic (Yun et al., 1998). Human *IGF2* has five promoters (huP1 and P0–P3) while mouse *Igf2* has only 4 (P0–P3) (Stringer et al., 2012). The intergenic region between *IGF2* and *H19* contains CCD (the Centrally Conserved DNase I hypersensitive domain), which has tissue specific enhancer function in mice that independent of imprinting (Ainscough et al., 2000; Koide et al., 1994; Nativio et al., 2009). The *IGF2/H19* locus also contains two non-coding RNAs, *PIHit* and *Nctc1* that display a strong active chromatin signature (Wamstad et al., 2014). *PIHit* acts as a tissue-specific long noncoding RNA gene (Court et al., 2011), while *Nctc1* has been described as an enhancer RNA in mouse (Eun et al., 2013). Unlike CS6 and *Nctc1* are muscle-specific, *PIHit* is highly expressed in liver and very low expressed in other tissues (Court et al., 2011). Unlike in mouse, the *IGF2/H19* gene locus has four CTCF binding sites in human, namely ICR, CCD, CTCF-AD and CTCF-Ds. Through these sites, CTCF regulates the interaction of promoters and enhancers through cohesion or PRC2-mediated higher-order chromatin conformation (Li et al., 2008; Nativio et al., 2009).

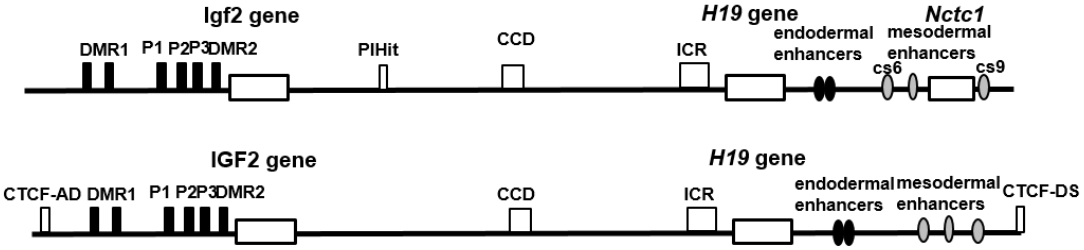

Figure 1.2 Schematic representation of the *IGF2/H19* gene locus in mouse (top) and human (bottom). Schematic representation of the *IGF2/H19* locus in mouse and human. *IGF2* and *H19* genes (white boxes) are displayed together with the downstream endodermal enhancers (black ovals), the centrally conserved domain (CCD), and the ICR (white box), as well as the upstream promoters of *Igf2* (black boxes): DMR1, P1, P2, P3, DMR2. Apart from these, there are another two CTCF binding sites, CTCF-AD (white box) on the upstream of *IGF2*, and CTCF-Ds (white box) on downstream of *H19*.

1.1.2.2 The Afp/Alb gene locus

Embryonic or fetal antigens have been identified in most tumors providing strong support for the view that malignancy is a disorder of differentiation. A well-known model of differentiation and neoplastic gene regulation is the *ALB* (albumin)-*AFP* (α-fetoprotein) locus (Kajiyama et al., 2006). AFP, the main component of mammalian fetal serum, is synthesized by the visceral endoderm of the yolk sac and by fetal liver, and reactivated in liver tumors. As an important marker for liver tumors, AFP blood level change is widely used in clinical practice (Lazarevich, 2000). Unlike *AFP*, *ALB* expression starts from hepatocyte specification, rises to adult levels by E14 (embryo day of 14), and persists in mature liver where its gene transcripts reach a maximum level (Tilghman and Belayew, 1982). Due to the different expression stage of hepatocytes, the alterations of transcripts level of *AFP* and *ALB* are used for identifying hepatic differentiation.

The albumin and α-fetoprotein genes are adjacent on mouse chromosome 5, and are subject of a common regulation by a variety of liver-enriched transcription factors (Kajiyama et al., 2006; Taube et al., 2010). In both genes, promoter-proximal controls mediate developmental regulation while distant enhancers drive high level expression. The *AFP* gene has three characterized enhancers, E3 (-6.1 kb), E2 (-4.3 kb) and E1 (-2.7 kb), while *ALB* has one enhancer at -9.9 kb (Lazarevich, 2000) (Figure 1.3). All the enhancers bind multiple C/EBP and HNF isoforms (Kajiyama et al., 2006; Taube et al.,

2010). In addition, *AFP* repression is mediated by elements, extend from about -900 to -250 bp (Kajiyama et al., 2006), through binding p53 to displace Foxa1 at the distal promoter of *Afp* (-850 bp) in mouse (Taube et al., 2010). Disruption of differentiation is seen in many types of cancers and considered as an important step in cancer progression. However, it remains to be seen whether cancer cells derive from mature cells which de-differentiate to an embryonic stage of development driven by the de-repression of a previously silent oncofetal gene.

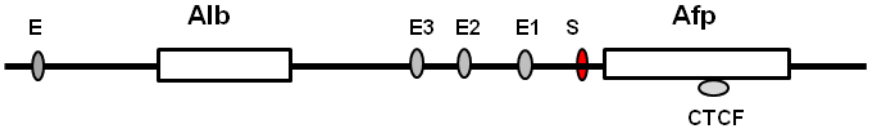

Figure 1.3 Schematic representation of the *Alb/Afp* gene locus in mouse. *Alb* and *Afp* genes (white boxes) are displayed together with enhancers (gray ovals) and silencer (red oval), and CTCF binding at the middle of *Afp* gene. *Afp* gene has three enhancers while *Alb* has one enhancer.

1.2 Sirtuin 6 (SIRT6)

1.2.1 SIRT6 and its enzymatic activities

Sirtuins, the class III NAD-dependent deacetylase, are highly conserved from bacteria to human protein (Kugel and Mostoslavsky, 2014). The founder member of this group is Sir2 (silent information regulator-2), which was initially shown to extend lifespan in budding yeast (Imai et al., 2000). Mammals have seven sirtuins (SIRT1-7), with different subcellular localizations and specific substrates, and display diverse biological functions. Sirt3, Sirt4 and Sirt5 are found in mitochondria, and Sirt1 and Sirt2 are both located in nucleus and cytosol, while Sirt6 and Sirt7 are exclusively located in the nucleus (Michishita et al., 2005).

Sirtuin proteins contain a conserved catalytic domain, and require NAD^+ for their enzymatic activity as deacetylase, mono-ADP-ribosyltransferase and deacylase (Yuan et al., 2013). To data, SIRT6 is the only one that has been reported to have all three lysine modifying enzyme activities. Firstly, SIRT6 exhibits nucleosome-dependent deacetylase activity (Gil et al., 2013). Its substrates include histone markers like H3K9 (Michishita et al., 2008), H3K56 (Michishita et al., 2009; Yang et al., 2009) and non-histone protein such

as CtIP (C-terminal binding protein interacting protein)(Kaidi et al., 2010) and GCN5 (Dominy et al., 2012). Compared with deacetylation, SIRT6 displays a relatively weak ADP-ribosyltransferase activity. The substrates of ADP-ribosyltransferase so far validated are PARP1 (poly(ADP-ribose) polymerase 1) (Liszt et al., 2005) and KAP1 (KRAB-associated protein 1) (Van Meter et al., 2014). Similar with Sirt5, that removes malonyl and succinyl groups on target protein, SIRT6 efficiently removes long-chain fatty acyl groups, such as myristoyl lysine, from TNF-α (tumor necrosis factor-α) to promote its secretion (Jiang et al., 2013).

1.2.2 SIRT6 function

SIRT6-deficient mice are small and develop abnormalities at 2–3 weeks of age that include profound lymphopenia, lordokyphosis, a curved spine, heart failure and loss of subcutaneous fat. These severe phenotypes ultimately lead to death at about 1 month (Mostoslavsky et al., 2006). At the cellular level, loss of Sirt6 leads to increased glucose uptake, hypersensitivity to DNA damage, and genomic instability (Mostoslavsky et al., 2006). These phenotypes provide the first insight into the distinct functions of SIRT6 (Figure 1.4).

1.2.2.1 SIRT6 and genome integrity

The well-studied biological function of SIRT6 appears to be in maintenance of genome integrity. From the phenotype of Sirt6 knockout (KO) mouse like increased sensitivity to DNA-damaging agents and a number of chromosomal abnormalities, SIRT6 was initially hypothesized to be required in facilitating BER (base excision repair) (Mostoslavsky et al., 2006). Moreover, it has been shown that SIRT6-depleted cells exhibit abnormal telomere structures by increasing the acetylation level of H3K9ac (Michishita et al., 2008) and H3K56ac (Michishita et al., 2009), which resemble defects in Werner syndrome, a premature ageing disorder. A number of studies point that SIRT6 is also involved in DSB repair (double-strand break repair), and more specifically in HR (homologous recombinant). For example, SIRT6 was first found to mono-ADP-ribosylate and activate PARP1, followed enhancing DSB repair induced by oxidative stress (Mao et al., 2011).

Because PARP1 is important for both DSB repair and BER, overexpression of SIRT6 also rescues the decline of BER in aged fibroblasts (Xu et al., 2015). Moreover, SIRT6 interacts with DNA-PK (DNA- dependent protein kinase) (McCord et al., 2009) and SNF2H (SWI/SNF related matrix-associated actin-dependent regulator of chromatin; also known as SMARCA5) (Toiber et al., 2013) to promote DNA DSB repair by deacetylating H3K9ac and H3K56ac, respectively. Interestingly, the first non-histone substrate found for SIRT6 deacetylatase activity is CtIP, which is responsible for DNA end resection (Kaidi et al., 2010). Overall, both deacetylase and ADP-ribosyltransferase activities of SIRT6 are required for genomic stability in regulating DNA repair and telomere maintenance.

1.2.2.2 SIRT6 and aging related disease

Accumulating evidences show that SIRT6 acts as a transcriptional regulator by physically associating with the transcription factors to participate in regulating aging related disease including inflammation, metabolism and heart disease. Similarly with SIRT1, SIRT6 also regulates gene expression by physically interacting with the RelA subunit of NFκB (nuclear factor kappa B), leading to the deacetylation of histone H3K9ac at promoters of NFκB target genes. This deacetylation ultimately decreases NFκB-dependent apoptosis and senescence (Kaidi et al., 2010). Notably, RelA heterozygosity rescues the early lethality and aging-related phenotypes of SIRT6-knockout mice. In addition, the role of SIRT6 as an eraser of long-chain fatty acyl groups is more efficient compared to its deacetylation-activity. One particularly relevant example for this SIRT6 function is the removal of myristoyl lysine from TNF-α to promote its secretion (Jiang et al., 2013). TNF-α can activate NFκB, both known as proinflammatory cytokines in numerous inflammatory diseases. These studies therefore suggest that SIRT6 plays an important role in inflammation through deacetylation and deacylation activities.

As mentioned above, SIRT6-knockout mice display severe hypoglycemia phenotypes that eventually lead to death at about 4 weeks of age (Mostoslavsky et al., 2006). These abnormalities correlate with the glucose metabolism disorders. SIRT6 is recruited to promoters of multiple glycolytic genes by associating with Hif-1α (hypoxia inducible factor

1α) and serves as a co-repressor of Hif-1α, silencing its target genes through deacetylation of H3K9ac on the promoters (Zhong et al., 2010). Consistently, the glucose-metabolic abnormalities are rescued by treating with a Hif-1α inhibitor or knockdown Hif-1α with shRNA in Sirt6-deficient mice (Zhong et al., 2010). Another paper has revealed that SIRT6 also negatively regulates AKT phosphorylation through inhibition of a subset of upstream molecules. The absence of SIRT6 consequently leads to a cascade of phosphorylation events and enhances activation of AKT, resulting in hypoglycemia (Xiao et al., 2010). It was subsequently demonstrated that SIRT6 interacts with and deacetylates and activates GCN5 (acetyltransferase general control non-repressed protein 5), which catalyzes acetylation of PGC-1α (peroxisome proliferator-activated receptor-γ coactivator 1-α), the master regulator of gluconeogenesis that stimulates hepatic glucose production (Dominy et al., 2012). Another study confirmed that SIRT6 regulates glucose metabolism not only through impacting on glycolysis, but also by functioning at gluconeogenesis (Kim et al., 2010).

Further evidence for the role of SIRT6 in aging has been observed in cardiac hypertrophy and heart failure. There is evidence for decreased levels of SIRT6 in both human and mouse failing hearts (Kugel and Mostoslavsky, 2014). SIRT6 serves as a negative regulator of cardiac hypertrophy by directly attenuating IGF (insulin-like growth factor) signaling through physically associating with c-Jun and deacetylating H3K9ac on c-Jun target promoters. SIRT6-knockout mice develop cardiac hypertrophy and heart failure, while SIRT6 overexpression transgenic mice are blocked theses response (Sundaresan et al., 2012). c-Jun is also known to locate downstream of AKT in the IGF signaling pathway. Thus, SIRT6 regulates IGF signaling through different pathway in a tissue- and context-dependent manner. Intriguingly, over-expression of SIRT6 alters the IGF signaling specifically in white adipose tissue, and extends the lifespan of male (but not female mice) by 15 %. Altogether, SIRT6 acts as a key modifier responsible for modulating lifespan through regulating aging-related metabolism and signaling pathways.

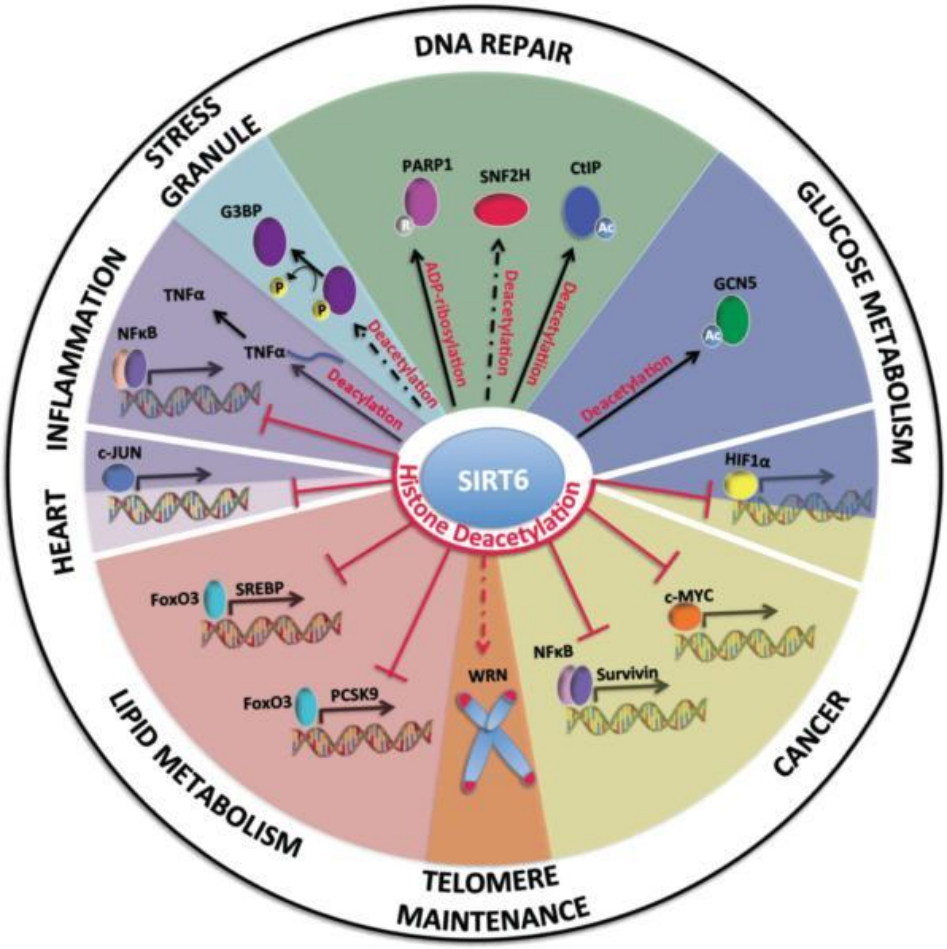

Figure 1.4 SIRT6 cellular functions and their impact on organismal biology and disease (Kugel and Mostoslavsky, 2014). SIRT6 primarily functions as a H3K9 and H3K56 histone deacetylase that decreases chromatin accessibility for transcription factors such as nuclear factor κB (NF-κB), c-JUN, Foxo3, MYC, and hypoxia inducible factor 1α (HIF1α) to their respective target promoters, and thus inhibits expression of their target genes. SIRT6 can also regulate protein activity through direct deacetylation of GCN5 (general control non-repressed protein 5) and CtIP [C-terminal binding protein (CtBP) interacting protein] and ADP-ribosylation of poly-(ADP-ribose) polymerase 1 (PARP1). SIRT6 has also been found to interact with SNF2H to enhance its recruitment to sites of damage thereby enhancing DSB repair. In addition, SIRT6 associates with telomeric chromatin and deacetylates histone H3 lysine 9 (H3K9) and H3 lysine 56 (H3K56), leading to stabilization of WRN (Werner syndrome protein) and contributing to telomere maintenance. SIRT6 function has now been expanded to include cytosolic roles in stress-granule (SG) formation through the promotion of G3BP dephosphorylation and tumor necrosis factor α (TNF-α) secretion by lysine deacylation. These cellular functions impact upon many aspects of health and disease such as DNA repair, telomere maintenance, SG formation, glucose/lipid metabolism, inflammation, cardiac hypertrophy, and cancer. Unbroken arrow, SIRT6 directly modifies the protein or directly affects histone deacetylation at the promoters of target genes. Broken arrow, SIRT6 deacetylation activity is necessary, but is not direct. Red arrows, histone deacetylation; Ac, acetylation; P, phosphorylation; R, ADP-ribosylation. Figure is taken from Kugel, S., and Mostoslavsky, R. (2014). Chromatin and beyond: the multitasking roles for SIRT6. Trends in biochemical sciences *39*, 72-81.

1.2.1.3 SIRT6 and cancer

There is a controversial discussion about the role of SIRT6 in tumor progression as SIRT6 may have dual functions as an oncogene and tumor suppressor. The initial evidence that SIRT6 might act as an oncogene was the observation that SIRT6 expression increased 4-fold in CLL (chronic lymphocytic leukemia) patients compared with healthy volunteers (Wang et al., 2011a). Recently, the expression of SIRT6 also showed up-regulation in head and neck squamous cell carcinoma (Lu et al., 2014) and skin cancer (Ming et al., 2014). However, accumulating studies tend to support SIRT6 as a tumor suppressor. SIRT6 is down-regulated in several human cancers including colorectal cancer, pancreatic cancer, squamous cell carcinoma, breast cancer, prostate cancer, hepatocellular carcinomas (HCC) and lung cancer (Han et al., 2014; Lai et al., 2013; Lin et al., 2013; Marquardt et al., 2013; Yuan et al., 2013). Direct evidence is given by the observation that Sirt6 deletion induces the number, size and aggressiveness of tumors in a conditional Sirt6 knockout mouse model (Sebastian et al., 2012). Previous study also showed that a decreased level of SIRT6 in human hepatocytes predisposes them to form oncogenic hepatocellular carcinomas. This transformation causes metabolic changes and global hypomethylation consistent with a prooncogenic phenotype including up-regulation of established HCC biomarkers (Marquardt et al., 2013). By contrast, overexpression of SIRT6 induces massive apoptosis in a variety of cancer cells but not in normal cells (Van Meter et al., 2011). The previous described sections about glycolysis also provide strong support for the role of SIRT6 as tumor suppressor. SIRT6-deletion actives HIF1α-dependent glycolytic genes and leads to increased uptake of glucose as well as enhanced glycolysis together with an inhibited mitochondrial respiration (Zhong et al., 2010). This abnormality is reminiscent of the aerobic glycolysis in tumor cells. Indeed, the tumor formation in the absence of Sirt6 is independent of oncogene activation, but SIRT6-knockout MEFs (mouse embryonic fibroblasts) exhibits enhanced aerobic glycolysis. A recent study has also shown that E2F1 enhances glycolysis via suppressing SIRT6 transcription in bladder and prostate cancer cell lines (Wu et al., 2015). At the cellular level, SIRT6 inhibits ribosomal gene expression by co-repressing MYC transcriptional activity to control the tumor growth (Sebastian et al., 2012). In

addition, SIRT6 represses Survivin expression by reducing histone H3K9 acetylation and NFκB activation, and the increased SIRT6 expression at the liver cancer initiation stage markedly impairs liver cancer development (Min et al., 2012).

1.3 Cell-type specific gene regulation

During the development of multicellular organisms, each cell acquires its specific fate through a precisely controlled pattern of gene expression (Figure 1.5). The complex patterns of cell-type specific gene expression are thought to be achieved by combinatorial binding of TFs (transcription factors) to *cis*-regulatory elements, such as enhancers, promoters, silencers, and insulators (Kron et al., 2014; Smith and Shilatifard, 2014). Among those, enhancers play a central role in driving cell-type-specific gene expression (Calo and Wysocka, 2013).

1.3.1 Enhancers

Enhancers are distal-acting elements that enable precise spatiotemporal patterns for the process of cellular differentiation. Generally, enhancers could be recognized by tissue-specific transcription factors due to the specific DNA motif that they display. In addition to transcription factors, enhancers are distinguished by their epigenetic features. Enhancers with H3K27me3 and H3K4me1 mark poised enhancers while with H3K27ac and H3K4me1 modifications they act as active enhancers (Creyghton et al., 2010; Zentner et al., 2011). Considering the importance of enhancers in the maintenance of the precise spatiotemporal patterns of gene expression, it is easily conceivable that changes in enhancer activity contribute to the misregulation of tumor-relevant genes. For example, endodermal enhancers are shown to be necessary for the activation of *Igf2* and *H19* genes upon induction of liver carcinogenesis (Vernucci et al., 2000). Cancer cells also exploit enhancers to reprogram global gene expression favoring carcinogenesis (Akhtar-Zaidi et al., 2012). Emerging evidence indicates that large enhancer clusters have high transcription-factor occupancy and regulate lineage-specific programs as well as function as key oncogenic drivers in many tumor cells (Loven et al., 2013; Parker et al.,

2013; Smith and Shilatifard, 2014). These enhancer clusters including stretch enhancers, super-enhancer and transcription initiation platforms (TIP) that ensure robust control of cell identity (Smith and Shilatifard, 2014). The *IGF2/H19* hepatic control region overlaps with stretch enhancers in hepatocellular carcinoma (Parker et al., 2013). Thus, enhancer malfunction is suggested as the main cause of tissue-specific cancer development (Herz et al., 2014). Large-scale studies recently have demonstrated cancer cells could disrupt enhancer activity at oncogenes or other genes important in tumor pathogenesis (Hnisz et al., 2013). The alterations of enhancer activity can promote a 'cell identity crisis', in which enhancers associated with oncogenes and multipotentiality are activated, whereas those promoting cell fate commitment are inactivated (Kron et al., 2014).

1.3.2 Modification of enhancer chromatin

Recently, large-scale epigenomic mappings are effectively used to identify chromatin marks for enhancers. The chromatin signature that most reliably predicts enhancers is the relative occupancy of the monomethylated (H3K4me1) compared to the trimethylated of H3 lysine 4 (H3K4me3) (Heintzman et al., 2007). Specifically, active promoters are marked by H3K4me3, whereas enhancers are marked by H3K4me1. However, H3K4me1 is not only enriched at distal enhancers, but coincides with a "window of opportunity" to active enhancer, for example through promoting the incorporation of the histone H2AZ variant, resulting in less compacted chromatin structure, facilitating recruitment of transcription factors (Calo and Wysocka, 2013; Hoffman et al., 2010) (Figure 1.5A and B). Interestingly, instead of being tightly linked to enhancer activity, H3K4me1 marks hypomethylated DNA regions (Fernandez et al., 2015), as it interfere with the binding of Dnmt3L, an essential cofactor of DNA methyltransferases Dnmt3a/b (Calo and Wysocka, 2013). These functions of H3K4me1 in the context of enhancers provides a platform for the binding of pioneer factors and nucleosomal depletion, since pioneer factors like Foxa1 binds at genomic regions showing local DNA hypomethylation (Serandour et al., 2011).

In the context of H3K4me1, the additional recruitment of H3K27ac could switch inactive/poised enhancer into active enhancers, leading to a higher transcription of nearby genes (Creyghton et al., 2010) (Figure 1.5A). Surprisingly, further studies

identified that H3K27me3 together with H3K4me1, but lacking of H3K27ac, were enriched at enhancers in ESCs (Rada-Iglesias et al., 2011; Zentner et al., 2011). These elements are termed poised enhancers and will drive gene expression during differentiation, although they do not have this ability in pluripotent cells (Rada-Iglesias et al., 2011) (Figure 1.5C). Intriguingly, poised enhancers are already looped to their target promoters in ESCs, which might be mediated by Polycomb complex PRC2 (Calo and Wysocka, 2013; Weth et al., 2014).

Table 1.1 Histone marks

Histone marks	Types	Functions
H3K4me1	active	Enriched in enhancer and super-enhancer regions (Heintzman et al., 2007; Loven et al., 2013); marks hypomethylated DNA regions (Fernandez et al., 2015); promotes the incorporation of the histone H2AZ variant (Calo and Wysocka, 2013).
H3K4me3	active bivalent	Enriched at promoters (Heintzman et al., 2007); transcription-start site maker (Lloret-Llinares et al., 2012); stimulates preinitiation complex formation (Lauberth et al., 2013).
H3K9me3	repressive	Enriched in promoter and poised enhancer regions (Zentner et al., 2011); heterochromatin marker (Lehnertz et al., 2003; Peters et al., 2002; Schotta et al., 2004).
H3K27me3	repressive bivalent	Enriched at subsets of cis-regulatory elements, including poised enhancers (Rada-Iglesias et al., 2011; Zentner et al., 2011); mark of the inactive X chromosome (Rougeulle et al., 2004).
H3K9ac	active	Enriched in active enhancer and promoter regions (Ernst et al., 2011; Zentner et al., 2011); mediates the recruitment of TFIID (Agalioti et al., 2002).
H3K27ac	active	Enriched in active enhancer and super-enhancer regions (Creyghton et al., 2010; Loven et al., 2013).
H4K8ac	active	Enriched in active enhancer and promoter regions (Ernst et al., 2011; Zentner et al., 2011); mediates the recruitment of SWI/SNF complex (Agalioti et al., 2002).
H2AZ	active	Enriched at both active and poised enhancers and promoters, alters the nucleosome stability and chromatin accessibility (Creyghton et al., 2008; Jin and Felsenfeld, 2007; Valdes-Mora et al., 2012).

Besides H3K4me1/3, H3K27ac and H3K27me3, other histone modifications are used to decorating distal regulatory regions (Table 1.1). For instance, H3K9ac, H3K18ac, H4K8ac and histone crotonylation were observed at putative enhancers (Ernst et al., 2011; Tan et al., 2011; Zentner et al., 2011). H3K9ac is critical for the recruitment of TFIID, and H4K8ac mediates recruitment of the SWI/SNF complex, a chromatin remodeling complexes; both are required for the recruitment transcription complexes at enhancers (Agalioti et al., 2002). Moreover, H3K9me3, the mark of heterochromatin, is enriched at poised enhancers (Zentner et al., 2011). A large number of studies demonstrate that histone variants H2AZ and H3.3 are enriched at both active and poised enhancers and promoters of multiple cells (Creyghton et al., 2008; Hu et al., 2013; Jin and Felsenfeld, 2007; Li et al., 2012a; Valdes-Mora et al., 2012). Nucleosomes containing H2AZ and H3.3 are less stable and therefore easier for pioneer factor to displace from DNA (Jin and Felsenfeld, 2007; Li et al., 2012a).

1.3.3 Pioneer factors

Generally, the initial recognition of enhancers requires pioneer transcription factors. Pioneer factors, a class of TFs such as GATA, FOXA and Pu.1, have the ability to binding at the regions of silent chromatin and open the compacted chromatin, subsequently initial a cascade of events leading to recruitment of chromatin remodelers and downstream TFs (Wamstad et al., 2014). Insight into the regulation of liver-specific gene activity in mouse embryos led to the identification of the FOXA proteins as ‘pioneer factors’ whose binding to enhancers and promoters enable chromatin access for other tissue-specific transcription factors (Cirillo et al., 2002b; Zaret, 1999). Earlier studies have found that the forehead box structure is similar to that of linker histone H1, which facilitates FOXA to displace histone H1 in a SWI/SNF-independent manner (Clark et al., 1993). Moreover, FOXA displays an unusual property during the cell cycle; it remains associated with condensing chromosomes during mitosis, while most sequence-specific TFs appear to be released (Caravaca et al., 2013). These special qualities—avid binding to condensed chromatin and similar structure with histone H1—might be critical manifestations of the ability of pioneer factors to stably mark enhancers for future use (Levine et al., 2014).

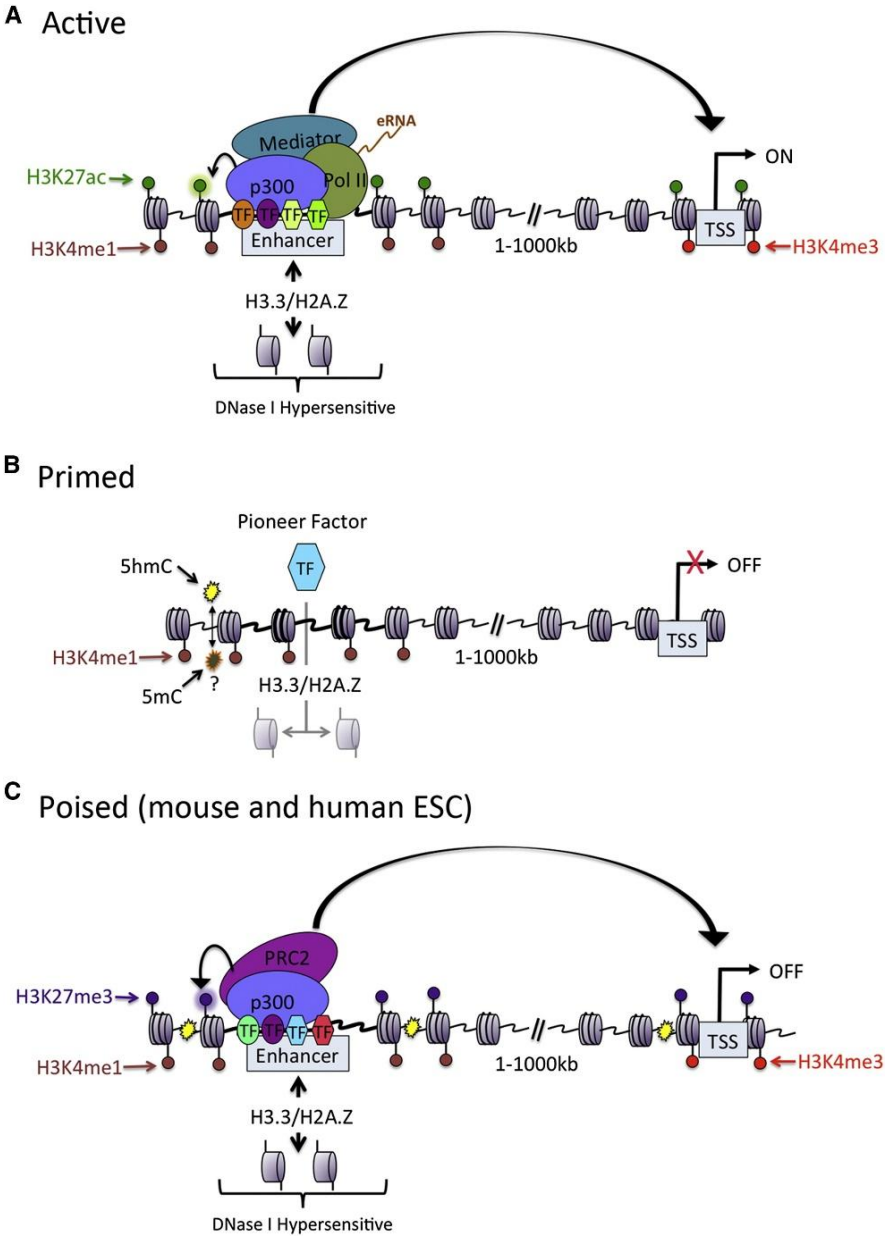

Figure 1.5 Epigenetic features of active, primed, and poised enhancers. (A) Schematic representation of the major chromatin features found at active enhancers. Enhancers are associated with incorporation of hypermobile nucleosomes containing H3.3/H2A.Z histone variants, which compete for DNA binding with TFs. TFs in turn recruit co-activator proteins that can modify and remodel nucleosomes. H3K4me1 and H3K27ac are the predominant histone modifications deposited at nucleosomes flanking enhancer elements. (B) Prior to activation, enhancers can exist in a primed state, characterized by the presence of H3K4me1. Other features that have been associated with enhancer priming are presence of pioneer TFs, hypermobile H3.3/H2A.Z nucleosomes, DNA 5mC hypomethylation, and hydroxylation (5hmC). (C) Schematic representation of the chromatin landscape surrounding poised enhancers found in human and mouse ESCs. A subset of "primed" enhancers in ESCs is also marked by H3K27me3 and associated with PRC2. These enhancers are bound by TFs and co-activators and communicate with their target promoters. Figure is taken from Calo, E., and Wysocka, J. (2013). Modification of Enhancer Chromatin: What, How, and Why? Molecular Cell *49*, 825-837.

1.3.4 Foxa1 and Foxa2 in endodermal development, hepatic differentiation and cancer development

The vertebrate forkhead boxA (FOXA) gene family comprises Foxa1, Foxa2 and Foxa3, which are encoded by different genes and have the conserved forkhead box. The Foxa family has been found to play important roles in multiple stages of mammalian life, especially during early development. For example, mouse embryos homozygous for a null mutation of Foxa2 result in embryonic lethality at embryo day of 11 (E11) and show severe phenotypes in structures related to all three germ layers, with absence of the notochord, abnormalities of the somites and neural tube, and failure to form the gut tube, although endoderm cells are present (Friedman and Kaestner, 2006; Weinstein et al., 1994). However, neither Foxa1 nor Foxa3 is required during early mouse embryogenesis as both Foxa1$^{-/-}$ and Foxa3$^{-/-}$ embryos appear normal at birth, likely owing to differences in their spatial and temporal expression domains and/or functional compensation by the remaining Foxa factors (Le Lay and Kaestner, 2010).

Foxa is expressed throughout the developing foregut of early mouse embryos. The timing of Foxa family gene expression during embryogenesis, combined with the many liver-specific Foxa target genes, has been interpreted as evidence that Foxa genes regulate hepatogenesis (Friedman and Kaestner, 2006). To circumvent these early functions outside the endoderm, CRE recombinase-mediated inactivation of Foxa2 was carried out specifically in the foregut endoderm of embryos with a Foxa1 homozygous null mutation (Zaret, 2008). Strikingly, the only known model of a completely ‘liver-less’ in vertebrate was induced by the Foxa1/2 (Foxa1 and Foxa2) deletion, which revealed that Foxa1 and Foxa2 are redundantly necessary to activate the hepatic differentiation program. Specifically, these Foxa1/2 double-null embryos are completely deficient in hepatic specification, as neither liver bud development nor expression of the earliest liver marker Afp is evident (Lee et al., 2005).

Despite that the essential roles in early development and organogenesis, both Foxa1 and Foxa2 exhibit the pivotal role in cancer progression, mainly due to their pioneer function to open chromatin structure, which facilitates binding of other transcriptional

regulators, with subsequent initiation of tissue-specific transcriptional programs. For instance, FOXA1/2 and estrogen receptor (ER) or androgen receptor (AR) frequently bind to adjacent *cis*-regulatory elements in their target genes in human prostate or breast cancer cell lines, respectively, and that the recruitment of ER or AR to their targets depends on FOXA (Carroll et al., 2005; Lupien et al., 2008; Yu et al., 2005). Moreover, FOXA1 may also inhibit metastatic progression of luminal subtype breast cancers by controlling differentiation through enhancing the expression of the negative cell cycle regulator p27Kip1 and the cell adhesion molecule E-cadherin (Nakshatri and Badve, 2007; Yamaguchi et al., 2008). More interestingly, both Foxa1 and Foxa2 account for the sexual dimorphism in liver cancer. Specifically, HCC is completely reversed in Foxa1- and Foxa2-deficient mice after diethylnitrosamine-induced hepatocarcinogenesis. Co-regulation of target genes by Foxa1/2 and either ERα or AR was increased during hepatocarcinogenesis in normal male or female mice, respectively, but was lost in Foxa1/2-deficient mice (Li et al., 2012b). In addition, Foxa2 was found to suppress the metastasis of hepatocellular carcinoma partially through matrix metalloproteinase-9 inhibition, which is also associated with HCC progression (Wang et al., 2014).

1.4 Polycomb group protein and its role in gene silencing

1.4.1 PRC2 core components and its enzymatic activities

The Polycomb group of protein contains Polycomb repressive 1 (PRC1) and PRC2, which is initially referred to its critical role in regulating body segmentation in Drosophila (Lewis, 1978). The core canonical PRC2 complex consists of EZH2 (enhancer of zeste), the zinc-finger-containing protein SUZ12 (suppressor of zeste12), the WD40-repeat protein EED (embryonic ectoderm development) and RBAP46/48 (also known as Rbbp7/4) (Figure 1.6) (Margueron and Reinberg, 2011). EZH2 is the core catalytic subunit mediating H3K27 trimethylation, while Suz12 and EED are required for the methyltransferase activity, because EZH2 itself lacks enzymatic activity. RbAp46/48 functions as a histone chaperones to enhance the histone binding (Volkel et al., 2015).

PRC2 is primarily known for its role in epigenetic gene silencing and X chromosome inactivation via trimethylation of H3K27, the classic substrate of EZH2 (Cao et al., 2002; Plath et al., 2003). A number of studies have shown PRC2 also exhibits methyltransferase activity on linker histone H1, which is important for transcriptional repression (Kuzmichev et al., 2004; Kuzmichev et al., 2005; Martin et al., 2006; Xu et al., 2010). Furthermore, previous studies showed EZH2 catalyzes non-histone proteins such as GATA4 and RORα (Volkel et al., 2015). No matter the histone substrates or non-histone substrates, all the methylation activities point the repressive role of PRC2 in various biological process, including development, adult homeostasis and cancer (Vizan et al., 2015). For example, PRC2 mediates transcriptional repressive states or creates silenced or poised enhancers through the H3K27me3 modification to regulate the cell identity and differentiation (Creyghton et al., 2010; Zentner et al., 2011).

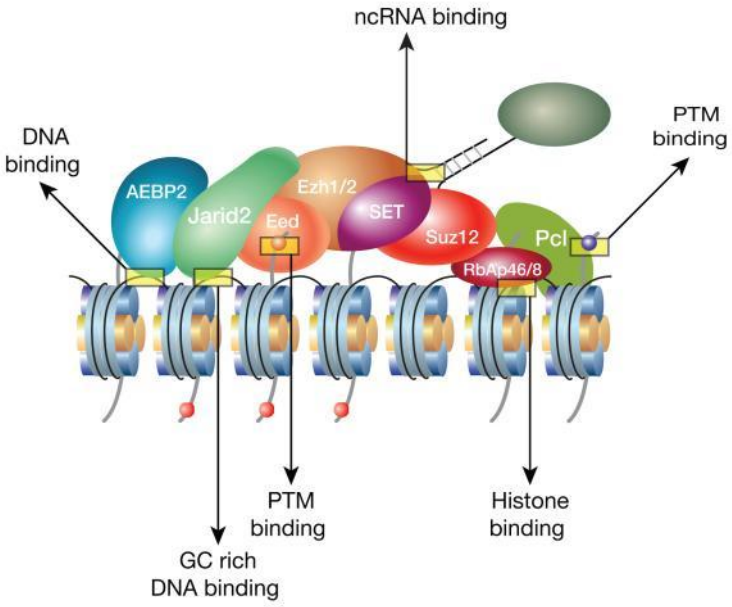

Figure 1.6 Multiple interactions of PRC2 with chromatin (Margueron and Reinberg, 2011). Schematic representation of PRC2 holoenzyme at chromatin. Putative interactions with either DNA or histones that could explain PRC2 recruitment are highlighted. The proteins are involved are indicated in this picture. Figure is taken from Margueron, R., and Reinberg, D. (2011). The Polycomb complex PRC2 and its mark in life. Nature *469*, 343-349.

Apart from post-translational modifications (PTM) of histones, PRC2 mediates gene silencing through directly controlling the DNA methylation (Vire et al., 2006).

Accumulating evidence has demonstrated the PTMs of PRC2 proteins are critical for their stabilities and subcellular locations, as well as the role in repression and regulation of tumor progression. The PRC2 proteins are targeted for phosphorylation, sumoylation, ubiquitylation and acetylation (Niessen et al., 2009; Wan et al., 2015). EZH2 phosphorylation by AKT or CDK1 inhibits its enzymatic activity (Cha et al., 2005; Wei et al., 2011; Wu and Zhang, 2011), whereas the acetylation of EZH2 decreases the phosphorylation and increases its stability and suppression (Wan et al., 2015). Both EZH2 and SUZ12 could be sumoylated, although the exact biological role is unclear (Riising et al., 2008).

1.4.2 PRC2 in differentiation

PRC2 has been linked to lineage commitment to establish proper execution of developmental gene expression program (Creyghton et al., 2008; Hu et al., 2013). There are two straightforward hypothesis that explain the maintenance of stem-cell pluripotency in the context of PRC2-mediated gene repression (Margueron and Reinberg, 2011). The first model is in keeping with the function of PRC2 in repressing numerous developmental regulators in ES cells, which is required for the maintenance of pluripotency and that are poised for activation during ES cell differentiation (Boyer et al., 2006; Lee et al., 2006). Conversely, PRC2 inactivation promotes differentiation during myogenesis and epidermis formation (Caretti et al., 2004; Ezhkova et al., 2009). Notably, H2AZ and PRC2 occupancy is interdependent at promoters in ES cells and H2AZ dynamic redistribution is necessary in mediating cell fate transitions upon induction of differentiation (Creyghton et al., 2008). However, some studies draw the attention to the second hypothesis that PRC2 is required for silencing of pluripotency genes upon ESC differentiation, such as *Suz12*$^{-/-}$ ES cells fail to form a proper endodermal layer and are impaired in proper differentiation (Pasini et al., 2007). Recently, Polycomb protein EED was also proved to regulating silence of pluripotency genes including Oct4, Nanog and Sox2 upon ESC differentiation (Obier et al., 2015).

1.4.2 PRC2 in hepatic cancer

In the context of HCC, emerging evidence has indicated that frequent aberrant expression of PRC2 proteins and their downstream molecular effects in promoting tumor growth and metastasis. The most widely investigated protein EZH2 is frequently upregulated in primary HCC and the upregulation of EZH2 is correlated to poor prognosis of HCC (Cai et al., 2011b; Sasaki et al., 2008). Interestingly, high expression of H3K27me3 is also detected in HCC tissue microarrays, and the increased H3K27me3 in HCC significantly correlated with large tumor size, poor differentiation, advanced clinical stage, vascular invasion as well as shorter survival of HCC patients (Cai et al., 2011a). These studies indicate that the dysregulated EZH2-H3K27me3 epigenetic mark has a profound role in hepatocarcinogenesis.

The underlying molecular mechanisms of EZH2 upregulation in HCC are attributed to aberrant silencing of EZH2 target genes (Au et al., 2013; Chen et al., 2007). EZH2 represses target genes through H3K27-dependent (e.g. CDKN2A) and H3K27-independent (e.g. TP53) mechanisms in hepatocellular carcinoma (Gao et al., 2014). Moreover, EZH2 promotes HCC cell motility and metastasis by repressing tumor suppressor miRNAs included miR-125b, miR-139-5p, miR-101, let-7c and miR-200b in of H3K27-dependent model (Au et al., 2012). Last but not least, EZH2 may directly interplay with other signaling pathway such as Wnt pathway to drive hepatocarcinogenesis (Cheng et al., 2011).

However, it is controversial of the expression of Suz12 in HCC. The mRNA expression of Suz12 is increased in liver tumors of mice treated with the carcinogen DEN (Kirmizis et al., 2003), while SUZ12 protein is reduced during HBV X protein-mediated transformation, owing to the phosphorylation-mediated proteasomal degradation (Wang et al., 2011b). Due to the limited studies of other PRC2 component, involvement of other core subunits such as SUZ12 and EED is certainly urges further investigations. Taken together, dysregulated PRC2 proteins do not only result in aberrant gene and miRNA expressions but may also directly interplay with other signaling pathway to drive hepatocarcinogenesis.

1.5 Aims of the study

HCC is the fifth most common cancer globally but, owing to the lack of effective treatment options, represents the third leading cause of neoplasm-related mortality (Zender et al., 2006). Its incidence is increasing worldwide because of the dissemination of hepatitis B and C virus infection, alcohol intake, toxins and hemochromatosis (Clark et al., 2015; Singal and El-Serag, 2015). Hence, it is particularly important to afford an effective early detection and diagnosis confirmation. Fortunately, the well-established HCC biomarkers offer great hope, such as AFP test is already used to help monitor the person's response to therapy and to monitor for cancer recurrence in clinical. Similarly, other oncofetal genes like *H19* and *IGF2* exhibit high level in HCC patients, which also suggest much potential clinical utility for *IGF2* and *H1*9 testing in the context of liver cancer (Ariel et al., 1998; Couvert et al., 2012; Morace et al., 2012), to assist in more effective early detection and diagnosis confirmation of HCC. Interestingly, data from Prof. Strand lab identified the up-regulation of these HCC genes including *Afp, Igf2, H19* and glypican-3 is Sirt6-dependent in hepatocytes. However, how Sirt6 regulates the expression of these biomarkers is not well characterized and is the focus of this study.

Sirt6, an important regulator of lifespan and aging-related disease, performs its multiple roles via its enzymatic reactions that include deacetylation, deacylation and ADP-ribosylation. Accumulating studies have revealed that SIRT6 plays pivotal roles in fatty liver-related disease, such as fatty liver (Kim et al., 2010; Tao et al., 2013; Yang et al., 2011; Yang et al., 2014), diabetes and obesity (Dominy et al., 2012; Palmer et al., 2011; Zhong et al., 2010), as well as liver tumor formation (Min et al., 2012). Specifically, SIRT6-deletion actives HIF1α-dependent glycolytic genes and leads to increased uptake of glucose as well as enhanced glycolysis together with an inhibited mitochondrial respiration (Zhong et al., 2010). At the cellular level, SIRT6 represses Survivin expression by reducing histone H3K9 acetylation and NFκB activation, and the increased SIRT6 expression at the liver cancer initiation stage markedly impairs liver cancer development (Min et al., 2012). However, neither model could explain the pro-oncogenic phenotype

and impaired liver function in the Sirt6-deficient mice, suggesting additional mechanisms must contribute to the mutant phenotype of SIRT6-deficient mice.

In addition, the expression level of oncofetal genes directly linked to the histopathological onset and development of the liver tumor. SIRT6 expression level is significantly decreased in both premalignant and malignant stages of hepatocarcinogenesis (Marquardt et al., 2013; Zhong et al., 2010). The lab of Prof. Strand also identified the surprising congruency between the human hepatoma cell lines and the Sirt6-deficient hepatocytes. Given the importance of SIRT6 in hepatocyte function and development of liver tumor, investigating the molecular mechanism between Sirt6 and these oncofetal genes will be beneficial for the prevention and/or therapeutic treatment of HCC and liver-related diseases.

2 Materials and methods

2.1 Instruments and equipment

Name	Company
Zeiss cLSM-710NLO	Carl Zeiss MicroImaging GmbH
Cell culture microscope wilovert 30 standard	Hund, Wetzlar, Germany
Cell culture flowbank (S-2000 1.5)	Heto-Holten, Danmark
GFL type 1004 waterbath	Milian Labware, USA
Mx3000P qPCR machine	Startagene, USA
Covaris® M220	Life Technology, Germany
Centrifuge 5415 R	Eppendorf, Hamburg, Germany
ChemiDoc™ XRS	Bio-Rad Laboratories GmbH
Wet Western blot transfer apparatus	benchfly, USA
Trans-Blot® Turbo™ Transfer System	Bio-Rad Laboratories GmbH
Protein Blotting Equipment	Bio-Rad Laboratories GmbH
Leica light microscope	Leica, Germany
MyCycler (thermo cycler)	Bio-Rad Laboratories GmbH
UV/Visible spectrophotometer ultrospec 3000	Pharmacia biotech, Freiburg, Germany
Eppendorf Thermomixer® Dry Block Heating Shaker	Eppendorf, Hamburg, Germany
pH-Meter Toledo 320	Mettler Toledo, Switzerland
Nandrop ND-1000	Spectrophotometer
Rollers	Stuart, United Kingdom
4°C/-20°C refrigerator	Bosch, Germany
-80°C refrigerator	Ultra-Low technology, USA

2.2 Chemicals

Acetic acid	Applichem, Darmstadt, Germany
Acrylamide	Merck, Darmstadt, Germany
AEBSF	Sigma-Aldrich, Munich, Germany
Agarose	CalBiochem, Germany
APS	Sigma-Aldrich, Munich, Germany
Bovine Serum Albumin	Applichem, Darmstadt, Germany
Boric Acid	Applichem, Darmstadt, Germany
2-Butanol	Applichem, Darmstadt, Germany
Benzonase	Sigma-Aldrich, Munich, Germany
CDP Star	Tropix, Bedford, USA
Collagen R	Serva, Heidelberg, Germany
DEA	Tropix, Bedford, USA
Dimethyl sulfoxide (DMSO)	Pharmacy, Universitätsmed. Mainz
DTT	Sigma-Aldrich, Munich, Germany
DPBS	Sigma-Aldrich, Munich, Germany
DPBS with EDTA	Sigma-Aldrich, Munich, Germany
EDTA	Applichem, Darmstadt, Germany
EGTA	Applichem, Darmstadt, Germany
Ethanol	Roth, Karlsruhe, Germany
Ethidium Bromide	Sigma-Aldrich, Munich, Germany
Fetal Bovine Serum (FCS)	Biochrom AG, Berlin, Germany
Fluoromount-G™ mounting medium	Beckman Coulter, Fullerton (CA), USA
Glycine	Sigma-Aldrich, Munich, Germany
Glycerol	Sigma-Aldrich, Munich, Germany
Hepes	Sigma-Aldrich, Munich, Germany
IGEPAL	Sigma-Aldrich, Munich, Germany
I-Block	Tropix, Bedford, USA

L-Glutamine	Sigma-Aldrich, Munich, Germany
Lithium chloride	Roth, Karlsruhe, Germany
Methanol	Roth, Karlsruhe, Germany
Monopotassium phosphate	Merck, Darmstadt, Germany
N-Ethylmaleimide (NEM)	Sigma-Aldrich, Munich, Germany
Nitroblock II	Tropix, Bedford, USA
NZ Amine® Broth	Sigma-Aldrich, Munich, Germany
Potassium chloride	Merck, Darmstadt, Germany
Perchloric acid	Sigma-Aldrich, Munich, Germany
2-Propanol	Applichem, Darmstadt, Germany
Protease Inhibitor cocktail	Roche, Mannheim, Germany
Paraformaldehyde	Carl Roth GmbH, Karlsruhe, Germany
PhosSTOP Phosphatase Inhibitor	Roche, Mannheim, Germany
Sodium butyrate	Sigma-Aldrich, Munich, Germany
Sodium chloride	Roth, Karlsruhe, Germany
Sodium dodecyl sulfate (SDS)	Sigma-Aldrich, Munich, Germany
Sodium hydroxide	Merck, Darmstadt, Germany
Sodium orthovanadate (Na3VO4)	Sigma-Aldrich, Munich, Germany
Sodium chloride (NaCl)	Carl Roth GmbH, Karlsruhe, Germany
TEMED	Applichem, Darmstadt, Germany
Triton X-100	Merck, Darmstadt, Germany
Trichostatin A (TSA)	Sigma-Aldrich, Munich, Germany
Tris	Sigma-Aldrich, Munich, Germany
Triton X-100	Sigma-Aldrich, Munich, Germany
Tween 20	Sigma-Aldrich, Munich, Germany
Tryptone	Sigma-Aldrich, Munich, Germany
Yeast Extract	Sigma-Aldrich, Munich, Germany

2.3 Medium, gels and reagents

2.3.1 Medium

Escherichia coli

LB medium

10 g Trypton

5 g Yeast extract

10 g Sodium chloride

add 1 L with ddH_2O

pH 7.0 with NaOH

sterilization by autoclaving

LB agar plates

1 L LB medium

15 g Agar

sterilization by autoclaving

addition of antibiotics after cooling to 50-60 °C

Mammalian cells

DMEM medium for Hep3B cells

Advanced DMEM supplemented with

10% FCS

1% Gibco Pen Strep

1% L-Glutamine

1% Hepes Buffer

DMEM-pmHep(primary mouse hepatocyte)

Gibco DMEM supplemented with

10% FCS

1% Gibco Sodium pyruvate

1% Gibco Pen Strep

1% L-Glutamine

1% Hepes Buffer

2.3.2 Gels and reagents

Agarose gel electrophoresis

TBE (Tris-Borate-EDTA) buffer

90 mM Tris-HCl pH 8.0

90 mM Boric acid

2.5 mM EDTA pH 8.0

Agarose gel (1% w/v)

1 g agarose

100 mL TBE buffer

0.1 µg/mL Ethidium bromide

Agarose gel electrophoresis

Ethidium bromide

10 mg/mL in ddH_2O

Loading buffer (6X)

0.2% Bromophenol blue

30% Glycerol

100 mM EDTA, pH 8.0

SDS gels

Table 2.1 Resolving gel composition (for 4 gels)

Reagents	Resolving gel (%)			
	8%	10%	12%	15%
30% Acrylamide (ml)	10.8	13.3	15.5	20
1.8 M Tris-HCl (pH-8.8) (ml)	8.0	8.0	8.0	8.0
H_2O (ml)	20.6	18.1	15.9	11.5
10% SDS (µl)	400	400	400	400
10% APS (µl)	200	200	200	200
TEMED (µl)	8.0	8.0	8.0	8.0

Stacking gel 2.25 mL Acrylamide-bis

3 mL 0.6 M Tris pH 6.8

9.5 mL dH_2O

150 µL SDS (10% w/v)

75 µL APS (10% w/v)

7.5 µL TEMED

SDS PAGE

2X SDS-PAGE sample buffer

40 mL 10% SDS (w/v)

10 mL 1 M Tris-HCl pH 6.8

10 mL 2-Mercaptoethanol

20 mL Glycerol

2.2 mg Bromphenol blue

Add 100 mL with dH_2O

10X SDS-PAGE running buffer

30.25 g TRIS

144 g Glycin

850 mL dH_2O

100 mL 10% SDS (w/v)

Add 1 L with dH_2O

Western blot

10X Western blotting buffer

30 g Tris

144 g Glycin

Add 1 L with dH_2O

1X Western blotting buffer

100 mL 10X Western blotting buffer

200 mL Methanol

add1 L with dH_2O

I-Block solution

100 mL 10X PBS

2 g Tropix I-Block™

1 mL Tween 20

Add 1 L with dH_2O

Assay Buffer

10.6 g Tropix® DEA

500 µL 2 M $MgCl_2$

Add 1 L with dH_2O

pH 9.5 with HCl

Nitro-Block-II solution

Nitro-Block-II™ 1:200

in Assay Buffer

CDP-Star solution

CDP-Star® 1:1000

in Assay Buffer

2.4 Antibodies

The primary antibodies used are as follows: anti-SIRT6 (Sigma), anti-SIRT6 (Cell Signaling), anti-Foxa1 (MyBiosourse), anti-Foxa2 (R&D), anti-CTCF (Cell Signaling), anti-CTCF (Millipore), anti-Rad21 (Abcam), anti-Rad21 (Santa Cruz), anti-Suz12 (Cell Signaling), anti-Suz12 (Abcam), anti-EZH2 (Cell Signaling), anti-IGF2 (Abcam), anti-HP1β (Active Motif), anti-Rbbp7 (Santa Cruz), anti-PIAS1(Abcam), anti-c-Myc (Sigma), anti-Flag (Sigma), anti-HA (Cell Signaling) anti-Acetylated Lys (Cell Signaling), anti-Acetylated Lys (Abcam), anti-Crotonylysine (PTM Biolabs), anti-Sumo1 (Cell Signaling), anti-Sumo2/3 (Cell Signaling), anti-Ubiquitin (Cell Signaling), anti-Histone H1.2 (Abcam), anti-Histone H1.4 (Sigma), anti-Histone H1.4 (Bioss), anti-H2AZ (Active Motif), anti-H3K4me1 (Active Motif), anti-H3K4me3 (Active Motif), anti-H3K9me3 (Active Motif), anti-H3K9ac (Cell Signaling), anti-H3K9ac (Active Motif), anti-H3K27me3 (Active Motif), anti-H3K27ac (Abcam), anti-H4K8ac (Cell Signaling), anti-Histone H3 (Cell Signaling), and anti-Rabbit IgG (Cell Signaling) or anti-Mouse IgG (Millipore) or anti-Goat IgG (PeproTech) as negative controls.

The secondary antibodies for Western blot: anti-rabbit immunoglobulin ALP-conjugated (Sigma), anti-mouse immunoglobulin ALP-conjugated (Sigma), anti-goat immunoglobulin ALP-conjugated (Sigma), anti-mouse immunoglobulin HRP-conjugated (R&D), anti-mouse immunoglobulin HRP-conjugated (Cell Signaling), anti-rabbit immunoglobulin HRP-conjugated (Cell Signaling), and anti-goat immunoglobulin HRP-conjugated (Santa Cruz).

Fluorescence secondary antibodies were all from Molecular Probes: Alexa-Flour-488 mouse-anti-rabbit, Alexa-Flour-488 goat-anti-mouse, Alexa-Flour-555 mouse-anti-rabbit, Alexa-Flour-555 goat-anti-mouse. Hoechst were used to staining nucleus.

2.5 Molecular biological methods

2.5.1 Cell culture

Mice of the strain 129-Sirt6$^{tm1Fwa/J}$ were obtained from Jackson Laboratory. Hepatocytes from Sirt6$^{-/-}$ and Sirt6$^{+/+}$ mice were isolated from mouse livers by hepatic portal vein

perfusion as described before (Teufel et al., 2010). Conditional Sirt6-knockout mice were also established by breeding between SIRT6 conditional allele and Albumin-cre lines. All mice were maintained in the central laboratory animal facility (ZVTE) of Johannes Gutenberg University and all the guidelines concerning animal handling were strictly followed. Hep3B was cultured in advanced DMEM supplemented with 10% fetal bovine serum, 1% L-glutamine, 1% HEPES (PAA) and 1% penicillin–streptomycin.

2.5.2 Transfection assays and expression analysis

Hep3B cells were transfected using Lipofectin™ reagent (Invitrogen) according to manufacturer's instruction. Plasmid including pcDNA, *SIRT6*-Myc and Foxa2-Flag were transfected into cells seated in 6-well plate. Cells were incubated with transfection reagent for 6 h at 37°C, followed by a change to normal culture medium and then harvested after 48 hours. Expression analysis was done by qPCR on reverse transcribed RNA, Western blot or Co-IP. Primers are listed in Table 2.

2.5.3 Genomic engineering by CRISPR-Cas9

The clustered regularly interspersed palindromic repeats (CRISPR)/CRISPR associated (Cas) 9 nuclease system was used to introduce enhancer deletion mutations in Hep3B cells following recently published protocols (Canver et al., 2014).

2.5.3.1 CRISPR design and creation

SgRNA-specifying oligo sequences were designed to optimize uniqueness and have limited off-targets using an online tool (http://crispr.mit.edu/). The sequences flanking mEnh-*H19/Igf2* distal targeted by the CRISPR constructs (Figure 2.1) are:

sgRNA-Ds: GAGGGTATCTGGTTGCCCGC **CGG**

sgRNA-Cs: CACCgGAGTGCGGGCAACTGCCGTT **TGG**

sgRNA-E1: CACCgGCCCGGAAAGGCGGGTTAAC **TGG**

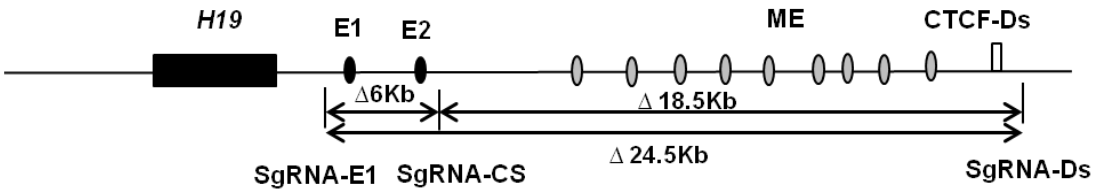

Figure 2.1 Schematic representation of CRISPR-based enhancer deletion strategy in Hep3B cells. *H19* genes (black boxes) is displayed together with the downstream endodermal enhancers (EE) (black ovals), mesodermal enhancers (ME) (gray ovals), and CTCF-downstream binding locus (CTCF-Ds) (white box). The black lines with two arrows indicate the predicted cleavage of EE, ME and full enhancers region, respectively.

2.5.3.2 Oligo annealing and cloning into pX459 plasmid

The plasmid pX459 (Addgene #48139) expresses a human codon-optimized SpCas9 and chimeric guide RNA expression plasmid, following previously published guide-lines (Cong et al., 2013).

a. Phosphorylate and anneal each pair of oligos:

oligo 1 (100 µM)	1 µl
oligo 2 (100 µM)	1 µl
10X T4 Ligation Buffer (NEB)	1 µl
ddH_2O	6.5 µl
T4 PNK (NEB)	0.5 µl
Total	10 µl

Anneal in a thermo cycler using the following parameters:

37°C 30 min

95°C 5 min and then ramp down to 25°C at 5°C /min.

Dilute the annealed oligo 1:200.

b. Set up digestion-ligation reaction:

100ng pX459	X µl
phosphorylated and annealed oligo duplex from step 1 (1:200 dilution)	2 µl
10X Tango buffer	2 µl
10mM ATP	1 µl
10mM DTT	1 µl
FastDigest BbsI (Fermentas)	1 µl
T7 ligase(NEB)	0.5 µl
ddH_2O	Y µl
Total	20 µl

Incubate the ligation reaction in a thermo cycler:

37°C 5 min

23°C 5 min, Cycle the previous two steps for 6 cycles (total run time 1 hour)

4°C hold until ready to proceed

c. Transformation with 1-2 µl of the final product into XL-1 blue competent cells, pick colony and sequence verify.

2.5.3.3 Transfection

Transfection experiments were performed as described previously. Hep3B cells were plated at a density of 0.5 million/ml on 10 cm^2 plates 24 hours before transfection. Cells were triple transfected using Lipofectin^{TM} reagent (Invitrogen) according to manufacturer's instruction with 7.5 µg of each CRISPR plasmid and 0.5 µg of pGFP. To enrich for deletion, the top 5% GFP^+ cells were sorted via FACS Aria cell sorter (BD Biosciences) 48 hours post-transfection. Then cells were immediately diluted in 96 well-plates with Hep3B medium for recovery 48 hours. After that, 1 mg/mL of puromycin (Sigma) was supplemented to the cell culture media for 5 days to select for the transfected clones.

2.5.3.4 Screening clones

Genomic DNA was isolated from clonal CRISPR targeted Hep3B cell lines using High Pure PCR Template Preparation Kit (Roche). To screen deletion clones, distal enhancer-spanning PCR primers were designed which flank the outside of the CRISPR sgRNAs. Given efficient CRISPR cuts and repairs of DNA through non-homologous end joining, about 420bp product is amplified by PCR. Subsequently, a qPCR-based genotyping method was designed to quantify the DNA copy number of the targeted regions relative to control regions. qPCR copy number primers were designed inside the targeted region to quantify the efficiency of CRISPR deletion as creating a biallelic or monoallelic deletion. Primers are listed in Table 2.

2.5.4 DNA-methylation

Genomic DNA of mouse hepatocytes was extracted with the Gentra®Puregene®Kit (Qiagen) according to the manufacturer's instructions. Bisulfite conversion of 500 ng DNA

per sample was performed with the EZ DNA Methylation-Direct™-Kit (Zymo) according to the manufacturer's specifications. Quantification of DNA methylation was studied by pyrosequencing on the PyroMark Q96 ID instrument using PyroMark Gold Q96 reagents (Qiagen). Primers are listed in Table 2.

2.5.5 Chromosome conformation capture (3C)

Chromosome conformation capture (3C) technology (Figure 2.2) is based on formaldehyde crosslinking of interacting chromatin segments, followed by restriction digestion and intramolecular ligation of crosslinked fragments. Ligation products are subsequently analyzed by PCR using primers specific for the restriction fragments of interest. Here, 3C was performed using *BamHI* (Promega) as previously described (Court et al., 2011). Standard curves for qPCR have been generated from the RP23 BAC (Invitrogen). The sequence of primers used for qPCR quantification of 3C products are shown previously (Court et al., 2011).

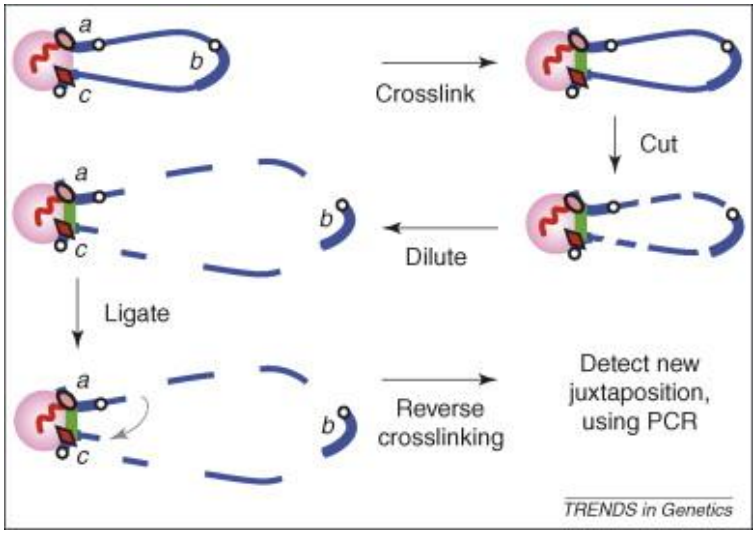

Figure 2.2 The 3C method (Marenduzzo et al., 2007). A loop containing genes *a*, *b* and *c* is shown. 3C involves fixation to crosslink DNA sequences that lie next to each other (usually through DNA–protein–DNA links; green), before cutting with a restriction enzyme, dilution and ligation. Dilution favors intramolecular ligation: that is, the end of one DNA molecule in a DNA–protein–DNA complex is joined to the end of the second DNA molecule in the same complex more frequently than to the end of a different molecule or complex. Then, two DNA sequences that were initially in close proximity are ligated (i.e. *a* with *c*, but not *a* with *b*), and (after reversing the crosslinks) the novel juxtaposition is detected by PCR. Figure is taken from Marenduzzo, D., Faro-Trindade, I., and Cook, P.R. (2007). What are the molecular ties that maintain genomic loops? Trends in Genetics 23, 126-133.

2.5.6 ChIP and reChIP

ChIP (Chromatin Immunoprecipitation) was done as described previously (Kashyap et al., 2013). Cells were firstly treated with 1% formaldehyde to form cross-linking of protein-DNA and then the chromatin DNA was sonicated. The cross-linked protein-DNA was immunoprecipitated and thus precipitating the DNA associated with protein. qRT-PCR was performed to value the enrichment of protein and the data was normalized against the input. For reChIP assay after the first immunoprecipitation, beads were eluted in 10mM DTT and diluted with reChIP dilution buffer and subjected to a second immunoprecipitation. ChIP primers are shown in Table 2.

Requirements

1 x PBS =2.33 ml 10 x PBS + 21 ml dH_2O

Fixation solution: 0.27 ml 37% Formaldehyde (room temperature) in 10 ml cell culture medium

Glycine-Stop-Fix solution: 1 ml 10 x Glycine buffer+1 ml 10 x PBS+8 ml dH_2O

Cell scraping solution = 1 x PBS + 5 µl 100 mM PMSF

SDS lysis buffer: 1% SDS, 10 mM EDTA, 50 mM Tris-HCl (pH 8.1), Protease inhibitor cocktail (PIC)

ChIP dilution buffer:

A: 0.01% SDS, 1.1% Triton X-100, 1.2 mM EDTA, 16.7 mM Tris-HCl (pH 8.1), 167mM NaCl, PIC (Fresh)

B: 20 mM Tris/HCl (pH 8.0); 1% Triton X-100; 150 mM NaCl; 2 mM EDTA, PIC.

Protein A/G agarose

Low salt wash buffer: 0.1% SDS, 1% Triton X-100, 2 mM EDTA, 20 mM Tris-HCl (pH 8.1), 150 mM NaCl.

High salt wash buffer: 0.1% SDS, 1% Triton X-100, 2 mM EDTA, 20 mM Tris-HCl (pH 8.1), 500 mM NaCl.

LiCl wash buffer: 0.25 M LiCl, 1% IGEPAL, 1% deoxycholic acid, 1 mM EDTA, 10mM Tris-HCl (pH 8.1).

TE buffer: 10 mM Tris-HCl (pH 8.0), 1 mM EDTA.

Rechip buffer: 20 mM Tris/HCl (pH 8.0); 0.1% Triton X-100; 150 mM NaCl; 2 mM EDTA,

PIC (Fresh).

Elution buffer: 100 mM $NaHCO_3$, 1% SDS.

5 M NaCl

RNase A (10 mg/ml)

Proteinase K (10 mg/ml)

2.5.6.1 In vivo cross-linking and lysis

pmHep cells were grown in 100 cm^2 plate up to the confluency of 80% in 10 mL of DMEM.

a. 270 µl of 37% formaldehyde was added to the culture plate and incubated on a shaking platform for 7-8 min at room temperature.

b. Pour fixation solution off and wash by adding 10 ml ice cold 1 x PBS, and then pour off.

c. 5 mL Glycine-stop-fix solution was added and the plate was swirled to mix and rock at room temperature for 5 min. Addition of glycine quenches unreacted formaldehyde.

d. The plate was then kept on ice and the media was aspirated carefully and the cells were washed twice with ice cold 1 x PBS.

e. After washing, 1 mL of ice cold PBS including 5 µl 100mM PMSF was added to the plate and cells were scraped, collected and centrifuged at 700 g for 10 min at 4°C. If freezing the pellet, add 1 µl 100 mM PMSF and PIC and store at -80°C.

f. The cell pellet was then resuspended in SDS lysis buffer (+PIC) and kept on ice. 3 M cells use 130 µl SDS lysis buffers, 10M cells use 720 µl SDS lysis buffers and PIC.

2.5.6.2 Sonication to shear DNA

a. To shear the DNA cells lysate was transferred in Snap-Cap microTUBE and sonication was performed 12 min under 75 Watts by Covaris, with 5% duty cycle at 7°C to gain 200-700 bp DNA fragments. (If use 1 ml miliTUBE, sonication was performed 15 min under 75 Watts by Covaris with 10% duty cycles.)

b. After sonication the sample was clarified by spinning it at 14,000 rpm at 4°C for 10 min. The supernatant containing sheared cross-linked chromatin was transferred to the new microfuge tube.

c. Use the Nandrop to measure the concentration of the DNA.

2.5.6.3 Chromatin shearing efficiency analysis

a. Take about 20 µg DNA of the sheared sample, transfer to 1.5 mL microcentrifuge tube.

b. Add 1µL of RNaseA (10 mg/ml) and incubate at 37 °C for 30 min.

c. Add 1µL of Proteinase K (10 mg/ml) and reverse crosslink by heating at 65°C overnight (O.N).

d. Purify DNA using Qiagen QIAquick PCR Purification Kit, Cat. No. 28104.

e. Resuspend pellet with 15 µL dH_2O.

f. Add 1 volume of loading dye to 3-5 volumes of purified DNA. (NOTE: The use of loading dye without Bromophenol Blue is recommended. Bromophenol Blue migrates at ~300 bp and interferes with smear analysis)

g. Load 300~600 ng of purified DNA per lane.

h. Resolve on 1% agarose TAE gel (including Ethidium Bromide) run at 75 V for 1 hour.

i. Destain and view gel with a UV light source and record image.

2.5.6.4 Immunoprecipitation of cross-linked protein/DNA

a. 80 µg for histone makers or 250 µg for transcription factors was diluted with ChIP dilution buffer (+PIC) to a final volume of 1 ml.

b. 60 µl of Protein A/G agarose beads were added to the diluted sample and incubated at 4°C for 1 hour with constant agitation. This pre-clearing step removes the protein and DNA that binds nonspecifically to the Protein A/G agarose.

c. The supernatant was collected by brief centrifugation at 3000 g for 1 min.

d. 25 µl of sample was saved as Input (Usually from the histone makers or IgG).

e. 1-5 µg of antibody was added to rest of the sample and the sample was incubated for overnight at 4°C with rotation (+Ab).

f. The protein-antibody complex was precipitated by adding 60 µl of Protein A/G agarose to the sample and incubating the sample at 4°C for 3 hours with continuous rotation.

g. The Protein A/G agarose was collected by centrifugation at 3000 g for 1 minute and the supernatant fraction was discarded.

h. The Protein A/G agarose was then washed with 500 µl cold 1 x low salt wash buffer wash buffer and wash for 10 minutes with rotation at 4°C and discard supernatant.

i. Add 500 µl cold high salt wash buffer and wash 10 minutes with rotation at 4°C, discard supernatant.

j. Add 500 µl cold LiCl salt wash buffer and wash 10 minutes with rotation at 4°C, discard supernatant.

k. Add 500 µl cold TE buffer to wash twice with rotation at 4°C, each 10 minutes and discard supernatant.

(For reChIP: After step 8 of immunoprecipitation of cross-linked protein/DNA, wash the beads once more with high salt wash buffer. Then incubate the beads with 50 µl 10 mM DTT for 30 min at 37°C with constant shaking (950 rpm). The beads were collected by brief centrifugation at 3000 g for 1 min. Supernatant was collected and repeat step b, collect all the supernatant into a new tube. Then add 900 µl reChIP buffer (+PIC) and take 25 µl as input. Add the second primary antibody and repeat step e-k of immunoprecipitation of cross-linked protein/DNA.)

2.5.6.5 Elution of protein/DNA complexes

a. 100 µl of elution buffer (pre-warmed at 37°C) was added to the washed Protein A/G agarose beads and constant shaking at 1250 rpm at room temperature for 30 minutes.

b. The beads were collected by brief centrifugation at 3000 g for 1 minute.

c. Supernatant was collected and the elution step was repeated once more with 100 µl of elution buffer.

d. For the input, 15 µl elution buffers added in.

2.5.6.6 Reverse cross-link to free DNA and DNA purification

a. Eluates as well as the input controls were subjected to reverse cross-linking by add 5 M NaCl 8 µl and 2 µl, respectively. Incubate at 65°C with constant shaking at 950 rpm O.N.

b. Cool the sample to RT, then add 1 µl RNaseA and incubated at 37°C for 30 min.

c. To digest proteins, add 1 µl of Proteinase K (10 mg/ml) and incubated at 42°C for 1h.

d. Incubated the sample at 67°C for 20 min to stop the reaction.

e. Purify DNA using Qiagen QIAquick PCR Purification Kit, Cat. No. 28104.

f. Resuspend pellet with 100 µl dH_2O.

2.5.6.7 Real-*Time polymerase chain reaction (qPCR) and data analysis*

The input was diluted 1:10 again (For reChIP, the input do not need to be diluted) and then analyzed by qRT-PCR using specific primers together with the purified DNA samples. 2 µl of purified DNA and 100 nM of primers were used in 20 µl of reaction volume. Ct values (number of cycles required for the fluorescent signal to cross the threshold) were used for performing the calculation which consists on evaluating the fold difference between experimental sample and normalized input (Lin et al., 2012). ΔCt (normalized to the input samples) value for each sample.

ΔCt [normalized ChIP] = (Ct [ChIP] - (Ct [Input] -Log2 (Input Dilution Factor).

Where Input Dilution Factor = (fraction of the input chromatin saved)$^{-1}$ × Input dilution factor before qPCR=40×10=400.

2.5.7 Co-immunoprecipitation (Co-IP)

Cells were lysed in IP lysis buffer and the extracts were incubated overnight with the indicated antibodies. IP-antibody complexes were then captured on protein A/G agarose beads (Roche), and then detected by western analysis. Specifically:

a. Aspirate media out, and wash the cells with PBS 1 time. Then wash with 5 ml ice-cold PBS/Phosphatase Inhibitors (10xPBS 0.5 ml, distilled water 4.25 ml, Phosphatase Inhibitors 0.25 ml).

b. Add lysis buffer in and put the flask on ice for 5-10 min.

Lysis buffer: 50 mM Tris-HCl PH7.5, 150 mM NaCl, 1% Triton-100, 1 mM EGTA, 2 mM EDTA and Protease inhibitor (Roche), Phosphatase inhibitor (Roche), sodium orthovanadate.

c. Collect the cells by scrape. And centrifuge it for 5 min, 14,000 g in pre-cooled at 4°C.

d. Take the supernatant into a new tube (Cytoplasm). Resuspend the pellet (nuclear fraction) in 100 µl Complete Digestion buffer by pipetting up and down more than 5 times.

100 µl Complete Digestion buffer: 100 mM PMSF 0.5 µl, digestion buffer 98.5 µl, PIC 1 µl.

e. Add 0.5 µl Enzymatic Shearing cocktail. Vortex gently for 2 seconds and incubates 30 min at room temperature.

f. Add 2 µl 0.5 M EDTA to stop the reaction. Vortex gently for 2 seconds and place on ice

for 5 min.

g. Centrifuge 10 min, 14,000g in pre-cooled at 4°C.

During this time, take 60 µl Protein-A/G-Agarose (beads) into new tube, wash it with 500 µl IP wash buffer for 3 times, each for 5 min, 4°C.

h. Transfer supernatant into new tube and add 500 µl IP Incubation buffer or the cytoplasm part, pipetting them and take 100 µl out into a new tube (IP-input). Take the rest 500 µl into washed beads tube and add 1-5 µg antibodies. Incubate overnight, 4°C.

Add 100 µl 2xloading buffers in the IP-Input, cook at 99°C, 5 min.

i. Take the supernatant out, and wash the beads with IP wash buffer for 3 times, each for 500 µl. Add 30-100 µl 2xloading buffer in, cook at 99°C, 5 min. This is IP-sample.

2.5.8 Immunofluorescence (IF) and proximity ligation assay (PLA)

Cells were grown on chamber slides and fixed with paraformaldehyde or methanol according to the datasheets of antibodies. For IF, Alexa-Flour-488 conjugated or Alexa-Flour-546 conjugated secondary antibodies (Molecular Probes) were used for visualization. Hoechst (Molecular Probes) was used for nuclear staining. The detail of the protocol is:

a. Plate the cells in chamber slide (glass) over night.

b. Wash with DPBS 1 time.

c. a. PFA fix: put 4% PFA (diluted with DPBS) 100 µl to fix, 15 min room temperature. (Or 1% PFA 40 min, 2% PFA 30 min, 3% PFA 20 min)

d. Methanol fix. Put 150 µl ice-cold methnol (100%) into each well at room temperature 2 min. Open the cover, -20°C 15-20 min.

(1) Methnol/aceton fix. Mix the ice-cold aceton (100%) and methnol (100%) 1:1, put 150 µl into each well at room temperature 2 min. Open the cover, -20°C 15-20 min.

(2) Acetonal fix. Put 150 µl ice-cold aceton (100%) into each well at room temperature 2 min. Open the cover, -20 °C 15-20 min.

e. Wash with ice-cold 1xPBS for 3 times, each time 5 min. (Stored at 4°C)

Attention: Some Ab requires damasking (denature of protein binding surface, using 10 mM Natirum Glrate +0.02% tween 20 at 99°C 20 min)

f. Add 50 µl 0.2% Saponin (fresh) in PBS for cells, room temperature 20 min. For tissue, 1% Saponin in PBS is used.

g. Blocking (3% BSA and 0.1% Triton X-100 in PBS, fresh), room temperature 30 min.

h. Add 1°Ab in 150 µl blocking buffer, 4°C overnight, or room temperature 2 hours.

i. Wash with ice-cold PBST for 3 times, each time 5 min.

j. Add 2°Ab (1:200) +Hoechst (1:5,000) (diluted with DPBS) in 100 µl blocking buffer, room temperature 30-60 min, dark (covered it with aluminum paper). Hoechst can be used in no more than 2 weeks.

k. Wash with ice-cold 1xPBS for 3 times, each for 5 min with shaking, dark (covered it with aluminum paper). Wash with dH_2O 1 time, 5 min.

i. Take the plastic out, and add a big drop of mounting medium on the slide, covers it with glass. Keep it overnight at 4°C and watch under CLSM.

For PLA assay, the cells were followed the steps described in the user manual of Olink® Bioscience Company. A confocal laser-scanning microscope (Zeiss cLSM-710NLO, Carl Zeiss MicroImaging GmbH) was used for image collection.

Table 2.2 Primers

Primers for qRT-PCR	
Hu RPII	F: GCACCACGTCCAATGACAT
	R: GTGCGGCTGCTTCCATAA
Hu SIRT6	F: AGGATGTCGGTGAATTACGC
	R: TGGAACACCACACTGGAAGA
Hu H19	F: CTGAGCTTTCCTGTCTTTCC
	R: GAATGCTTGAAGGCTGCTCC
Hu IGF2	F: GTTATATTCTGCCTCGCCGG
	R: GAGTTGAGTCAAACACGGGC
Hu-PIHit	F: CCTAGACCCCTTCCATACCC
	R: CAAGGAATCTGCCTCTCCAG

Hu ALB	F: GTGAAACACAAGCCCAAGGCAACA
	R: TCCTCGGCAAAGCAGGTCTC
Hu-CYP3A4	F: TGTGCCTGAGAACACCAGAG
	R: GTGGTGGAAATAGTCCCGTG
Mu PoIR2B	F: CGACGAGGACATGCAATATG
	R: CGGCTCTTCAACTTCTCCAC
Mu PoIR2B	F: CGACGAGGACATGCAATATG
	R: CGGCTCTTCAACTTCTCCAC
Mu SIRT6	F: TGAGAGACACCATTCTGGAC
	R: TGCACATCACCTCATCCAC
Mu Lamin	F: AGAGCTCCTCCATCACCACCGT
	R: TGCCTGGCAGGTCCCAGATT
Mu H19	F: GAATCTGCTCCAAGGTGAAGC
	R: CAAAGCTATCTCCGGGACTC
Mu Igf2	F: GGAAGCTAGGAGGCTTAAAG
	R: CTTTAGGCACTTGCTGAGGG
Mu PIHit	F: TGGCAGGCAGCTTGGTAGTC
	R: AATGGCTGGGACAGAGCAGC
Mu Foxa1	F: ACAGGGTTGGATGGTTGTGT
	R: TGTTGCTGACAGGGACAGAG
Mu Foxa2	F: CCCATTCTGGACATGGTGAAA
	R: AGCACGCAGAAACCATAAATTAAA
Mu Runx2	F: CGGCCCTCCCTGAACTCT
	R: TGCCTGCCTGGGATCTGTA
Mu 91H	F: ATTGTTGGCCCCTTTCCAGGGC
	R: GCAGGCTCGCGTTGACAAGGAAC
Mu Alb	F: GACAAGGAAAGCTGCCTGAC
	R: TTCTGCAAAGTCAGCATTGG

Primers for CRISPR-cas9	
Dele-ctcf-Ds-F	F: GCCCCTCAGCTGGTACATAA
Dele-E1-R1	R: TTAGGCACCGAGGTCTTCAC
Dele-Cs1-F	F: GGCCTTTCTGGTGAAGTGAC
Dele-E1-R1	R: TTAGGCACCGAGGTCTTCAC
Dele-CTCF-Ds-F	F: GCCCCTCAGCTGGTACATAA
Dele-CS1-R1	R: GGAAGGGGAGCTCTTCAATC
Dele-CTCF-Ds-F	F: GCCCCTCAGCTGGTACATAA
Dele-CS1-R2	R: ACACCCACCTCTGAGCTGTC

Primers for ChIP	
Hu CTCF-AD	F: CTACCCAGACCCATCCACTGTAG
	R: CCACTCGCACATCAGTGCTT
Hu IGF2 P2	F: TCTGTGCCTACGAAGTCCCCAGAG
	R: GAAGCCCTCCCTGTCCACGTCCTGA
Hu IGF2 P3	F: TGCCTGCCCGGAGACCCCAGCTCAC
	R: CGCAGAGCGCCAAGGCCATGCTGAA
Hu CCD-CTCF	F: GGAGGAGGACAGAGGCAAGAG
	R: AACAAAATTTCAGCCGGTTCA
Hu H19_ICR _CTCF6	F: CTTGCATAGCACATGGGTATTTCT
	R: GTGACCCGGGACGTTTCC
Hu H19 E1	F: CTGGGTCTCGCTCCATAAAC
	R: ACAGAGAGGCACACGTAGGG
Hu H19 E2	F: CACAGCCTGGCCTTGACC
	R: TTCACAGGAAGCATTCGAGA
Hu BC2	F: CCCCAACTTGCCTGGACTTT
	R: ACACCCAGCAAGGAGCAAAA
Hu CTCF-Ds	F: TCTTGGCCCAGAGAGAAAGTG
	R: GCTTCTGAGCAGGTGCTTTCTT

Mu Igf2 DMR1	F: GCCAGAGATGAGCAAGGTTC
	R: CCTCAGCGTTTTCCTACCTG
Mu Igf2 P1	F: TTATGGAGTCGCCTTCGAGT
	R: GAGAAGTGACGAGGCCGATA
Mu Igf2 P2	F: CTGCTTAGCAAGTAGGTCCCTGTGA
	R: TGCTCAGTTAGAGGGTTACAAGGTAGGCGCA
Mu Igf2 P3	F: TCCAGCCCTTTCCTGTCTTCATCCTCTTCCA
	R: TACCCGGTGCCCTGACCACCCCACTG
Mu Igf2 DMR2	F: GTCCCCACATTTGCAGTTCT
	R: GTCCCCACATTTGCAGTTCT
Mu CCD-CTCF	F: AGCAAGAACCCCAAGTCTGA
	R: GTTAGGCAGACTCCGCTCTG
Mu H19_ICR_CTCF1	F: ACCCACAGCATTGCCATT
	R: GACCATGCCCTATTCTTGGA
Mu H19_ICR_CTCF2	F: GCCCATGACTATGGGATCAT
	R: TGTGTAAAGACCAGGGTTGC
Mu H19_ICR_CTCF3	F: AGGTTGGAACACTTGTGTTTCTGGAG
	R: TGGGCCACGATATATAGGAGTATGCT
Mu H19_ICR_CTCF4	F: CAAATGCCTGATCCCTTTGT
	R: GATCGATCGGTTCACTCTCC
Mu E1	F: AACATCAATCCGAGCCTGAC
	R: ACCAGTCTTTCCCAGCCTTT
Mu E2	F: TGTTAACCTGGCTCTGCCCTGC
	R: CTGCAGGTACAAACACGTAGG
Mu Anchor 0	F: TGCTCAGGAAGGTCAGAGGT
	R: TGCACTGCTGTGATTTCCTC
Mu CS6	F: GATGGTGTCTGTGTGGATGC
	R: CCTGTCTGCTTCTTCCCAAG
Mu Nctc1	F: ACATTCAGGCAGTGACCAAT

	R: GCTCCGACCTGAATATCTTG
Mu CS9	F: ATAAGTCCCAGGCTCGAGGT
	R: GGCCAAGGAGGATTTAGCTC
mAlb-E	F: CTGCGTTACAGCATCCACTC
	R: CGTCCGGAATGATGGTATTT
mAlb-P	F: GCAAACATACGCAAGGGA
	R: CAGAAAGACTCGCTCTAATATAC
mAfp enh 3	F: ACATTGCTGTAGCTCTGCTTGACC
	R: ACCGAGCTGCCTGTCGAACTTAAA
mAfp enh 2	F: AGTCAACAACAGGAGTCAGAGCAG
	R: CCACAGTTTGTGTGCTGACTGCAA
mAfp-enh 1	F: CACGGAGGAGTGGAAAGAAA
	R: CCTGTGACACGAAACATTGG
mAfp Distal Promoter	F: CTACATATGAAGCCTTAGCAAACATGT
	R: ACTCAGACGTTGGCGTGTCA
mAfp-P-middle	F: AGCTGGCTCATCAGGTTT
	R: CAGTAGTTCAGGCTATTCA
mAfp-Ctcf	F: CACATCCCTGAGCAGAGACA
	R: CCTTGCTAGCTTTCCCTTCC

Primers for methylation	
mIgf2 DMR0 P1 F	GGGAGAGTTAGGGTTTTTTAGTTAGTT
mIgf2 DMR0 P1 RBio	Bio-TCTAACCCCTCTACACAATTTAACC
mIgf2 DMR0 P1 S1	TTTTTGAAGAGGGGG
mIgf2 DMR0 P1 S2	GTTATAAGGAAAGTATGGTT
mIgf2 DMR0 P1 S3	GTTGTTTTTGTAAATGTGAA
mIgf2 DMR1 P1 F	TTGTATGTTTTGGTGGTTTTTTAAT
mIgf2 DMR1 P1 RBio	Bio-AAACCCTCTACTAAAAATCTCCTTT
mIgf2 DMR1 P1 S1	TGGATATTTTAAGGTGATTT

mIgf2 DMR1 P1 S2	AGGAAAAGGAAGGTAGG
mIgf2 DMR2 P1 FBio	Bio-TGTTTTGTGGAATTTTTAGGTAGGT
mIgf2 DMR2 P1 R	CCCCAAATCAAAAAATAAATAATCTC
mIgf2 DMR2 P1 S1	CAATATATCTCCAAAAAAC
mIgf2 DMR2 P1 S2	CCTTCAACCCCACC
mIgf2 DMR2 P2 F	TTTTTTAATATGATATTTGGAGATAGTT
mIgf2 DMR2 P2 RBio	Bio-CCACATAATTTAATTCACTAATAATTACTA
mIgf2 DMR2 P2 S1	ATGATATTTGGAGATAGTT
mIgf2 DMR2 P3 FBio	Bio-TTTTTTAATATGATATTTGGAGATAGTT
mIgf2 DMR2 P3 R	CCACATAATTTAATTCACTAATAATTACTA
mIgf2 DMR2 P3 S1	TTCACTAATAATTACTAAAC
mH19_CCD_F	AAGTTTAGAATTGGAGAGGTAGTAT
mH19_CCD_RBio	Bio-TCTCCACACAACCACAATCTTAC
mH19_CCD_S1	GTTTAGAAGGTAGAGGATAA
mH19_CCD_S2	AAGTGGTTTTGAGGAT
mH19_PIHit_F	AGAGTTAGAGGTGGTTTGGATAT
mH19_PIHit_RBio	Bio-AATCACTTCAACCTCCCAAAACTTTC
mH19_PIHit_S1	AGAGGTGGTTTGGATATTA
mH19 BamHI site 0_F	GGGTGTGGTATGGTTTGTT
mH19 BamHI site 0_RBio	Bio-CATAACCCCTACCCCCAAC
mH19 BamHI site 0_S	GGTTTGTTTAGGAAGG
mH19 Enh E1 P1 F	GTTAGTTTTGAGGGTAGATTAGGA
mH19 Enh E1 P1 RBio	Bio-ACTTTATATACACCTCCCTTAATCC
mH19 Enh E1 P1 S1	TTGAGGAAAAATAGATTTAAAATAT
mH19 Enh E1 P1 S2	GTGGTATTTAGGTTGTG
mH19 Enh E1 P2 F	GGAGGTATTAGGATGTAATGATATAGTT
mH19 Enh E1 P2 RBio	Bio-TATCAACACCACCATATCTACAACT
mH19 Enh E1 P2 S1	GGGTTAGTGTGTGGA

mH19 Enh E2 P1 F	TGTGGGGATTGTTTTGTAGTTGTATAATT
mH19 Enh E2 P1 RBio	Bio-CCCCTCACCAAAATCAACA
mH19 Enh E2 P1 S1	AGTTGTTTTTTATGAATTGTAAAT
mH19 Enh E2 P1 S2	GGATTGTTTTGTAGTTGTATAATT
mIgf2_DMR1_3C_F	GGGGGATTATAGAGAATTAGAGTTG
mIgf2_DMR1_3C_RBio	Bio-ACCTCTACTACCCAAACC
mIgf2_DMR1_3C_S1	AATTTGAGAAAGTGAGTTT
mIgf2_DMR2_3C_F	GGTTATTGTTGGATGATATGGATAGT
mIgf2_DMR2_3C_RBio	Bio-ACCCTCCATCTTATCTCTTCC
mIgf2_DMR2_3C_S	GGATAGTGGTATAGGTG
mH19_ICR_Pyro1_F	AAGGAGATTATGTTTTATTTTTGGA
mH19_ICR_Pyro1RBi	Bio-CCCACAACATTACCATTTATAAATTC
mH19_ICR_P1_S1new	GAATTAGTTGTGGGGTTTATA
mH19_ICR_Pyro2FBi	Bio-AAAGAATTTTTTGTGTGTAAAGATT
mH19_ICR_Pyro2_R	ATCAAAAACTAACATAAACCCCTAAC
mH19_ICR_Pyro2_S1	AACTCAATCAATTACAATCC
mH19_ICR_Pyro3_F	GGGTTTTTTTGGTTATTGAATTTTAA
mH19_ICR_Pyro3RBi	Bio-AATACACACATCTTACCACCCCTATA
mH19_ICR_Pyro3_S1	TGTTATGTGTAATAAGGGAA
mH19_ICR_Pyro4FBi	Bio-TTTTTGGGTAGTTTTTTTAGTTTTG
mH19_ICR_Pyro4_R	ACACAAATACCTAATCCCTTTATTAAAC
mH19_ICR_P4_S1new	CCATTTAACTATAACCAAATCTACA
mH19_ICR_P4_S2new	ACCTAAAATACTCAAAACTTTATCA

3 Results

3.1 Roles of Sirt6 on Foxa1/2-dependent *H19* and *Igf2* expression in hepatocytes

3.1.1 Tissue-specific gene expression of *H19* and *Igf2* in Sirt6-deficient mice

Experiments of the group of Prof. Strand have shown that established biomarkers of HCC are upregulated in Sirt6-deficient hepatocytes (Marquardt et al., 2013). To examine whether *H19* and *Igf2* were tissue-specifically expressed, qPCR data sets were generated in different tissues of mice, such as thymus, liver, colon, heart, muscle, spleen, kidney and brain. Figure 3.1 shows that upon loss of Sirt6, an increased expression of *H19* and *Igf2* was observed with the most prominent differences in liver and colon, which are of endodermal origin.

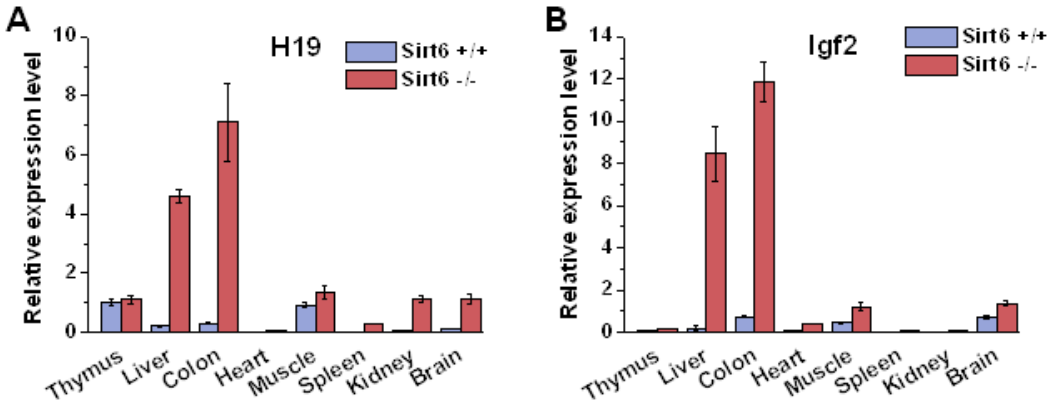

Figure 3.1 Expression of *H19* and *Igf2* in different tissues of Sirt6$^{+/+}$ and Sirt6$^{-/-}$ mice. Total RNA was extracted from different tissues of WT (blue) and Sirt6 KO (red) mice, including thymus, liver, colon, heart, muscle, spleen, kidney and brain. *H19* (A) and *Igf2* mRNA (B) were quantified by qPCR; quantification was normalized to RPII (RNA polymerase II). This experiment was repeated in two pairs of mice and a representative result was shown. Error bars indicate standard deviation (s.d).

To confirm the upregulated expression of *H19* and *Igf2* in the liver, *Sirt6*$^{Flox/Flox}$ and *Alb-Cre* mice were used. *Alb-Cre* mice are liver-specific Sirt6 deletion, which are generated by breeding of *Sirt6*$^{Flox/Flox}$ mice with the mice expressing the Cre recombinase driven by the albumin promoter. These mice were useful to overcome the early postnatal

lethality of Sirt6$^{-/-}$ mice and enable older mice to be analyzed. Figure 3.2 shows that loss of Sirt6 also induces gene expression in the liver-specific Sirt6 knockout mouse model: *H19* and *Igf2* increased about 60- and 4-fold, respectively. These results further confirmed that loss of Sirt6 is responsible for the up-regulation of *H19* and *Igf2* in hepatocytes.

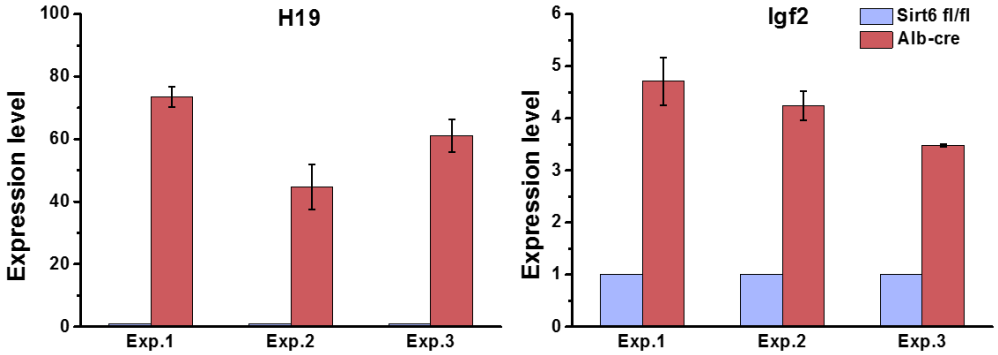

Figure 3.2 Expression of *H19* and *Igf2* in *Sirt6*$^{Flox/Flox}$ and *Alb-Cre* primary murine hepatocytes (pmHep). Total RNA was extracted from *Sirt6*$^{Flox/Flox}$ (blue) and *Alb-Cre* (red) primary murine hepatocytes. *H19* and *Igf2* mRNA were quantified by qPCR; quantification was normalized to RPII mRNA level; error bars indicate s.d. Exp indicates experiment, and 3 pairs of mice were used.

To further characterize the influence of Sirt6 on expression *H19* and *IGF2* gene, a cell culture model was selected. Hep3B cells transfected with a human SIRT6 expression vector were analyzed in comparison to Hep3B cells transfected with pcDNA control vector. Hep3B cells are characterized by low Sirt6 and high *H19* and *IGF2* expression in comparison to primary human hepatocytes (phHep). As shown in Figure 3.3, overexpression of SIRT6 decreased expression of *H19* and *IGF2* in Hep3B, 45% and 36%, respectively. Overall, these data indicate that SIRT6 can reduce expression of *H19* and *IGF2* mRNA.

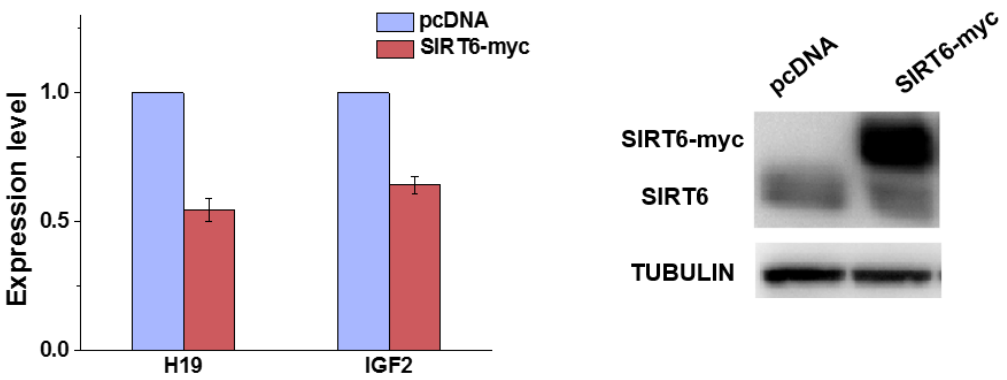

Figure 3.3 Overexpression of SIRT6 suppresses the expression of *H19* and *IGF2*. Expression of *H19* and *IGF2* mRNA when overexpression of SIRT6 in Hep3B (left). Hep3B cells were transfected with pcDNA (blue) or SIRT6-myc (red) plasmids. Forty eight hours following transfection, cells were collected to isolate RNA. Primers of indicated genes were used to quantify the mRNA level by qPCR; quantification was normalized to RPII, n=2, error bars indicate s.d. The right picture indicates the protein level of SIRT6 in this experiment. The transfected cells were isolated and the WB was performed with SIRT6 specific antibody. β-tubulin was used as a loading control.

3.1.2 Analysis of Sirt6-dependent histone modifications

3.1.2.1 Sirt6 alters enrichment of H3K9ac at the *Igf2/H19* gene locus

SIRT6 is shown to tightly bind to chromatin and is best characterized as a NAD^+ -dependent deacetylase of histone H3K9ac (Kugel and Mostoslavsky, 2014). To gain insight into how SIRT6 regulates the expression of *H19* and *Igf2*, the recruitments of Sirt6 was firstly analyzed by ChIP in pmHep, Hep3B pcDNA and SIRT6-myc cells. As shown in Figure 3.4B, Sirt6 was enriched at all the regions of the *Igf2/H19* gene locus in normal primary murine hepatocytes, and the binding reduced along with the deletion of Sirt6. By contrast, the occupancy of SIRT6 increased at all the analyzed locus when SIRT6 was overexprssed in Hep3B cells (Figure 3.4C).

As the classic substrate of Sirt6, the occupancy of acetylation of histone H3 lysine 9 was also analyzed at the *Igf2/H19* gene locus by ChIP with H3K9ac specific antibody. Consistent with the data of ChIP-Sirt6, Figure 3.5B shows that the occupancy of H3K9ac increased in Sirt6-deficient pmHep at the *Igf2/H19* gene locus with a prominent enrichment at enhancers region, from E1 to CS9 (Figure 3.5B).

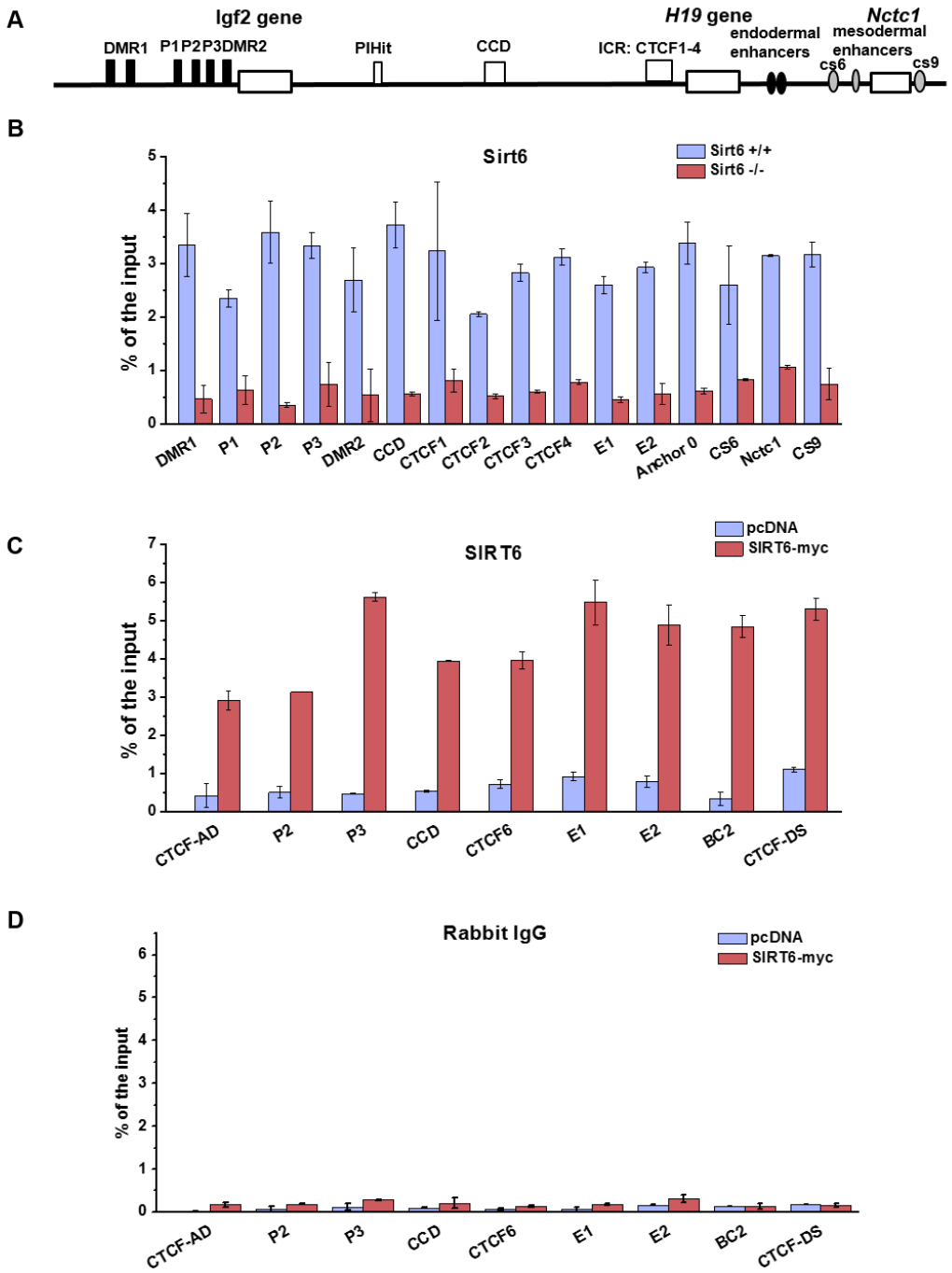

Figure 3.4 ChIP analysis of Sirt6 enrichment at the *Igf2/H19* gene locus in hepatocytes. (A) Schematic representation of the mouse *Igf2/H19* gene locus. *Igf2* and *H19* genes (white boxes) are displayed together with the downstream endodermal enhancers (black ovals), the centrally conserved domain (CCD) and the ICR (white box), as well as promoters of *Igf2* (black boxes): DMR1, P1, P2, P3 and DMR2. Occupancy of Sirt6 at the *Igf2/H19* gene locus was performed in pmHep (B), Hep3B pcDNA and Hep3B SIRT6-myc cells (C). The cells were cross-linked, sonicated and IP was performed using Sirt6 specific antibody. DNA was extracted from IP sample and PCR was performed using primers spanning the indicated regions. ChIP profiles of qPCR data were normalized to the input. These experiments were repeated 3 times and a representative result was shown. Error bars indicate s.d.

Moreover, the enrichment of H3K9ac showed the similar trend at all sites except CTCF-binding site upstream of IGF2 (CTCF-AD) in Hep3B cell in comparison with phHep (Figure 3.5C). H3K9ac also exhibited strongly enrichment both at the promoters of *IGF2* and enhancers region in Hep3B cells. Importantly, the occupancy of H3K9ac decreased at all sites in SIRT6 overexpressing Hep3B cells.

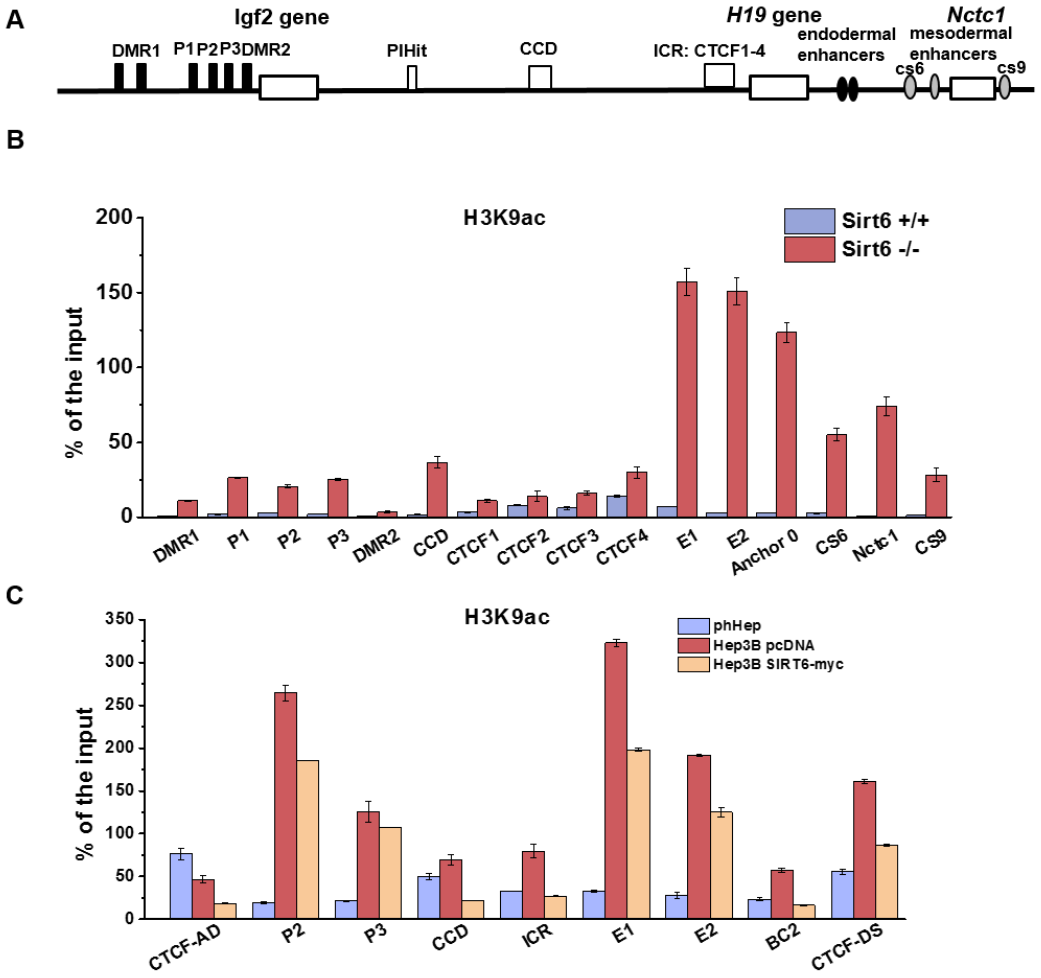

Figure 3.5 ChIP analysis of Sirt6-dependent enrichment of the histone mark H3K9ac at the *Igf2/H19* gene locus in hepatocytes. (A) Schematic representation of the mouse *Igf2/H19* gene locus (see also Figure 3.4 and Figure 1.2). (B) Enhanced H3K9ac binding at the enhancers region of the *Igf2/H19* gene locus when Sirt6 was deleted in pmHep. (C) Occupancy of H3K9ac in primary human hepatocytes (phHep), Hep3B pcDNA and Hep3B SIRT6-myc cells. The cells were cross-linked, sonicated and IP was performed using H3K9ac specific antibody. DNA was extracted from IP sample and PCR was performed using primers spanning the indicated regions. ChIP profiles of qPCR data were normalized to the input. These experiments were repeated three times and a representative result was shown. Error bars indicate s.d.

3.1.2.2 Characterization of the histone modifications of H3K27ac and H3K27me3 at the Igf2/H19 gene locus

Enhancers are classified into poised and active states according to their status of the H3K27 residues. Together with H3K4me1, H3K27me3 marks poised enhancers and a combination of H3K4me1 and elevated H3K27ac means an active enhancer state (Creyghton et al., 2010; Zentner et al., 2011). To understand the enhancer environment, ChIP assays of H3K27ac and H3K27me3 were firstly performed in hepatocytes, since poised enhancers can be activated through replacing H3K27me3 by H3K27ac.

As shown in Figure 3.6B, there was no strong signal in normal pmHep for most tested regions. However, H3K27ac was specifically enriched and sharply increased at endodermal enhancers (5-fold at E1 and 2.5-fold at E2) when Sirt6 was deleted. Unlike H3K27ac, H3K27me3 was enriched at all sites of this locus, but mainly at the promoters of *Igf2* in normal pmHep, including DMR1, P1, P2, P3 and DMR2, and the reduction of H3K27me3 occupancy at these sites were about 50% when Sirt6 was lost (Figure 3.6C), which is consistent with the data of ChIP-seq of H3K27me3 (data not shown). Interestingly, enrichments of H3K27me3 at the ICR and the enhancers region (E1-CS9) decreased more than 80%, especially at the E1 and E2 (91.1% and 92.2%, respectively).

Acetylation and methylation cannot co-occur on the same lysine 27 of histone H3 (Shlyueva et al., 2014), therefore, the analysis of the ratio of H3K27ac to H3K27me3 (H3K27ac/H3K27me3) was calculated, which is suggested as a new prognostic marker for HCC (Hayashi et al., 2014). Intriguingly, Sirt6 knockout caused the ratio specifically increased at the entire enhancers region, especially at endodermal enhancers (Figure 3.6D), which implies the importance of the enhancers region, especially E1. Altogether, Sirt6 not only controls the acetylation of histone H3 lysine 9, but also influences the trimethylation and acetylation of histone H3 lysine 27, especially at the enhancers region of the *Igf2/H19* gene locus. The ChIP data of H3K27me3 in Sirt6 normal expressing primary hepatocytes also indicates the enhancers region of the *Igf2/H19* gene locus is poised enhancers.

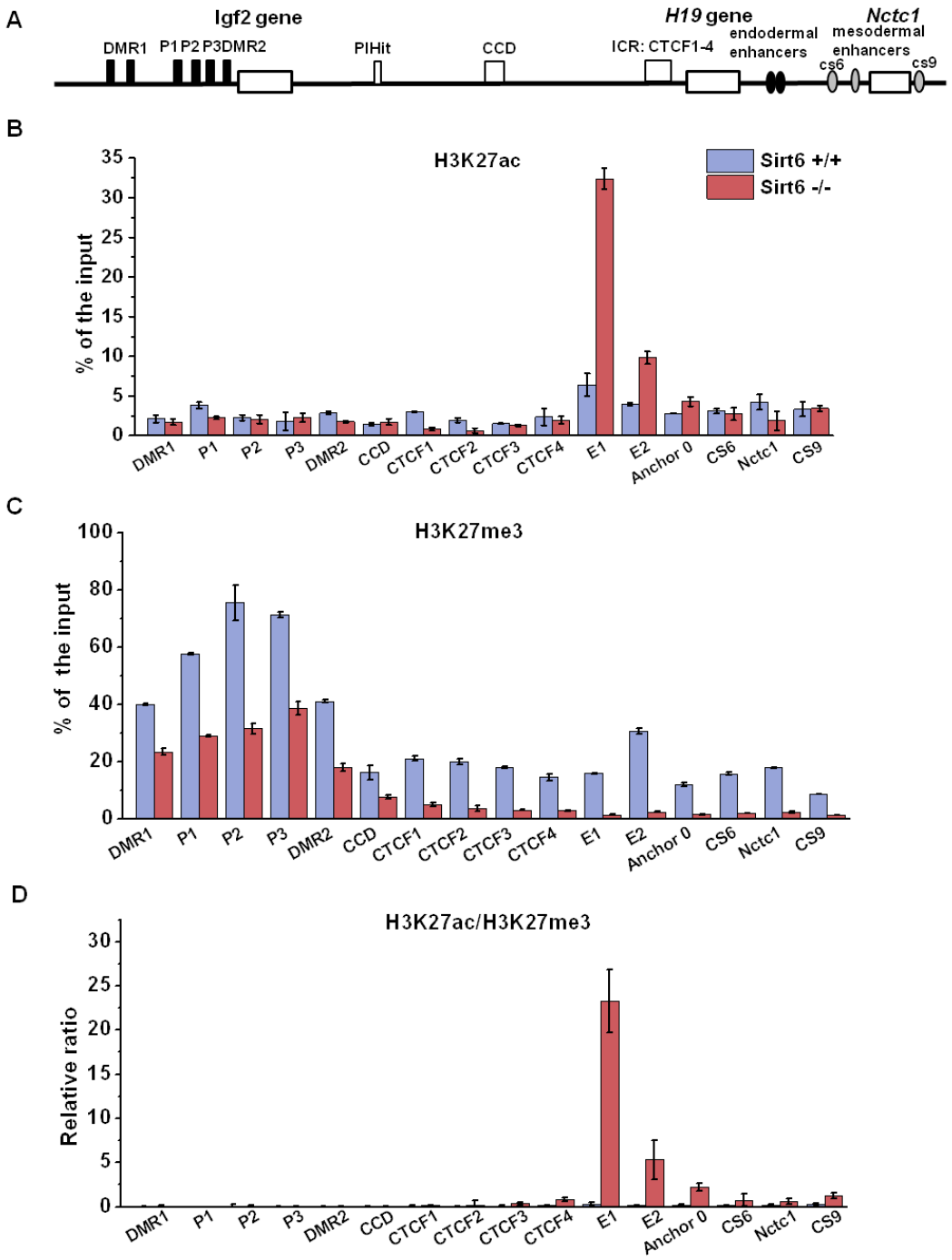

Figure 3.6 ChIP analyses of histone modifications of H3K27ac and H3K27me3 at the *Igf2/H19* gene locus in pmHep. (A) Schematic representation of the mouse *Igf2/H19* gene locus (see also Figure 3.4 and Figure 1.2). Sirt6$^{+/+}$ (blue) and Sirt6$^{-/-}$ (red) pmHep were used for ChIP. The cells were cross-linked, sonicated and IP was performed using H3K27ac (B) and H3K27me3 (C) specific antibodies. DNA was extracted from IP sample and PCR was performed using primers spanning the indicated regions of the *Igf2/H19* gene locus. ChIP profiles of qPCR data were normalized to the input. (D) Relative enrichment ratio of H3K27 modifications specially increased at enhancers region of the *Igf2/H19* gene locus. The H3K27 ratio is the enrichment of H3K27ac normalized with that of H3K27me3. These experiments were repeated three times and a representative result was shown. Error bars indicate s.d.

To gain more into Sirt6-dependent histone modification changes, ChIP profiles of H3K27ac and H3K27me3 were performed in phHep and Hep3B cells. Consistent with the above observations, the occupancy of H3K27ac increased about 10-fold at the enhancers region in Hep3B in comparison with that in phHep, together with about 5-fold at promoters of *IGF2* (P2-P3), which was different with that in pmHep (Figure 3.7B).

Correspondingly, enrichment of H3K27me3 exhibited the opposite trend with that of H3K27ac in Hep3B (Figure 3.7C), which reduced at most sites of the *IGF2/H19* gene locus except two CTCF binding sites (CTCF-AD and CTCF-Ds) with respect to that in phHep. Most importantly, the reduced occupancies of H3K27me3 at enhancers were more than 80% in Hep3B in comparison with in phHep. Moreover, the H3K27ac/H3K27me3 ratio in Hep3B displayed comparable results as in Sirt6 KO pmHep (Figure 3.7D), which underlines the importance of the enhancers region in liver cancers.

Thus, the enrichments of the repressive mark (H3K27me3) is down-regulated along with that of the active mark (H3K27ac) is up-regulated at enhancers region of the *Igf2/H19* gene locus when Sirt6 is deleted. Taken together, the alterations of trimethylation and acetylation at H3 lysine 27 at the *Igf2/H19* gene locus in hepatocytes are Sirt6-dependent.

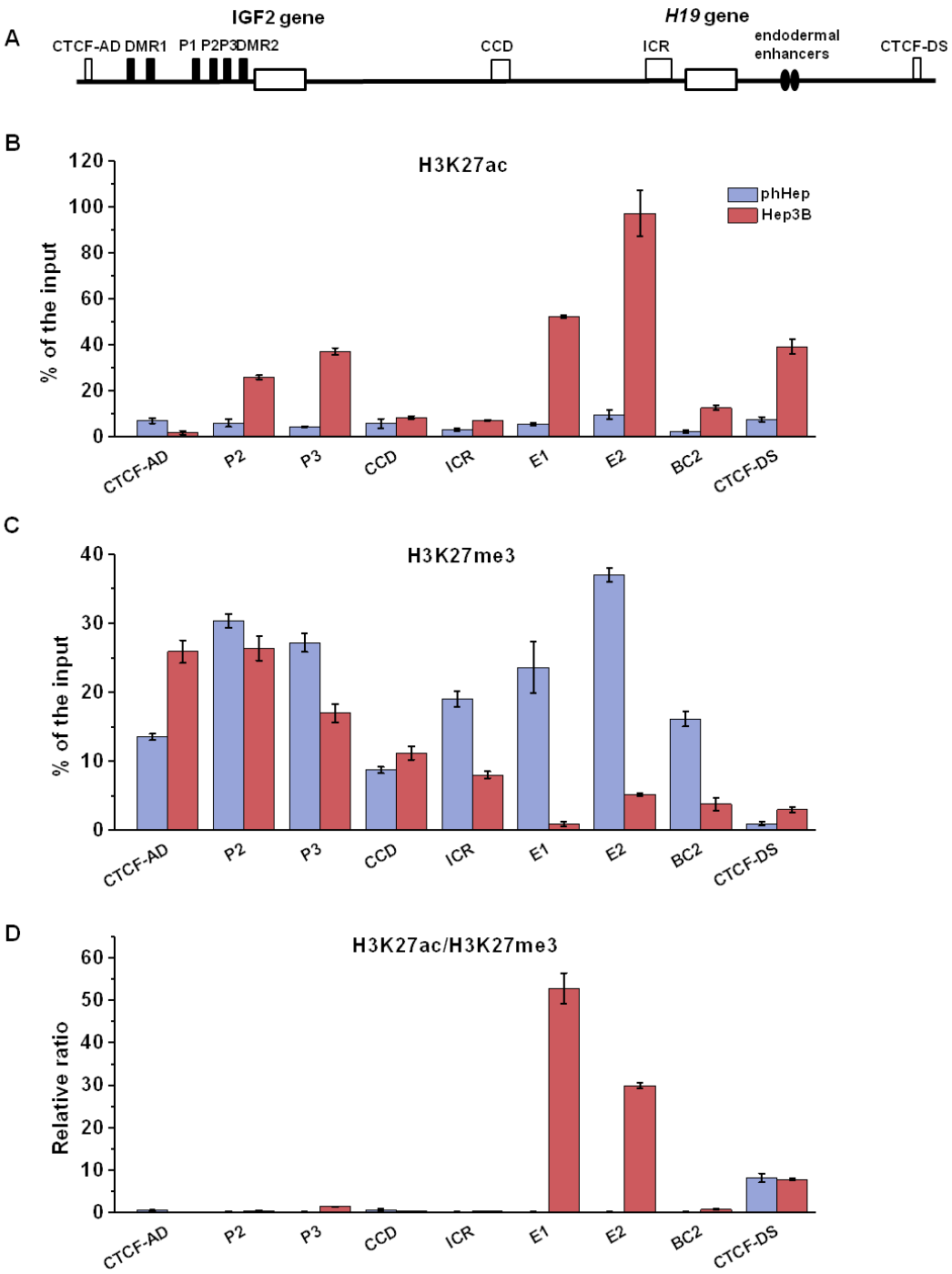

Figure 3.7 ChIP analyses of histone modifications of H3K27ac and H3K27me3 at the *IGF2/H19* gene locus in phHep and Hep3B cells. (A) Schematic representation of the human *IGF2/H19* gene locus (see also Figure 1.2). (B-C) phHep (blue) and Hep3B (red) were used for ChIP. The cells were cross-linked, sonicated and IP were performed with H3K27ac (B) and H3K27me3 (C) specific antibodies. DNA was extracted from IP sample and PCR was performed using primers spanning the indicated regions of the *IGF2/H19* gene locus. ChIP profiles of qPCR data were normalized to the input. (D) Relative enrichment ratio of H3K27 modifications specially increased at enhancers region of the *IGF2/H19* gene locus. The H3K27 ratio is the enrichment of H3K27ac normalized with that of H3K27me3. These experiments were repeated two times and a representative result was shown. Error bars indicate s.d.

3.1.2.3 Altered enrichments of H3K4me1 and H3K4me3 at the Igf2/H19 gene locus in Sirt6 knockout mice

Analysis of human primary and tumor cell lines has shown that enhancers region identified by virtue of H3K4me1 enrichment, as well as DNaseI hypersensitivity, display a cell type-specific distribution across the genome (Creyghton et al., 2010). ChIP profile of H3K4me1 at the *Igf2/H19* gene locus was characterized in mouse hepatocytes. As shown in Figure 3.8B, H3K4me1 was specifically enriched and sharply increased at the endodermal enhancers (E1-Anchor 0) and promoters of *Igf2* (P1-P3). However, loss of Sirt6 enhanced the occupancy of H3K4me1 at all the sites, especially at endodermal enhancers (E1-Anchor 0) (more than doubled). These data also emphasize the importance of the enhancers region when Sirt6 is lost.

The relative enrichment of H3K4me1 to H3K4me3 is currently considered the major epigenomic feature that can differentiate enhancers from promoters; therefore, ChIP of H3K4me3 was also performed in pmHep (Figure 3.8C). Unlike H3K4me1, the occupancy of H3K4me3 mainly focused at the promoters region of *Igf2* including P1-P3, and ICR region of *H19*, and exhibited an about 20% increase at these sites in the absence of Sirt6. Thus, the enhanced enrichment of H3K4me1 is mainly at the enhancers region of the *Igf2/H19* gene locus in Sirt6-defiicent mice, while that of H3K4me3 was prominent at the promoters and ICR. Furthermore, the relative ratio of enrichment of H3K4me1 with H3K4me3 was higher at endodermal enhancers (E1-Anchor 0) in normal primary murine hepatocytes. However, Sirt6 knockout enhanced the ratio not only at the endodermal enhancers, but also at the mesodermal enhancers like Cs6-Cs9 (Figure 3.8D). This data suggests that Sirt6 deletion facilities the enhancer property.

Moreover, these data together with the ChIP profiles of H3K27me3, H3K27ac in Sirt6 normal expressing primary hepatocytes confirms that the enhancers region of the *Igf2/H19* gene locus is poised enhancers. When Sirt6 is deleted, the poised enhancers switch into active enhancers with the activation of H3K27ac and H3K4me1, together with the removal of the bivalent repressive marker of H3K27me3.

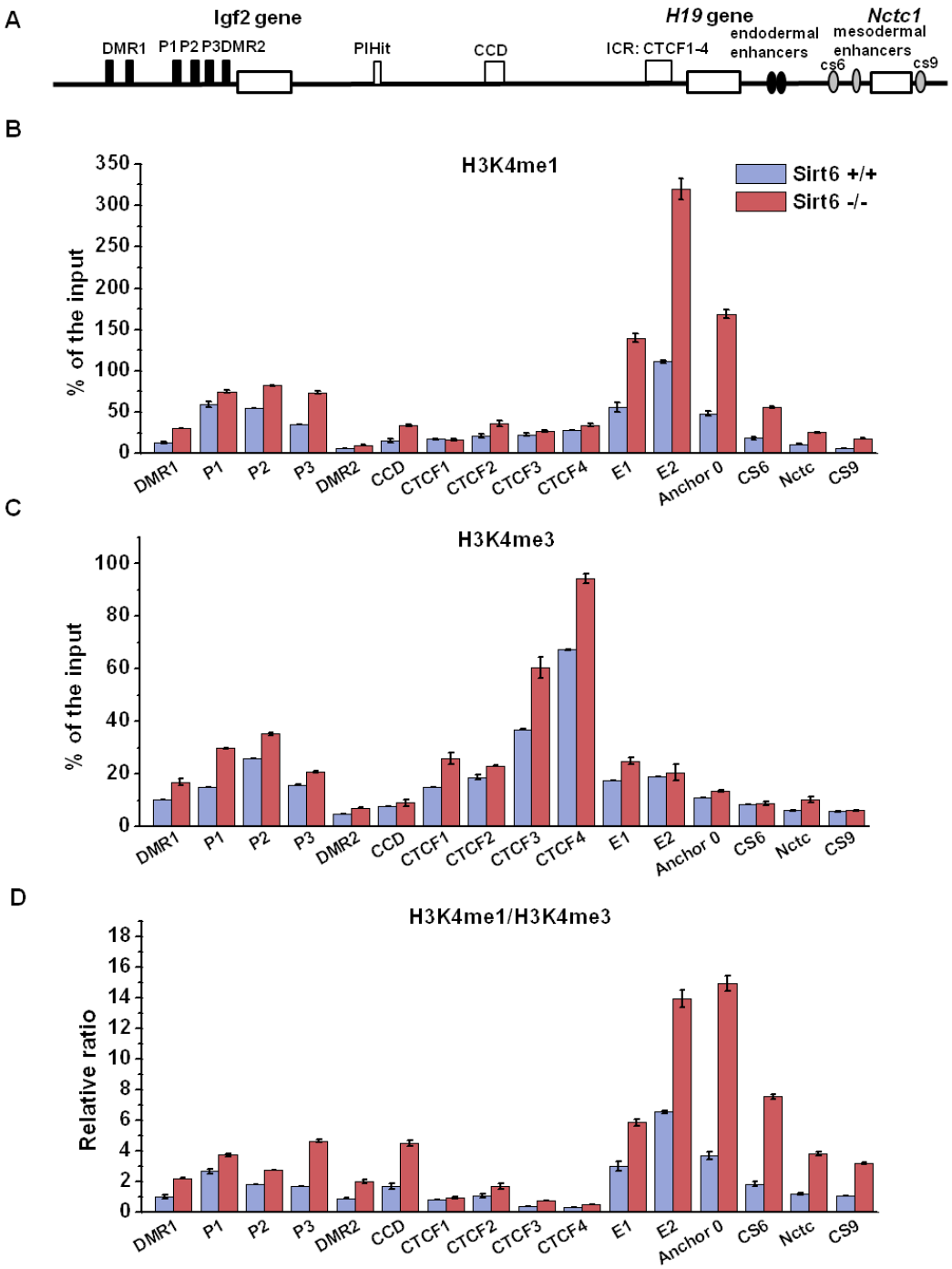

Figure 3.8 Sirt6-dependent enrichments of H3K4me1 and H3K4me3 at the *Igf2/H19* gene locus in pmHep. (A) Schematic representation of the mouse *Igf2/H19* gene locus (see also Figure 3.4 and Figure 1.2). Sirt6$^{+/+}$ (blue) and Sirt6$^{-/-}$ (red) pmHep were used for ChIP. The cells were cross-linked, sonicated and IP was performed with H3K4me1 (B) and H3K4me3 (C) specific antibodies. DNA was extracted from IP sample and PCR was performed using primers spanning the indicated regions of the *Igf2/H19* gene locus. ChIP profiles of qPCR data were normalized to the input. (D) Relative enrichment ratio of H3K4 modifications specially increased at enhancers region of the *Igf2/H19* gene locus. The H3K4 ratio is the enrichment of H3K4me1 normalized with that of H3K4me3. These experiments were repeated three times and a representative result was shown. Error bars indicate s.d.

3.1.2.4 Occupancies of H4K8ac and H3K9me3 at the Igf2/H19 gene locus in hepatocytes in Sirt6-deficient and wild-type mice

In contrast to the acetylation of K9 and K14 in histone H3 which is critical for the recruitment of TFIID, acetylation of histone H4K8 mediates recruitment of the SWI/SNF complex, a chromatin remodeling complexes. These modifications of the enhancer are required for the recruitment transcription complexes (Agalioti et al., 2002). Then ChIP profile of H4K8ac at the *Igf2/H19* gene locus was characterized in both Sirt6$^{+/+}$ and Sirt6$^{-/-}$ mice. Like other acetylated histone (e.g. H3K9ac and H3K27ac), H4K8ac is prominently enriched at the endodermal enhancers but, at E2 not E1 in normal pmHep. Loss of Sirt6 only specifically significantly increased the occupancy of H4K8ac at endodermal enhancers, including E1, E2 and Anchor 0 (Figure 3.9B). These results indicate that loss of Sirt6 maybe establishes an environment for transcription factors to initiate the transcription.

H3K27ac, H3K9ac, H4K8ac and H3K4me1/3 are active chromatin marks. To get better mechanistical insights, whether the Sirt6-dependent regulation was related with the heterochromatin was studied. ChIP profile of H3K9me3, the heterochromatin marker (Peters et al., 2002), was characterized at the *Igf2/H19* gene locus in Sirt6$^{+/+}$ and Sirt6$^{-/-}$ primary murine hepatocytes. However, the enrichment of H3K9me3 was not observed at the *Igf2/H19* gene locus in both Sirt6$^{+/+}$ and Sirt6$^{-/-}$ mice (Figure 3.9C). These data together with that of the bivalent marks, histone H3 lysine 4 trimethylation, implicate that Sirt6 is not associated with regulation of heterochromatin at the *Igf2/H19* locus in pmHep.

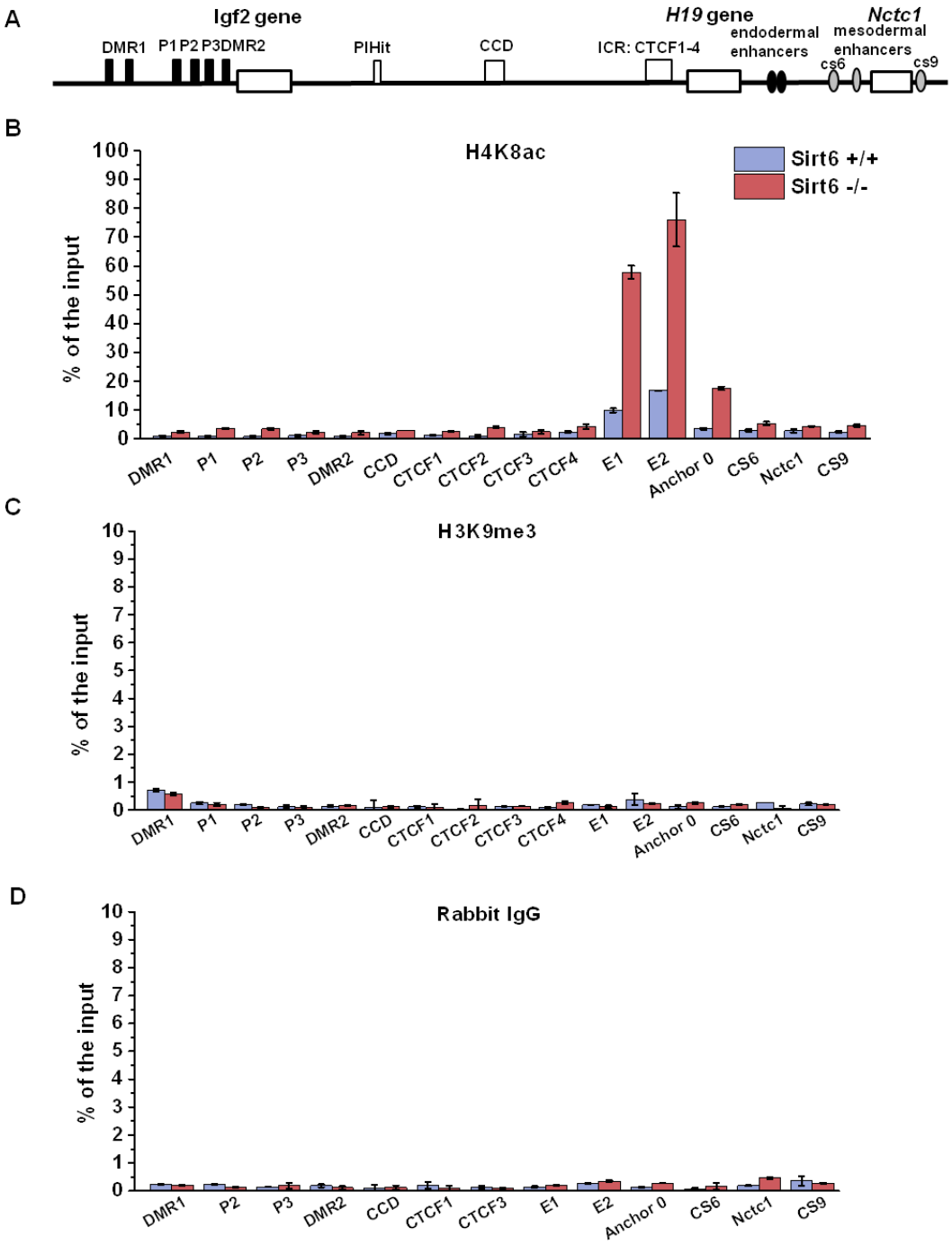

Figure 3.9 ChIP analyses of histone modifications of H4K8ac and H3K9me3 at the *Igf2/H19* gene locus when Sirt6 was lost. (A) Schematic representation of the mouse *Igf2/H19* gene locus (see also Figure 3.4 and Figure 1.2). Primary murine hepatocytes of Sirt6$^{+/+}$ (blue) and Sirt6$^{-/-}$ (red) mice were used for ChIP. The cells were cross-linked, sonicated and IP was performed using H4K8ac (B) and H3K9me3 (C) specific antibodies. Rabbit IgG was used as a negative control. DNA was extracted from IP sample and PCR was performed using primers spanning the indicated regions of the *Igf2/H19* gene locus. ChIP profiles of qPCR data were normalized to the input. These experiments were repeated three times and a representative result was shown. Error bars indicate s.d.

3.1.2.5 Analysis of protein level of histone markers in Sirt6 knockout mice

The above data indicates that the altered occupancies of some histone modifications are Sirt6 dependent. Then western blots and IFs of histone markers were performed to analyze whether Sirt6 deletion induces the histone modification alterations at the protein level. As shown in Figure 3.10, the normal primary murine hepatocytes had stronger signals of repressive markers H3K27me3 than the active markers of H3K9ac and H3K27ac; the signals of H3K9ac were strongly enhanced in Sirt6-deficient mouse, together with that of H3K27ac slightly increased, whereas the expression of H3K27me3 dramatically reduced. Consistent with the data of western blots, analysis of IF demonstrated the same results (Figure 3.11). These data also suggest acetylation and methylation could not co-occur on the same lysine 27 of histone H3, which is consistent with previous report (Shlyueva et al., 2014). Furthermore, these histone markers including H3K9ac, H3K27ac, H3K27me3 and H3, located in the nucleus, not the cytoplasm (Figure 3.11). Altogether, these data indicate that SIRT6 not only alters the histone modifications on chromatin, but also influences the proteins level of the histone marks, like H3K9ac, H3K27ac and H3K27me3.

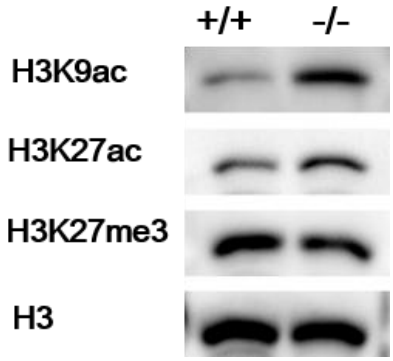

Figure 3.10 Western blots of H3K9ac, H3K27ac and H3K27me3 in Sirt6$^{+/+}$ and Sirt6$^{-/-}$ pmHep. H3K9ac, H3K27ac and H3K27me3 protein expression level were analyzed by western blots using samples from pmHep of Sirt6$^{+/+}$ and Sirt6$^{-/-}$ mice. Histone H3 was used as a control. Nitro-Block-II™ CDP-Star® detection system was used to visualize the bands. +/+ and -/- indicate Sirt6$^{+/+}$ and Sirt6$^{-/-}$, respectively. This experiment was repeated two times and a representative result was shown.

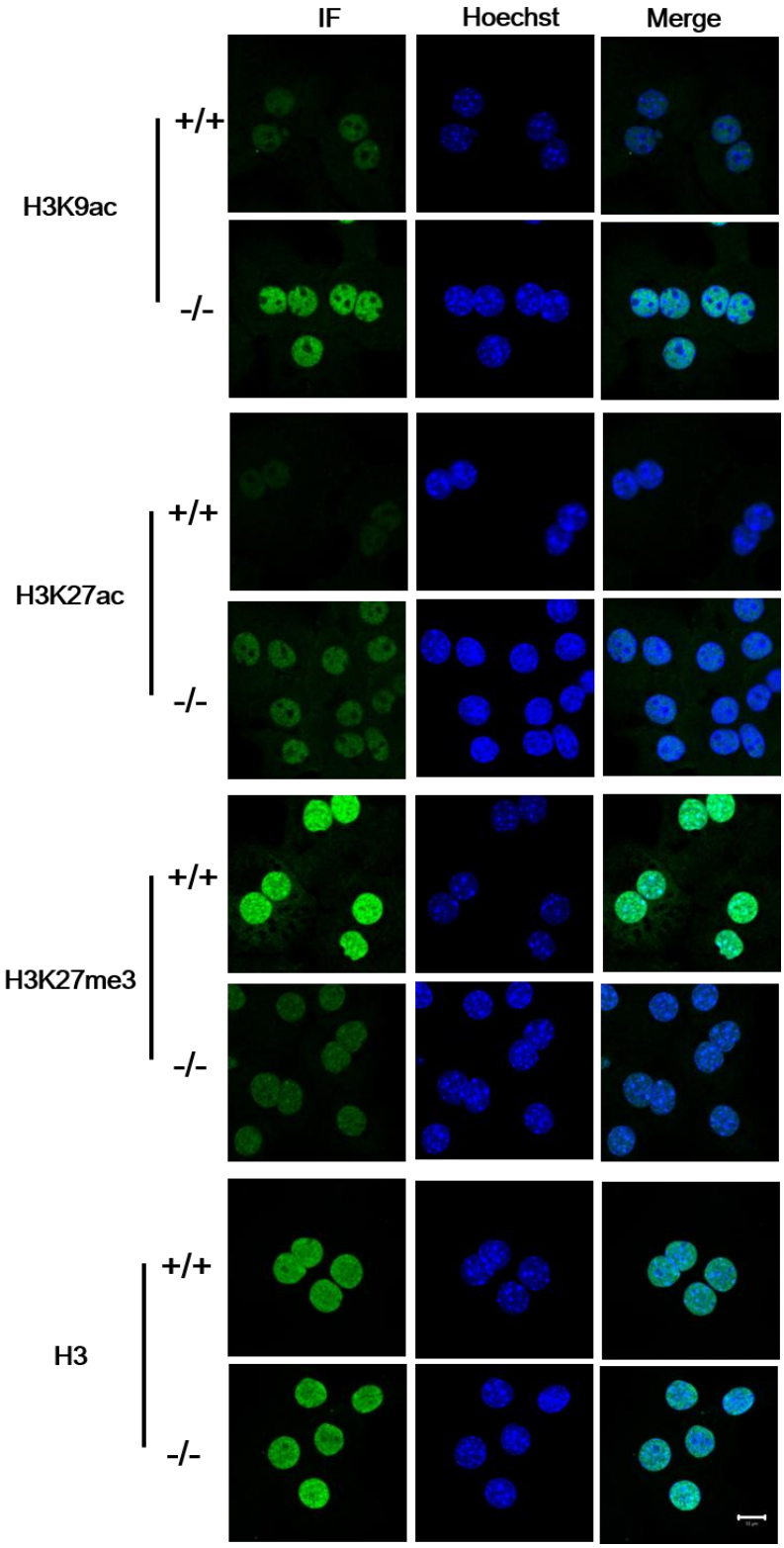

Figure 3.11 IFs of H3K9ac, H3K27ac and H3K27me3 in Sirt6$^{+/+}$ and Sirt6$^{-/-}$ pmHep. H3K9ac, H3K27ac, H3K27me3 and H3 specific antibodies were used to detect their protein levels in Sirt6$^{+/+}$ and Sirt6$^{-/-}$ primary murine hepatocytes by IF. Alexa-488 labeled secondary antibody was used. Hoechst was used to visualize the nuclear staining. +/+ and -/- indicate Sirt6$^{+/+}$ and Sirt6$^{-/-}$, respectively. This experiment was repeated three times and a representative result was shown. White scale bar is 10 µm.

3.1.2.6 Characterization of Sirt6-dependent occupancy of the histone variant H2AZ at the Igf2/H19 gene locus in murine hepatocytes

Numerous studies document enrichment of H2AZ at both poised and active enhancer region of multiple cell types, because nucleosomes containing H2AZ are biochemically less stable and therefore easier to displace from DNA than canonical nucleosomes (Jin and Felsenfeld, 2007). Thus, the occupancy of H2AZ at the locus of *Igf2/H19* in $Sirt6^{+/+}$ and $Sirt6^{-/-}$ primary murine hepatocytes was investigated. Consistent with earlier studies (Hu et al., 2013; Li et al., 2012a), H2AZ mainly enriched at the promoters and enhancers region in normal pmHep, such as E1, ICR and P2, etc. Similar with H3K4me1 and H3K9ac, the occupancy of H2AZ slightly doubled at promoters of *Igf2* and far more increased at the endodermal enhancers region (E1, E2 and anchor 0) (Figure 3.12B). The ChIP data demonstrated that loss of Sirt6 significantly enhanced H2AZ enrichments at endodermal enhancers.

Recently, some studies showed that histone acetylation as well as DNA methylation contribute to the somatic maintenance of *H19* and *Igf2* imprinting and expression (Pedone et al., 1999; Singh et al., 2010), and a gain of acetylated H2AZ (acH2AZ) is in concert with oncogene activation (Valdes-Mora et al., 2012). To test this hypothesis, ChIP of acetylated lysine was firstly performed (Figure 3.12C). Interestingly, the acetylated lysine only enriched at the endodermal enhancers (E1 and E2), not at the promoters in WT pmHep. Sirt6 deletion stimulated more than 10-fold enrichment of H2AZ at endodermal enhancers' sites, together with slightly increase at some of the *Igf2* promoters like DMR1, P1, and P2, as well as the ICR region of *H19*. Consequently, Sirt6 knockout also induces more acetylation modification at endodermal enhancers.

To examine the acH2AZ enrichment, then ChIP-reChIP analysis of acetylated H2AZ was performed in $Sirt6^{+/+}$ and $Sirt6^{-/-}$ pmHep. Strikingly, Sirt6 knockout promoted the increase of acetylation of H2AZ only at E1, and the increase is up to 34.5% in comparison with wild-type cells (Figure 3.12D). Thus, Sirt6 deletion not only enhanced the enrichment of H2AZ at endodermal enhancers, but more importantly, accumulation of acetylated H2AZ was observed at E1, which implies the critical role of this site.

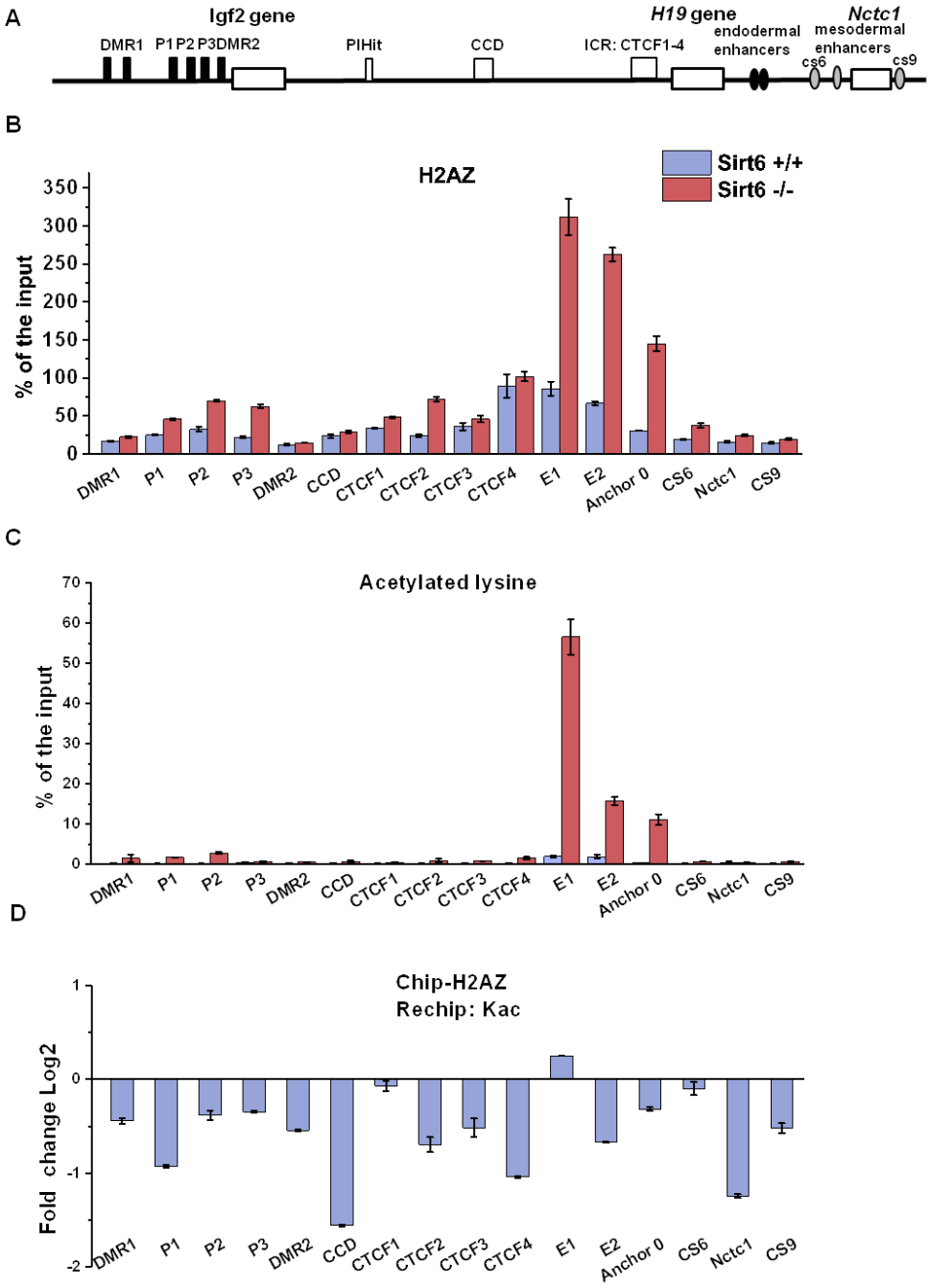

Figure 3.12 ChIP-reChIP analyses of H2AZ and acH2AZ occupancies at the *Igf2/H19* gene locus in pmHep. (A) Schematic representation of the mouse *Igf2/H19* gene locus (see also Figure 3.4 and Figure 1.2). Sirt6$^{+/+}$ (blue) and Sirt6$^{-/-}$ (red) pmHep were used for ChIP. The cells were cross-linked, sonicated and IP was performed using H2AZ (B) and acetylated lysine (Kac) (C) specific antibodies. DNA was extracted from IP sample and PCR was performed using primers spanning the indicated regions of the *Igf2/H19* gene locus. For acH2AZ reChIP (D), the 1st IP was performed with H2AZ specific antibody followed by the 2nd IP using antibody detecting acetylated lysine. ChIP and reChIP profiles of qPCR data were normalized to the input. Then the occupancy of acH2AZ in Sirt6$^{-/-}$ was normalizing with that in Sirt6$^{+/+}$. The experiments were repeated 3 times and a representative result was shown. Error bars indicate s.d.

In addition, lysine crotonylation (Kcr) is a newly discovered histone post-translational modification that is enriched at active gene promoters and potential enhancers in mammalian cell genomes (Tan et al., 2011). To explore whether this modification is involved into Sirt6-dependent regulation, ChIP analysis of crotonylated lysine occupancy at the *Igf2/H19* gene locus were performed in pmHep (Figure 3.13B). There were almost no strong signals at all the loci in Sirt6$^{+/+}$ pmHep. However, loss of Sirt6 induced strong signals at the endodermal enhancers, especially E1 (about 10.5-fold).

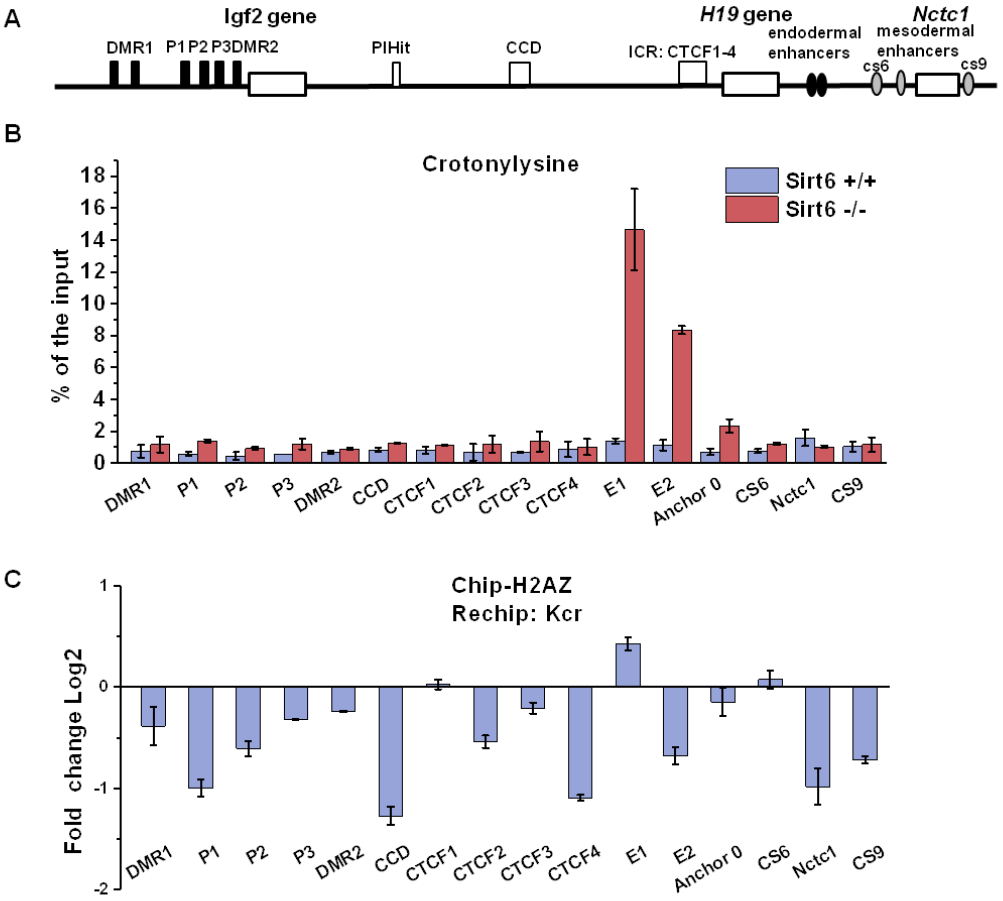

Figure 3.13 ChIP-reChIP analyses of crotonylated H2AZ occupancy at the *Igf2/H19* gene locus in pmHep. (A) Schematic representation of the mouse *Igf2/H19* gene locus (see also Figure 3.4 and Figure 1.2). Sirt6$^{+/+}$ (blue) and Sirt6$^{-/-}$ (red) pmHep were used for ChIP. The cells were cross-linked, sonicated and IP was performed with crotony lysine (B) specific antibody. DNA was extracted from IP sample and PCR was performed using primers spanning the indicated regions of the *Igf2/H19* gene locus. For Kcr-H2AZ reChIP (C), the 1st IP was performed with H2AZ specific antibody followed by the 2nd IP using antibody detecting crotonylated lysine. ChIP and reChIP profiles of qPCR data were normalized to the input. Then the occupancy of Kcr-H2AZ in Sirt6$^{-/-}$ was normalizing with that in Sirt6$^{+/+}$. These experiments were repeated three times and a representative result was shown. Error bars indicate s.d.

Furthermore, the reChIP was also performed to characterize the crotonylated H2AZ at the *Igf2/H19* gene locus. As shown in Figure 3.13C, the crotonylation of H2AZ also showed the comparable results as acetylated H2AZ. Most importantly, the alteration was observed at the unique site-E1. The aforementioned points clearly indicate that knocking out Sirt6 increases the modifications of acetylation and crotonylation, together with those modifications of H2AZ.

In summary, in combination with the data of active histone marks including H2AZ, H3K4me1, H3K4me3, H3K27ac and H4K8ac, together with that of the repressive mark H3K27me3, these imply the importance of the enhancers region of the *Igf2/H19* gene locus, and the histone modification alterations are Sirt6-dependent in hepatocytes.

3.1.3 Analysis of the methylation level at the *Igf2/H19* gene locus

Previously, the lab of Prof. Dr. Strand have showed that Sirt6 deficiency caused a global DNA hypomethylation of liver tissue (Marquardt et al., 2013). Because it is known that loss of methylation uncovers intronic enhancers to drive *IGF2* and *H19* expression (Blattler et al., 2014), a locus-specific analysis was performed in cooperation with lab of Prof. Ulrich Zechner. Analysis of DNA methylation levels of individual CpGs at the locus of *Igf2/H19* was investigated by pyrosequencing of bisulphite modified DNA from pmHep of $Sirt6^{+/+}$ and $Sirt6^{-/-}$ mice.

As shown in Figure 3.14, the hypermethylated sites (more than 80%) were *PIHit*, CCD and CS9, and mesodermal enhancers like CS6, *Nctc1* in WT pmHep. The middle methylated sites were 40%-60%, including DMR2, ICR region (i.e. CTCF 1-4) and E1, as well as the hypomethylated sites (less than 10%) are DMR1, E2 and P1-P3 (data not shown). After Sirt6 deletion, DNA methylation was reduced at the ICR, E2 and CS6, especially E1 from 40.1% to 15.3%. Moreover, among four CTCF-binding sites at the ICR, DNA methylation was reduced at three sites (CTCF1-3) in Sirt6-deficient hepatocytes. Consistent with the hypothesis, Sirt6 alters CpG island methylation at *Igf2/H19* gene locus, with a most prominent difference at E1.

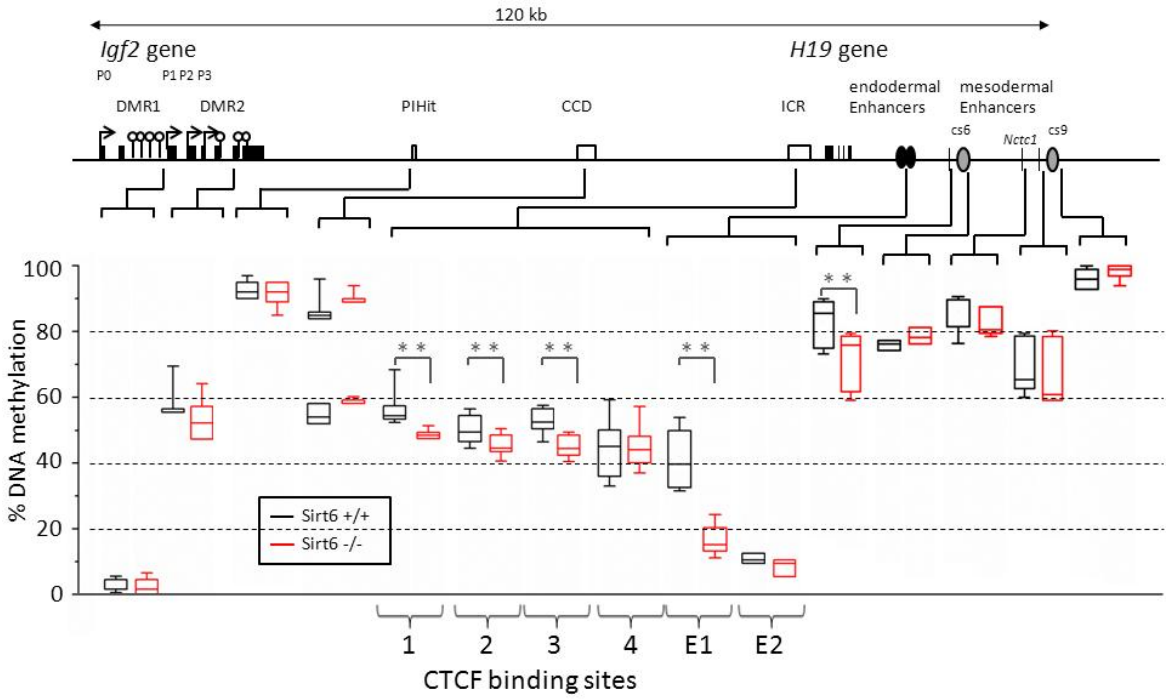

Figure 3.14 Methylation level at the *Igf2/H19* gene locus in Sirt6$^{+/+}$ and Sirt6$^{-/-}$ pmHep. DNA methylation levels of individual CpGs at the locus of *Igf2/H19* were determined by pyrosequencing of bisulphite modified DNA from pmHep. ICR and E1 show decreased methylation level in Sirt6 deficient pmHep (red). Box and whisker plots show mean, inter-quartile ranges, max and min values. Each box blot represents the average methylation score for a given number of CpGs in the respective pyrosequencing assay performed with more than three biological replicates. (Experiments were performed in cooperation with Dr. Matthias Linke and Prof. Ulrich Zechner, Institute of Human Genetics)

3.1.4 Characterization of chromatin loops at the *Igf2/H19* gene locus by chromosome conformation capture (3C)

Specific enhancer-promoter interactions are crucial for the switch from poised to active enhancers and play a role in the regulation of tumor-relevant genes (Calo and Wysocka, 2013; Wamstad et al., 2014). To determine the Sirt6-dependent chromatin conformation changes at the *Igf2/H19* gene locus, 3C-qPCR analyses with a *BamHI* restriction enzyme was performed. Primers within the ICR, DMR1 and *BamHI* site 0 (located 3.9 kb downstream from the endodermal enhancers) were used as anchors.

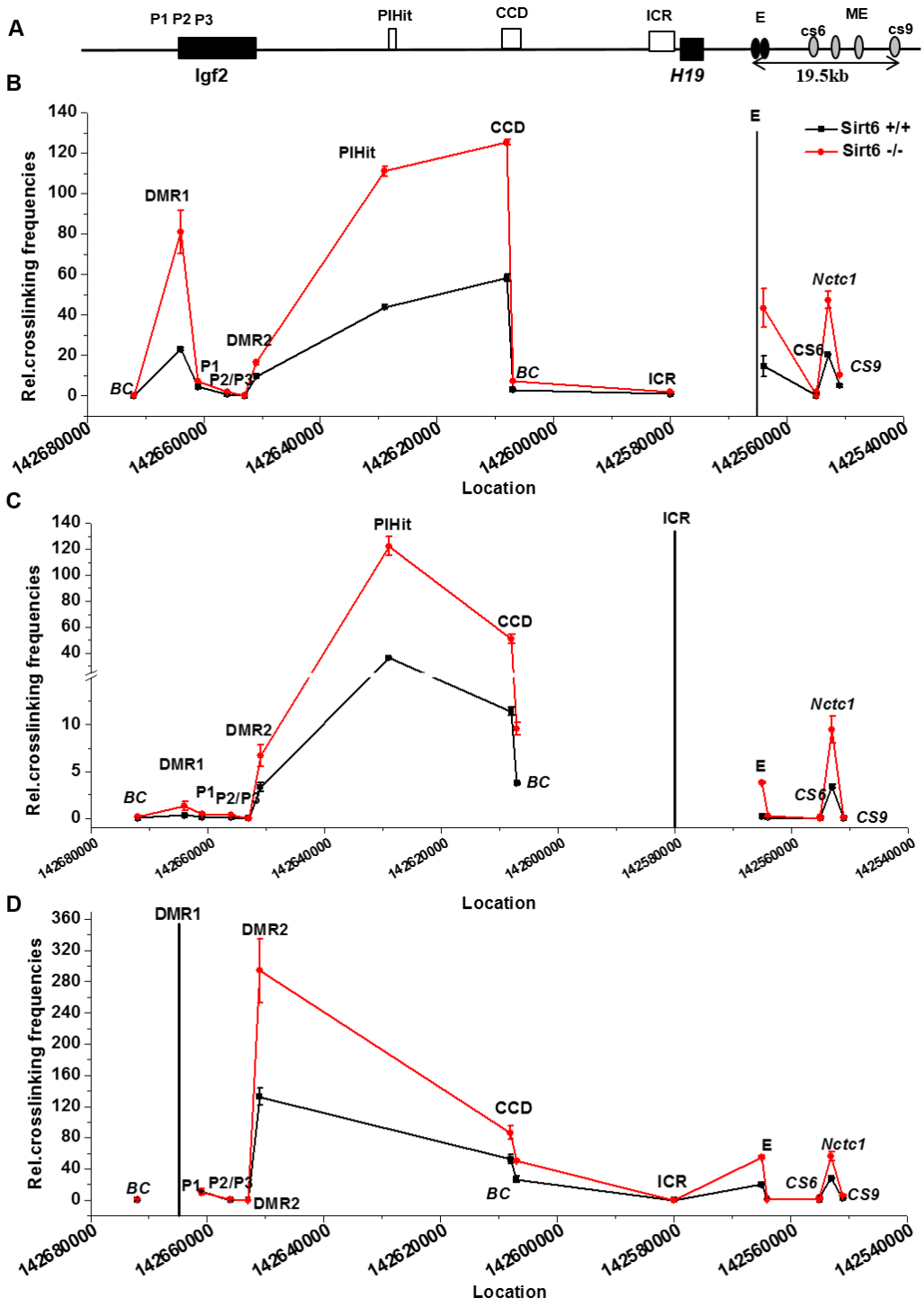

Figure 3.15 3C analysis of higher-order chromatin conformation at the *Igf2/H19* gene locus in Sirt6$^{+/+}$ and Sirt6$^{-/-}$ pmHep. (A) Schematic representation of the mouse *Igf2/H19* gene locus (also see Figure 3.4 and Figure 1.2). BC indicates the intervening regions between CTCF sites. (B-D) 3C analysis shows associations with the anchor sites of endodermal enhancer (B), ICR (C) and DMR1 (D). Black and red lines are profiles in Sirt6$^{+/+}$ and Sirt6$^{-/-}$ pmHep, respectively. BC indicates intergenic background control regions. X axis is the chromosome 7 locus according to Ensemble Release 80 (May 2015). Y axis is the relative crosslinking frequencies normalized with that of the BAC clone of the *Igf2/H19* gene locus. These experiments were repeated three times and a representative result was shown.

When the endodermal enhancer was used as an anchor, strong associations were detected with DMR1, *PIHit* and CCD in WT pmHep. Sirt6 deletion enhanced the above mentioned interaction with endodermal enhancer, such as DMR1 from 23.1 to 81.1. Interestingly, Sirt6 deficiency also amplified the associations with *Nctc1,* from 20.4 to 47.4 (Figure 3.15B). These data indicate the associations between endodermal enhancers and enhancer-related region including *PIHit*, CCD and *Nctc1* were significantly induced in Sirt6-deficient hepatocytes, as well as with the DMR1 of *Igf2*.

As shown in Figure 3.15C and D, usage of the ICR and DMR1 as anchor, the connection frequency between enhancers and promoters was substantially enhanced when Sirt6 is deleted. Specifically, both ICR and DMR1 showed significantly increased interaction with the CCD, endodermal enhancer and *Nctc1* in Sirt6 knockout hepatocytes. Interestingly, unlike in case of the ICR, the signal between the DMR1 and *PIHit* were not observed. This may be due to the fact that *PIHit* interacts with DMRs separately from that with endodermal enhancers (Court et al., 2011). The increased interactions between enhancers and *H19* ICR or *Igf2* DMR1 suggest that both genes should be highly expressed without Sirt6.

Moreover, recent studies suggest that promoter cross-talk might play a similarly critical role in organizing the genome and establishing cell-type specific gene expression (Eun et al., 2013). Analysis of 3C data confirmed that DMR1 raised the link with DMR2 in Sirt6 knockout pmHep (Figure 3.15C and D). The observation indicates that loss of Sirt6 increases the interaction among enhancers, promoters and enhancer-promoter, which can act cooperatively to enhance *H19* and *Igf2* expression.

As earlier reported, *PIHit* (Court et al., 2011) is a tissue-specific long noncoding RNA gene; while *Nctc1* is an enhancer RNA (Eun et al., 2013), which displays a strong active chromatin signature (Wamstad et al., 2014). Through analyzing the mRNA level, *Nctc1* was expressed in muscle, but not liver, and doubled in pmHep when Sirt6 was deleted. Unlike *Nctc1* were muscle-specific, *PIHit* was highly expressed in liver and especially in female mice. Moreover, the transcription of *PIHit* also showed significantly increase in Sirt6-deficient mice (Figure 3.16).

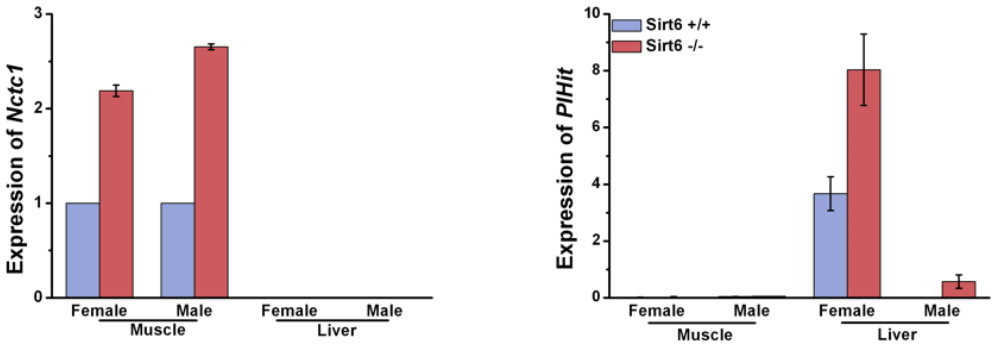

Figure 3.16 Expression of *Nctc1 and PIHit* in liver and muscle of Sirt6$^{+/+}$ and Sirt6$^{-/-}$ mice. Total RNA was extracted from muscle and liver of WT and Sirt6 KO mice, *Nctc1* (right) and *PIHit* (left) expression were quantified by qPCR; quantification was normalized to RPII. This experiment was repeated 2 times and a representative result was shown. Error bars indicate s.e.m.

3.1.5 Analysis of CTCF and cohesin binding at the *Igf2/H19* gene locus in the absence of Sirt6

Recent studies show that CTCF is the master organizer of genomic imprinting at the *H19/Igf2* locus (Han et al., 2008) and can also recruit the cohesin complex to insulator sites that are required for the insulator activity and higher-order chromatin conformation at the *Igf2/H19* gene locus (Nativio et al., 2009; Stedman et al., 2008; Yao et al., 2010). To examine whether CTCF and cohesion participate in the Sirt6-dependent regulation of the higher-order chromatin conformation, ChIP of CTCF and Rad21, a protein of cohesin complex, were performed at the *Ig2/H19* gene locus. Analysis of ChIP data confirmed that the two CTCF interaction sites both occupied by cohesin are specifically located at the CCD and ICR elements (Figure 3.17B and C). The enrichment of CTCF increased about 50% at both loci when Sirt6 was lost. Furthermore, Rad21 displayed the same trend in Sirt6-deficient cells. As previously reported, CTCF and cohesin normally co-localize at the unmethylated ICR (Stedman et al., 2008), which was confirmed by the methylation data (Figure 3.14). In addition, both CTCF and cohesin is involved in heterochromatin regulation (Chien et al., 2011). To analyze heterochromatin formation, binding of the heterochromatin marker HP1β was performed by ChIP. As shown in Figure 3.17D, no binding of HP1β at the entire locus could be detected at both Sirt6 expressing or deleted hepatocytes. These data together with that of H3K9me3 further demonstrated that Sirt6 is not associated with CTCF or cohesin to regulate heterochromatin organization at the

Igf2/H19 gene locus in pmHep.

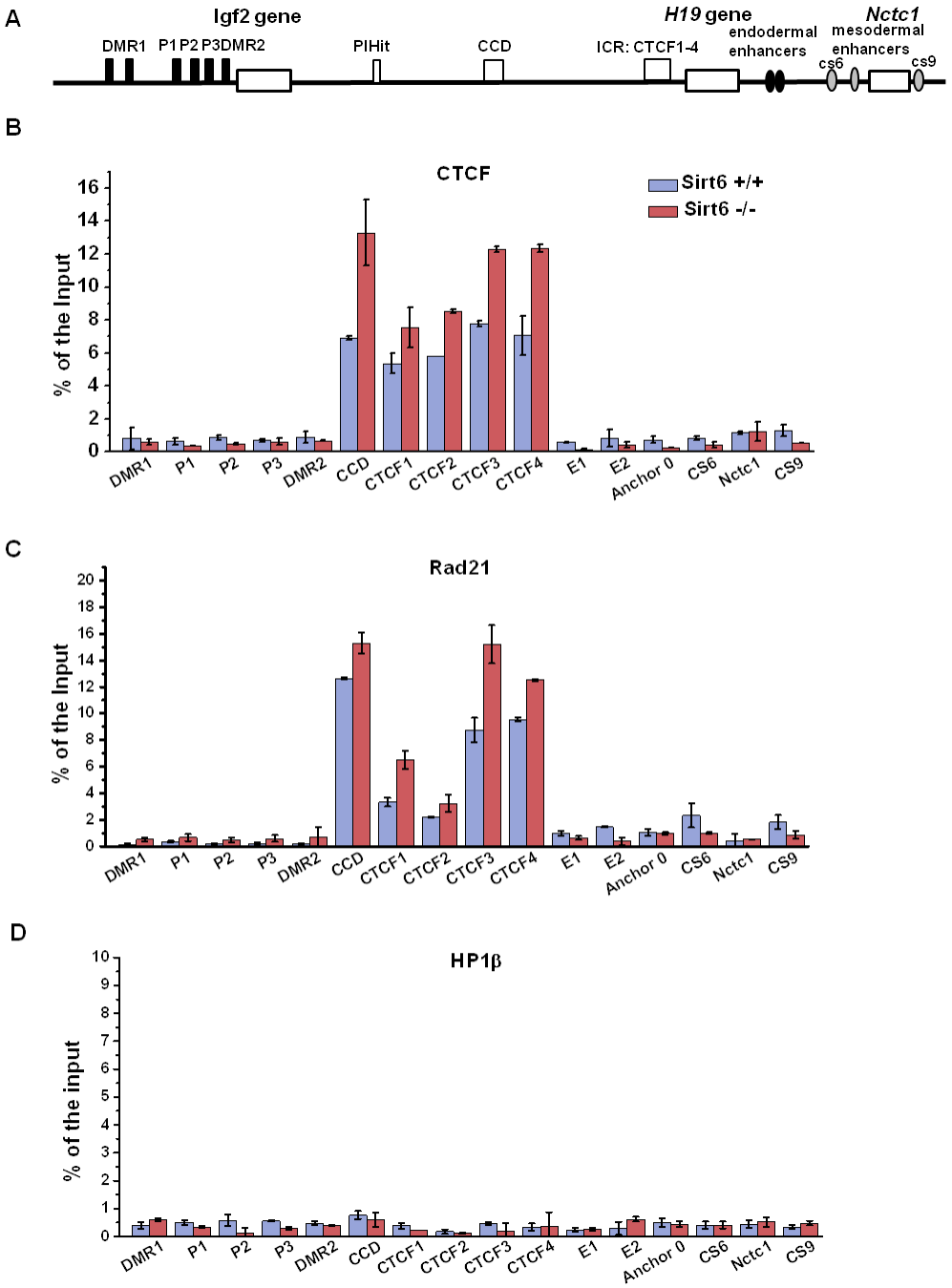

Figure 3.17 ChIP analyses of CTCF and Rad21 binding at the *Igf2/H19* gene locus in in Sirt6$^{+/+}$ and Sirt6$^{-/-}$ pmHep. (A) Schematic representation of the mouse *Igf2/H19* gene locus (see also Figure 3.4 and Figure 1.2). Sirt6$^{+/+}$ (blue) and Sirt6$^{-/-}$ (red) pmHep were used for ChIP. The cells were cross-linked, sonicated and IP was performed using CTCF (B), Rad21 (C) and HP1β (D) specific antibodies. DNA was extracted from IP sample and PCR was performed using primers spanning the indicated regions of the *Igf2/H19* gene locus. ChIP profiles of qPCR data were normalized to the input. These experiments were repeated three times and a representative result was shown. Error bars indicate s.d.

Cohesin and CTCF mediate tissue-specific transcriptional responses via long-range

chromosomal interactions, together with functionally serves as a transcriptional regulator (Schmidt et al., 2010; Zuin et al., 2014). To test whether these factors interacted with SIRT6 to participate in chromatin conformation and gene expression of *H19 and Igf2*, the interactions of these proteins should be analyzed. Based on primary results of the Prof. Strand group, RAD21 was identified as a potential interacting protein with Sirt6 by mass spectrometry (MS). To confirm the MS result, SIRT6 was immunoprepitated in Hep3B cells. As expected, SIRT6, CTCF and RAD21 were interacting reciprocally with each other (Figure 3.18A). These findings were confirmed by PLA (Proximity Ligation Analysis), which used SIRT6-Myc precipitated with CTCF, RAD21 and H3K9ac (Figure 3.18B). As described in Figure 3.15, the higher associations of three anchors with CCD and ICR with endodermal enhancers imply the important role of CTCF and cohesin when Sirt6 is lost.

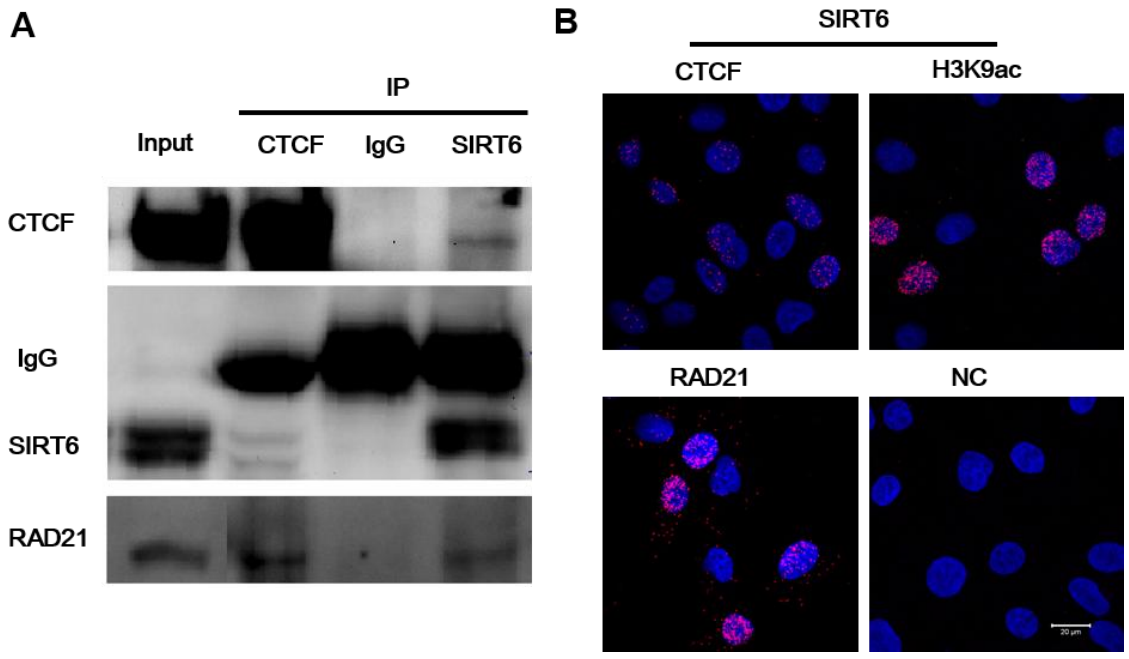

Figure 3.18 Detection of the interaction of CTCF, cohesin and SIRT6 by Co-IP and PLA in Hep3B cells. (A) Co-IP was performed using CTCF and SIRT6 specific antibodies in Hep3B cells. Rabbit IgG was used as a negative control. (B) Hep3B SIRT6-myc cells were plated on chamber slide and fixed with 4% PFA. PLA was performed using fluorescent microscopy images to determine the relative extents of interaction (red spots) between CTCF, RAD21 and SIRT6. As a negative control, proximity ligation was using PLA probes only. White scale bar is 20 µm. (PLA assays in cooperation with Henning Janssen and Dr. Dennis Strand)

3.1.6 Sirt6 in regulation of enrichments and modification of Foxa1/2

3.1.6.1 Sirt6 knockout enhances binding of Foxa1/2 at the Igf2/H19 gene locus

Activation of a gene is often associated with tissue-specific transactivation factors. It is known that Foxa1/2 (Foxa1 and Foxa2), members of liver-enriched transcription factors, have binding sites at the *H19* E1 enhancer to drive *H19* expression (Long and Spear, 2004). These findings prompted us to investigate whether Foxa1 and Foxa2 proteins are involved in the Sirt6-dependent regulation of the *Igf2/H19* gene locus. Remarkably, Foxa1 and Foxa2 are found to be enriched only at the E1 locus and the occupancies 4-fold increased in Sirt6-deficient pmHep (Figure 3.19).

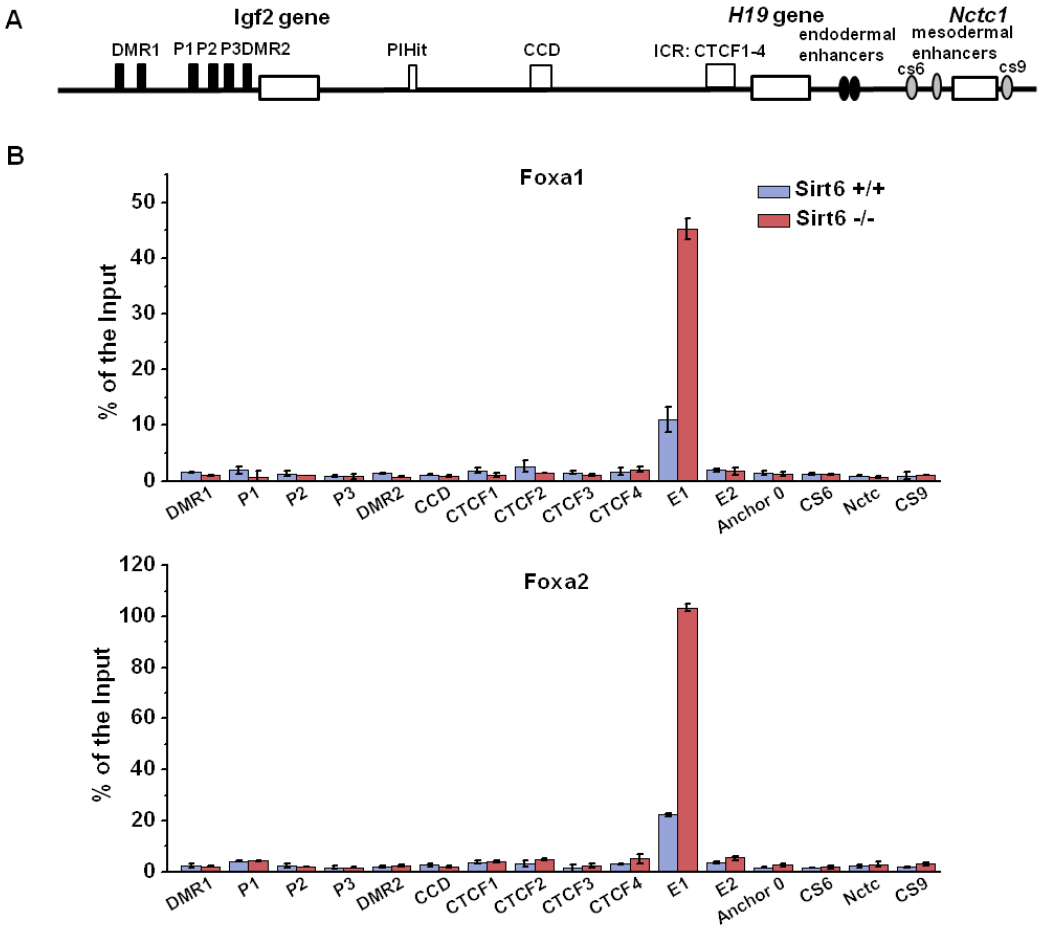

Figure 3.19 ChIP of Foxa1/2 binding at the *Igf2/H19* gene locus in the absence of Sirt6 in pmHep. (A) Schematic representation of the mouse *Igf2/H19* gene locus (see also Figure 3.4 and Figure 1.2). (B) ChIP analysis of Foxa1 and Foxa2 binding at the *Igf2/H19* gene locus in pmHep. Sirt6$^{+/+}$ (blue) and Sirt6$^{-/-}$ (red) pmHep were used for ChIP. The cells were cross-linked, sonicated and IP was performed using Foxa1 or Foxa2 specific antibodies. DNA was extracted from IP sample and PCR was performed using primers spanning the indicated regions. ChIP profiles of qPCR data were normalized to the input. These experiments were repeated three times and a representative result was shown. Error bars indicate s.d.

To gain better insight of the FOXA1/2 binding at the IGF2/H19 gene locus in the context of SIRT6, ChIP profiles of FOXA1 and FOXA2 were performed in phHep, Hep3B pcDNA and SIRT6-myc cells. Consistent with the above observations, the binding of FOXA1 and FOXA2 at E1 were consistently up-regulated in Hep3B tumor cells in comparison to phHep. However, the enrichment decreased about 20-25% when over-expression of SIRT6 in Hep3B cells (Figure 3.20). These data suggest SIRT6 regulates the expression of *H19* and *IGF2* through recruiting the pioneer factors, Foxa1 and Foxa2. Over-expression of SIRT6 could suppress the binding of the Foxa1 and Foxa2 at the unique site, E1.

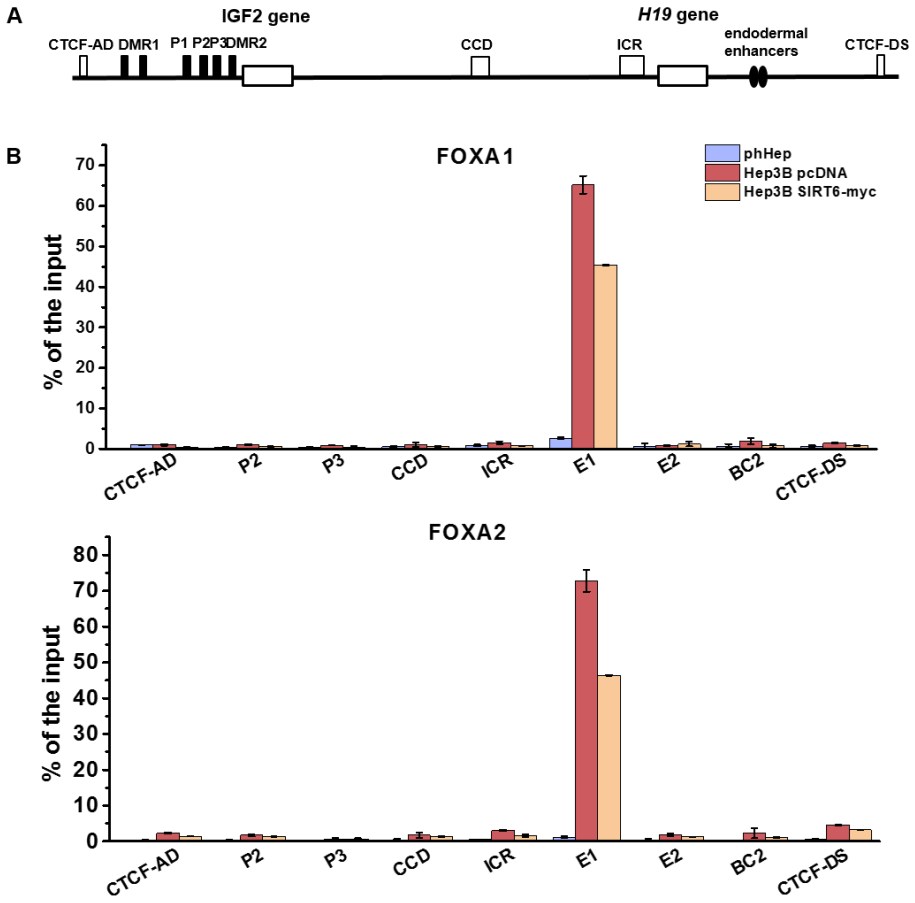

Figure 3.20 ChIP of Foxa1/2 binding at the *IGF2/H19* gene locus in phHep, Hep3B pcDNA and SIRT6-myc cells. (A) Schematic representation of the human *IGF2/H19* gene locus (see also Figure 3.4 and Figure 1.2). (B) ChIP analysis of FOXA1 and FOXA2 binding at the *IGF2/H19* gene locus. phHep, Hep3B pcDNA and Hep3B SIRT6-myc cells were used for ChIP. The cells were cross-linked, sonicated and IP was performed using FOXA1 or FOXA2 specific antibodies. DNA was extracted from IP sample and PCR was performed using primers spanning the indicated regions. ChIP profiles of qPCR data were normalized to the input. These experiments were repeated two times and a representative result was shown. Error bars indicate s.d.

3.1.6.2 Detection of acetylated Foxa2 in Sirt6$^{+/+}$ and Sirt6$^{-/-}$ pmHep

To investigate whether SIRT6 influences the acetylation level of Foxa2, immunprecipitation of acetylated lysine was performed and Foxa2 specific antibody used to detect the WB signals. As expected, an increased acetylation level of Foxa2 in Sirt6-deficient mice was observed (Figure 3.21A), which was further confirmed by proximity ligation assay (Figure 3.21B). These data suggest that Sirt6 regulates the acetylation level of Foxa2 *in vivo*.

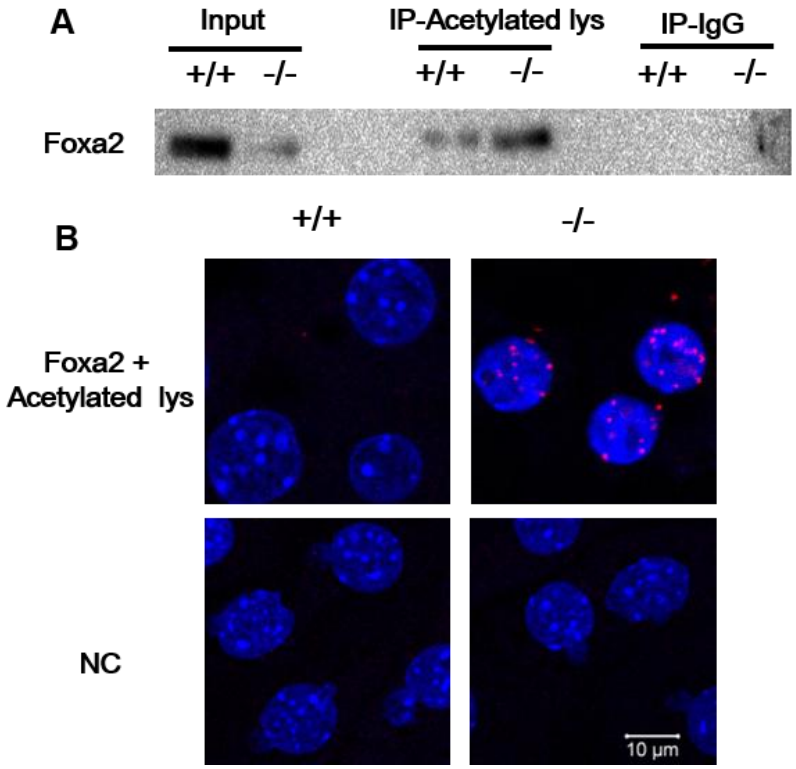

Figure 3.21 Detection of acetylation level of Foxa2 by Co-IP and PLA in Sirt6$^{+/+}$ and Sirt6$^{-/-}$ pmHep. (A) Primary murine hepatocytes of Sirt6$^{+/+}$ and Sirt6$^{-/-}$ were used. The Co-IP was performed using acetylated lysine antibodies and western blots were used to detect the signals. Rabbit IgG was used as a negative control. This experiment was repeated 3 times and a representative result is shown. (B) Sirt6$^{+/+}$ and Sirt6$^{-/-}$ pmHep were plated on chamber slide and fixed by 4% PFA. PLA signals (red) of protein-protein interactions of Foxa2 and acetylated lysine were visualized by confocal fluorescence microscopy. As a negative control, proximity ligation was performed using PLA probes only. +/+ and -/- indicate Sirt6$^{+/+}$ and Sirt6$^{-/-}$, respectively. White scale bar is 10 µm. This experiment was repeated three times and a representative result was shown. (PLA assays in cooperation with Henning Janssen and Dr. Dennis Strand)

Of note, it has been previously shown that Foxa2 acetylation facilitates its localization in the nucleus and promotes transcriptional activity in ob/ob and db/db mice (von Meyenn et al., 2013).

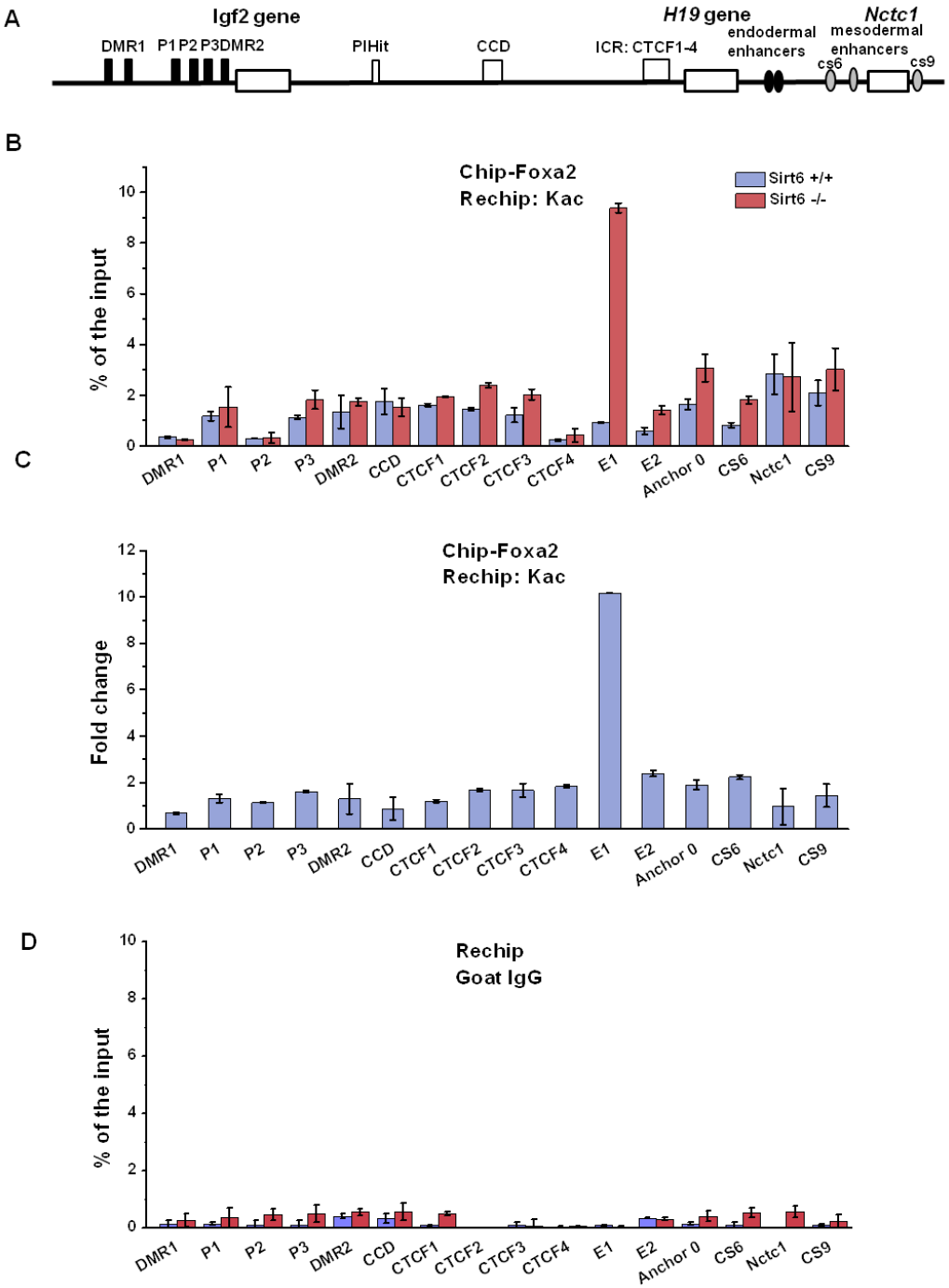

Figure 3.22 ChIP-reChIP of acetylated Foxa2 binding at the *Igf2/H19* gene locus in the absence of Sirt6. (A) Schematic representation of the mouse *Igf2/H19* gene locus (see also Figure 3.4 and Figure 1.2). $Sirt6^{+/+}$ and $Sirt6^{-/-}$ pmHep were used for reChIP. The cells were cross-linked, sonicated and the 1st IP were performed using Foxa2 specific antibody. Then 2nd IP were using acetylated Lysine (Kac) (B) specific antibody or rabbit IgG (D). DNA was extracted and PCR was performed using primers spanning the indicated regions of the *Igf2/H19* gene locus. reChIP profiles of qPCR data were normalized to the input. ReChip analysis of occupancy of acetylated Foxa2 in $Sirt6^{-/-}$ by normalizing with that in $Sirt6^{+/+}$(C). These experiments were repeated two times and a representative result was shown. Error bars indicate s.d.

To assess whether the acetylated Foxa2 is critical for the recruitment to E1, reChIP were performed to characterize the acetylated Foxa2 enrichment at the *Igf2/H19* gene locus. As shown in Figure 3.22B, the acetylated Foxa2 did not exhibit specifically binding sites in WT, but the binding is specifically at E1 of the *Igf2/H19* gene locus, and displayed about 10 times increase when Sirt6 was deleted (Figure 3.22B and C). These results indicate that the acetylated of Foxa2 specifically enriched at E1 when Sirt6 is lost, which is similar with acH2AZ.

3.1.6.3 Analysis of mRNA and protein level of Foxa2 when Sirt6 was lost

To analyze whether Foxa2 expression is regulated by SIRT6, qRT-PCR and WB were performed in pmHep. Interestingly, the protein level of Foxa2 decreased dramatically whereas the mRNA showed no significant difference in Sirt6-deficient mice (Figure 3.23A and B). These results suggest that SIRT6 regulates FOXA2 protein expression in post-transcriptional level, not RNA level.

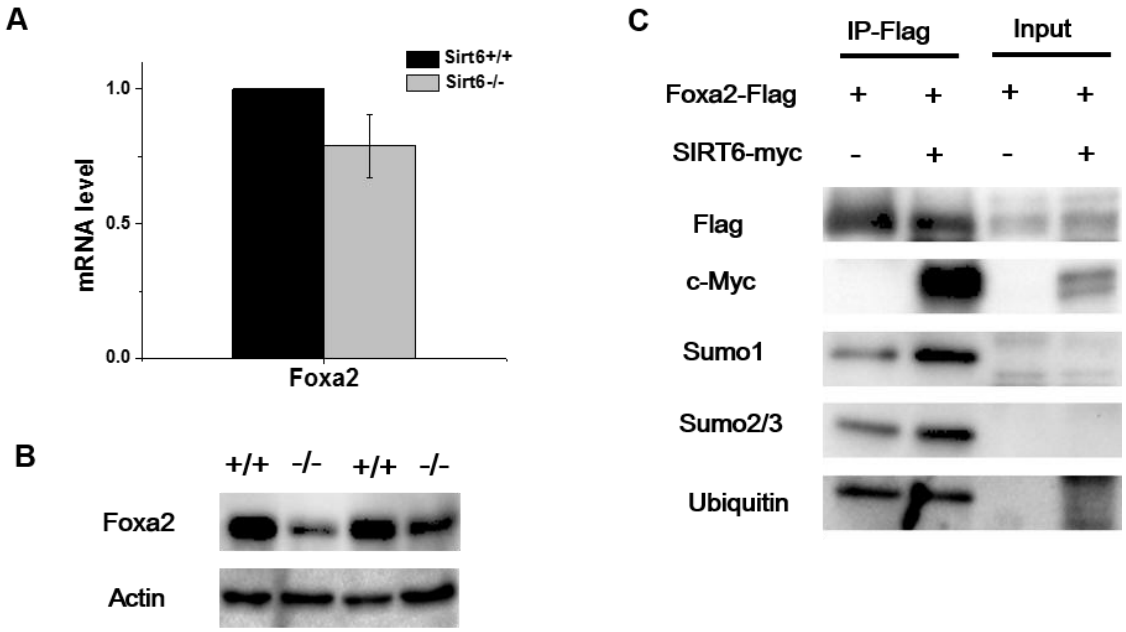

Figure 3.23 Detection of Foxa2 level by WB/qPCR and the PTM of FOXA2 by Co-IP. (A) Total RNA was extracted from pmHep of WT and Sirt6 KO mice. *Foxa2* mRNA expression level were quantified by qPCR; quantification was normalized to RPII; n=2, error bars indicate s.d. (B) Foxa2 protein expression level were analyzed by western blots using samples from pmHep of $Sirt6^{+/+}$ and $Sirt6^{-/-}$ mice. +/+ and -/- indicate $Sirt6^{+/+}$ and $Sirt6^{-/-}$, respectively. Actin was used as a control. (C) Hep3B cells were transfected with the indicated plasmid. Forty eight hours following transfection, lysated cells were immunoprecipiatated with mouse Flag specific antibody and IP complexes were detected using western blotting with antibodies as indicated.

As previously reported, preventing sumoylation by mutating the SUMO acceptor K6 to arginine resulted in downregulation of FOXA2 protein but not RNA expression (Belaguli et al., 2012). To identify whether SIRT6 regulates the modification of FOXA2, the sumo modification level of FOXA2 was examined through transfecting FOXA2-Flag plasmid together with/without SIRT6-myc plasmid. Indeed, over-expression of SIRT6 enhances the interactions of both Sumo1 and Sumo2/3 with Foxa2. However, there was no difference of the ubiquitination level of FOXA2 (Figure 3.23C). Thus, SIRT6 maybe deacetylate FOXA2 and then enhance its sumoylation to increase its stability.

3.1.7 Alterations of occupancy of histone H1 at the *Igf2/H19* gene locus when Sirt6 was deleted

It is known that pioneer factors are important for hepatic differentiation. Foxa1/2 can open compacted chromatin and displace the linker histone H1 to activate liver-specific genes (Cirillo et al., 2002a; Cirillo et al., 1998; Taube et al., 2010). Histone H1.2 and H1.4 variants are highly expressed in mouse liver (Popova et al., 2013; Vaupel and Mayer, 2007; Wisniewski et al., 2007), which is consistent with the gene expression microarray analysis (data not show). Based on these data, ChIP assays of histone H1.2 and H1.4 were performed.

As shown in Figure 3.24B and C, histone H1.2 was more enriched at DMR2, CCD and the enhancers region (E2-CS9) in Sirt6-deficient mice in compared with WT, whereas occupancy of H1.4 was more at P2. Most importantly, enrichments of both histone H1.2 and H1.4 showed a significant and specific reduction at E1, the known nucleosomes occupying region, when Sirt6 was deleted. This nucleosome occupancy is inversely correlated with the Foxa1/2 binding data at this site (Figure 3.19). Thus, these data indicate that Foxa1/2 could displace the histone H1 specifically at E1 when Sirt6 was lost.

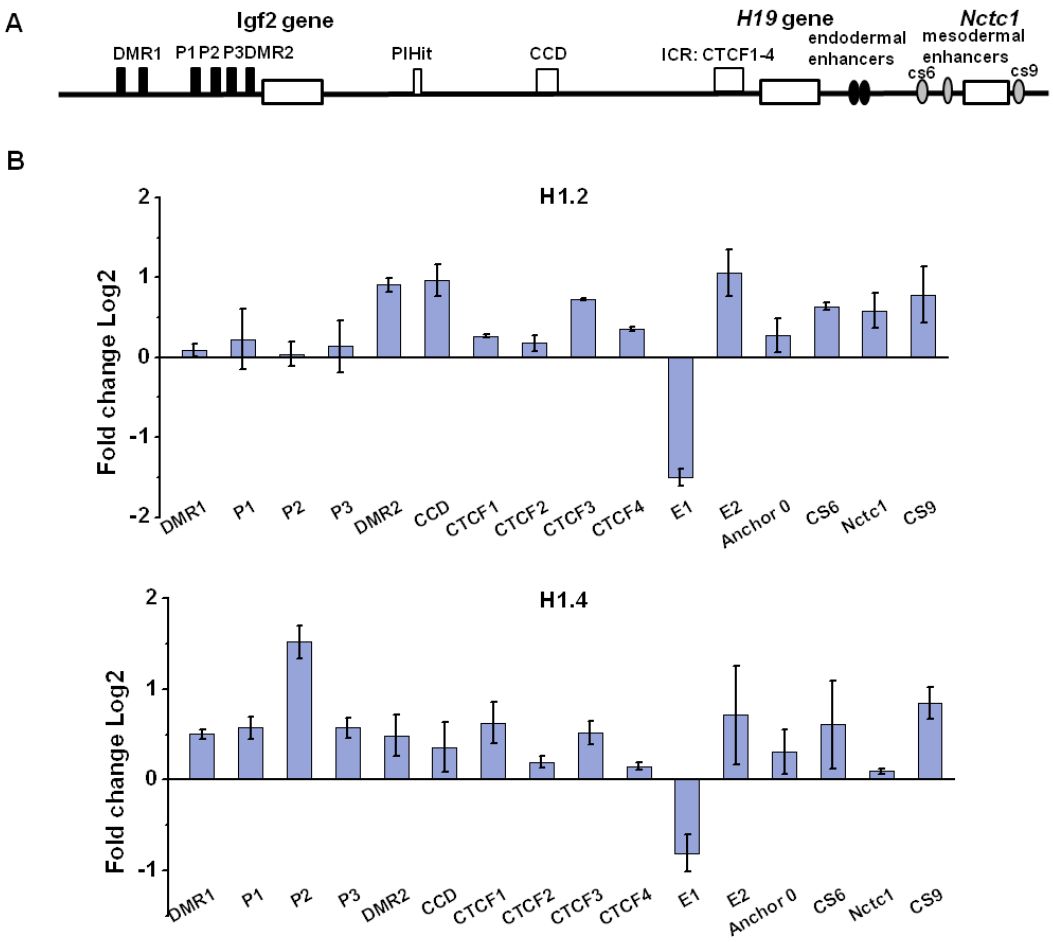

Figure 3.24 ChIP analysis of the occupancy of histone H1 at the *Igf2/H19* gene locus in Sirt6-deficent pmHep. (A) Schematic representation of the mouse *Igf2/H19* gene locus (see also Figure 3.4 and Figure 1.2). (B) Sirt6$^{+/+}$ and Sirt6$^{-/-}$ pmHep were used for ChIP. The cells were cross-linked, sonicated and IP was performed using histone H1.2 and H1.4 specific antibodies. DNA was extracted from IP sample and PCR was performed using primers spanning the indicated regions of the *Igf2/H19* gene locus. ChIP profiles of qPCR data were normalized to the input. The fold change indicates the occupancy of histone H1.2 or H1.4 in Sirt6$^{-/-}$ vs Sirt6$^{+/+}$. These experiments were repeated three times and a representative result was shown. Error bars indicate s.d.

Interestingly, primary hepatocytes of the SIRT6 KO mouse displayed a histone H1.4 protein abundance that was more cytoplasmic than nuclear (Figure 3.25A and B), followed by secretion into serum (Figure 3.25B). These data indicate that Foxa1/2 may function as pioneer factor to displace histone H1 to open the compacted chromatin, and this displacement led histone H1 to be secreted into supernatant.

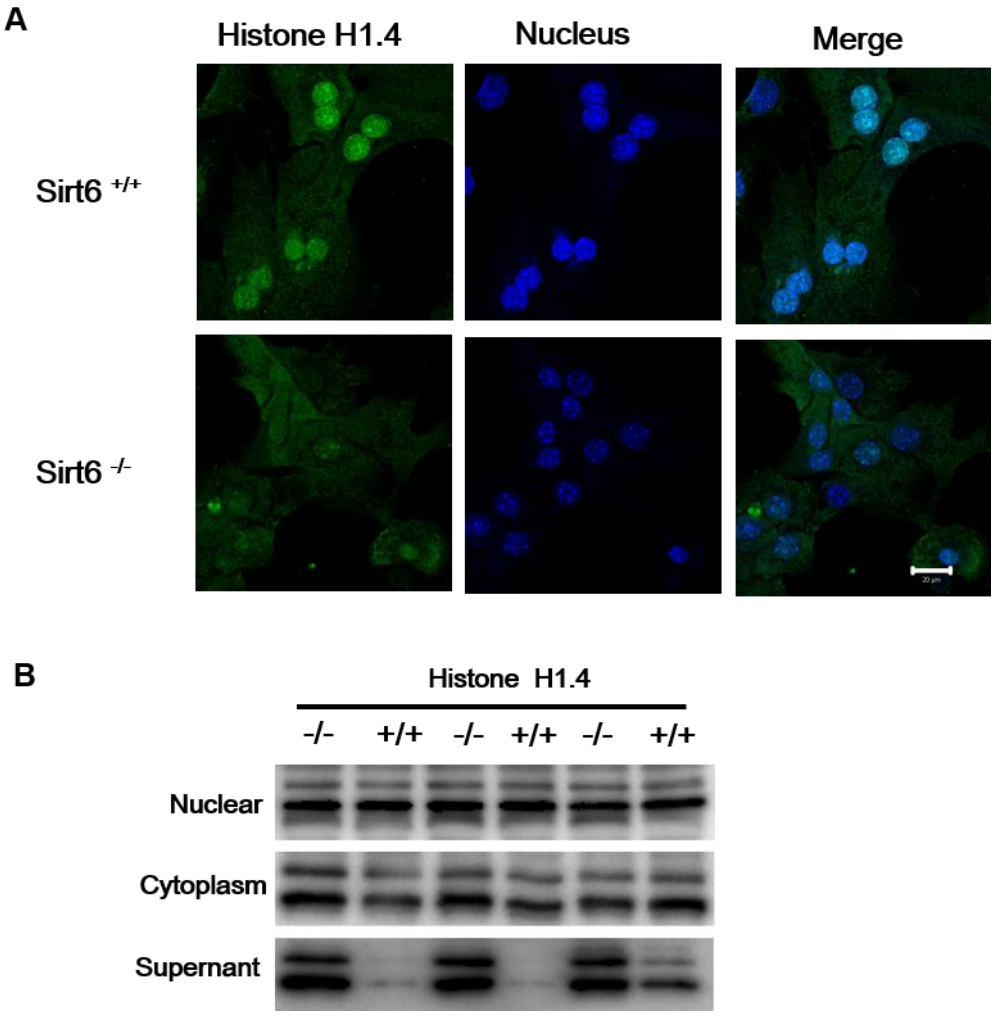

Figure 3.25 IFs and western blots of histone H1.4 in Sirt6$^{+/+}$ and Sirt6$^{-/-}$ pmHep. (A) Sirt6$^{+/+}$ and Sirt6$^{-/-}$ pmHep were plated on chamber slide and fixed with 4% PFA. The histone H1.4 protein was stained with H1.4 antibody. Staining was visualized using Alexa-488 labeled secondary antibody. Hoechst was used to visualize the nuclear. White scale bar is 20 μm. This experiment was repeated three times and a representative result is shown. (B) Sirt6$^{+/+}$ and Sirt6$^{-/-}$ pmHep were plated on 6-well plates and incubation overnight. The supernatant were collected and the proteins in nucleus and cytoplasm were isolated from the cell by Nuclear and Cytoplasmic Extraction kit. Anti-histone H1.4 was used to detect the bands by WB. +/+ and -/- indicate Sirt6$^{+/+}$ and Sirt6$^{-/-}$, respectively. This experiment was repeated three times and a representative result was shown.

3.1.8 Analysis of enhancers' type of *IGF2/H19* in Hep3B by CRISPR-cas9

The above ChIP results imply the importance of enhancers, as well as by some criterions including H3K4me1/H3K4me3 and H3K27ac/H3K27me3 ratios, which strongly indicate the enhancers region of *IGF2/H19* is more than a typical enhancer. Recent studies show super-enhancers and stretch-enhancers, which consist of clusters of enhancers, can stimulate higher transcriptional activity than typical enhancers (Whyte et al., 2013). This

promoted us to test whether the enhancers region of the *IGF2/H19* is a super-enhancer. The size of the complete enhancers region (from E1 to CS9) at the mouse *Igf2/H19* gene locus was firstly checked. With a size of 19.5 Kb, that region matches with that of the median size (19.4 Kb) of super-enhancer (Loven et al., 2013). Consistent with one of the criterion of super-enhancers, ChIP data of super-enhancer markers like H3K4me1 and H3K27ac (Hnisz et al., 2013; Loven et al., 2013; Whyte et al., 2013) were already shown. The occupancy of H3K4me1 doubled at the enhancers region with a loss of Sirt6, although that of H3K27ac specifically sharply increased at the endodermal enhancers (E1-Anchor 0).

The newly emerged CRISPR-Cas9 technology was used to delete different enhancers region of the *IGF2/H19* gene locus to check their properties. As shown in Figure 3.26A and C, three deletions were designed in Hep3B cells: endodermal enhancers (6 kb), mesodermal enhances (18.5 kb) and the entire enhancers region (24.5 kb), which is from upstream of E1 to CTCF-DS. Through screening the transfected clones, some monoallelic deletion and biallelic deletion clones were gained (Figure 3.26B). qPCR analysis was performed to quantify the effect of different deletions on *H19* and *IGF2* expression. In monoallelic deletion clones, both *H19* and *IGF2* showed a dramatical reduction when the endodermal enhancers (EE) were deleted, 80% and 97%, respectively (Figure 3.26D). Unfortunately, the bialllelic deletion clones of EE were not generated due to technical problems. Strikingly, the mesodermal enhancers (ME) deletion also caused a significantly drop of *H19* (62%) and *IGF2* (65%) expression. Moreover, in biallelic deletion clones, the expression of *H19* and *IGF2* induced by ME deletion was up to 91% and 98%, respectively. These data revealed that the ME is also responsible for the expression of both *H19* and *IGF2* expression regulation, although to a lesser extent as EE. Furthermore, the decrease of *H19* expression was up to 92% when the entire enhancers region was monoallelic deleted, while that of *IGF2* was 99.2%. There was almost no signal in biallelic deletion of the entire enhancers region. Altogether, these reveal that the entire enhancers region of the *IGF2/H19* gene locus may serve as a super-enhancer to contribute to the transcription of *H19* and *IGF2* in Hep3B cells.

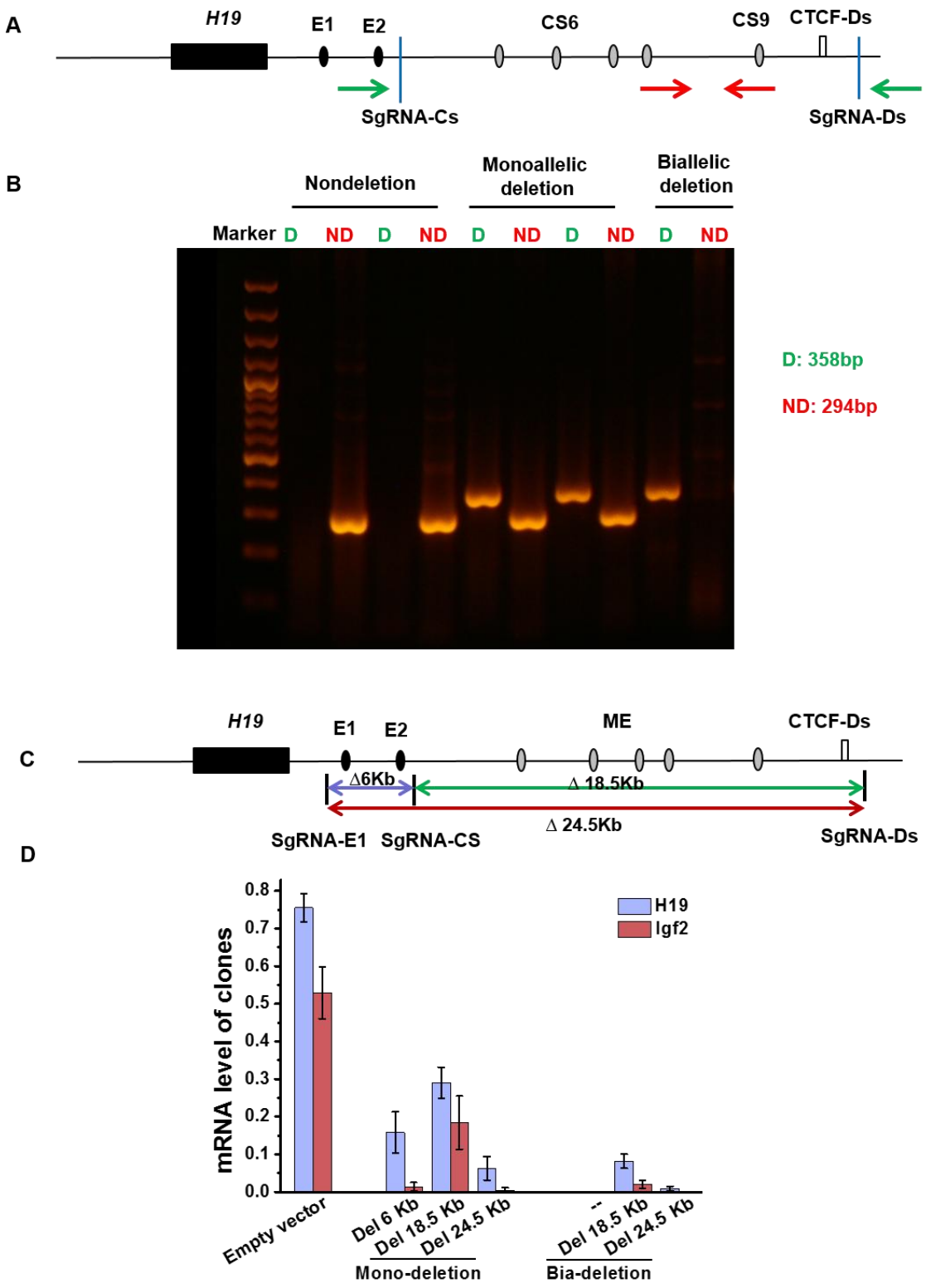

Figure 3.26 Expression of *H19* and *IGF2* genes after deletion of the enhancers region in Hep3B cells. (A) sgRNA deletion strategies of mesodermal enhancers. *H19* gene (black boxes) is displayed together with the downstream endodermal enhancers (E1 and E2) (black ovals), mesodermal enhancers (ME, e.g. CS6 and CS9) (gray ovals), and CTCF-downstream binding locus (CTCF-Ds) (white box). The sgRNA sites are shown in relation to the *IGF2/H19* gene locus. The green arrows indicate the position of PCR primers for deletion band amplification, and

the red arrows indicate the position of PCR primers for non-deletion band amplification. (B) PCR Screening of CRISPR/Cas9-mediated genomic deletion. Cells were transfected with 7.5 µg of each indicated sgRNA construct and 1 µg of a GFP expression construct. The top 5% of GFP^+ cells were sorted 2 days post-transformation and plated at limiting dilution. 14 days after plating, gDNA was extracted, and clones were screened for deletion by PCR. A representative screening agarose gel shows the detection of two nondeletion clones, two monoallelic deletion clones, and one biallelic deletion clones. As schematized in A, the red ND and green D refer to the nondeletion amplicon and the deletion amplicon, respectively. (C) Schematic representation of CRISPR-based enhancer deletion strategy in Hep3B cells. The blue, green and red lines with two arrows indicate the predicted cleavage of endodermal enhancers, ME and full enhancers region, respectively. (D) Relative expressions of *H19* (blue) and *IGF2* (red) in different enhancer-deletion clones. Total RNA was extracted from different enhancer deletion colonies. *H19* and *IGF2* mRNA were quantified by qPCR; quantification was normalized to RPII; n=3, error bars indicate s.e.m.

3.2 Sirt6 in hepatic differentiation genes regulation

3.2.1 Hepatic differentiation related gene expression in context of Sirt6

Previously publication by Prof. Strand and co-workers suggest that cell differentiation is one of the most significant pathway map folders from the Sirt6 knockout signature as determined by GeneGo analysis (Marquardt et al., 2013). Recently, a study identified thousands of enhancers that are bound by FOXA2 in a differentiation-dependent manner (Alder et al., 2014).Thus whether SIRT6 regulates Foxa2-dependent enhancer-driven differentiation genes in hepatocytes was investigated. Then the differentiation-related genes that recruit FOXA2 to their temporal enhancers during liver development (Alder et al., 2014) were analyzed from the microarray. As shown in Figure 3.27, almost all the embryonic hepatoblast markers were up-regulated, while the adult hepatocytes markers were down-regulated in the absence of Sirt6 in mouse liver. Strikingly, the up-regulated genes including *H19*, *Igf2*, *Gpc3* and *Afp* are oncofetal genes. This data is in line with the hypothesis that Sirt6 is involved in regulating these hepatic differentiation-related genes in a Foxa2-dependent manner.

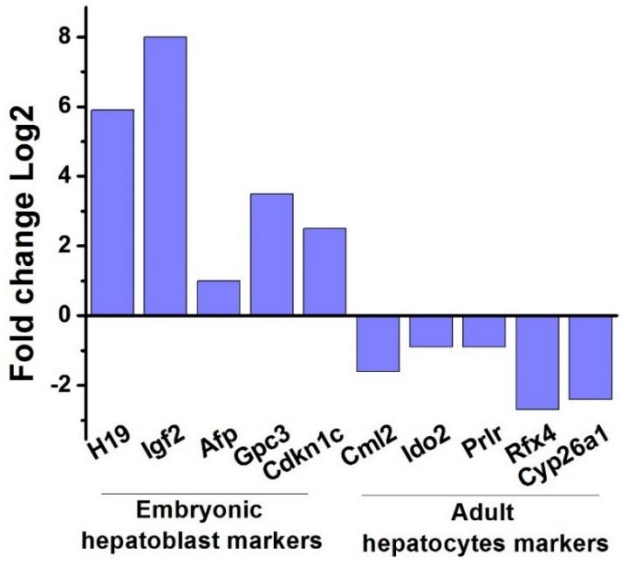

Figure 3.27 Expression of hepatic differentiation markers in the absence of Sirt6 by microarray. Differential expression of Foxa2 target genes in Sirt6$^{-/-}$ hepatocytes were analyzed. The expression signatures were generated using isolated primary mouse hepatocytes from WT and Sirt6-deficient livers at 3 weeks of age. The histogram displays fold changes in gene expression and the expression in Sirt6$^{+/+}$ pmHep was set to 1.

To confirm the microarray data, the relative mRNA level of the classic hepatoblast markers *H19*, *Igf2* and *Afp* as well as the differentiation markers of hepatocytes, *Alb* and *Cyp3a41* (Hannan et al., 2013), were quantified by qPCR. In Sirt6-deficient mice, oncofetal makers were dramatically elevated along with the differentiation markers that were significantly down regulated (Figure3. 28A). In contrast, this trend reversed when overexpressed SIRT6 was induced in Hep3B cells (Figure 3.28B), which confirmed that SIRT6 was required for lineage commitment in hepatocytes.

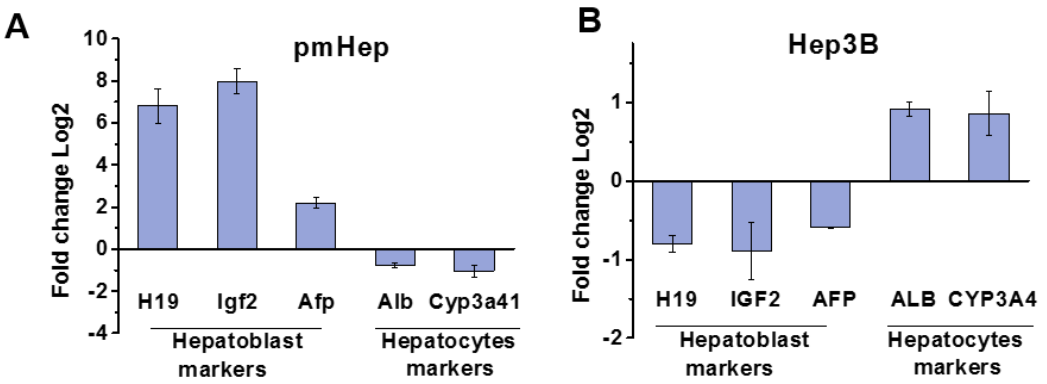

Figure 3.28 qRT-PCR analysis of expression of hepatic differentiation markers and oncofetal genes in hepatocytes. Relative expression of hepatoblast markers (*H19*, *Igf2* and *Afp*) and differentiation markers (*Alb* and *Cyp3a4*). (A) Total RNA was extracted pmHep of WT and Sirt6 KO mice. Primers of indicated gene were used to quantify the mRNA level by qPCR; quantification was firstly normalized to RPII; then mRNA expression level was analyzed in $Sirt6^{-/-}$ vs $Sirt6^{+/+}$; n=3, error bars indicate s.e.m. (B) Hep3B cells were transfected with pcDNA or SIRT6-myc plasmid. Forty eight hours following transfection, cells were collected to isolate RNA. Primers of indicated gene were used to quantify the mRNA level by qPCR; quantification was firstly normalized to RPII; then mRNA expression level was analyzed in Hep3B cell transfected with SIRT6-myc vs pcDNA, n=2, error bars indicate s.e.m.

3.2.2 Occupancy of Sirt6 and H3K9ac at the *Alb/Afp* gene locus in the absence of Sirt6

To gain insight into how Sirt6 regulates hepatoblast and hepatocytes markers, functional analysis of the *Alb/ Afp* gene locus was selected, since it is the classic model for hepatic differentiation. The recruitment of Sirt6 was firstly analyzed by ChIP assay in pmHep of WT and Sirt6 KO mice. As shown in Figure 3.29B, Sirt6 was enriched at all the regions of the *Alb/ Afp* gene locus in normal primary murine hepatocytes, and the binding reduced along with the deletion of Sirt6. As the classic substrate of Sirt6, the occupancy of acetylation of

histone H3 lysine 9 was also analyzed. Unlike the recruitment of Sirt6 in Sirt6-deficient murine hepatocytes, the occupancy of H3K9ac only increased at the enhancers and distant promoters of *Afp* (Figure 3.29B), which indicates H3K9ac contributes to the activation of *Afp*, not *Alb*.

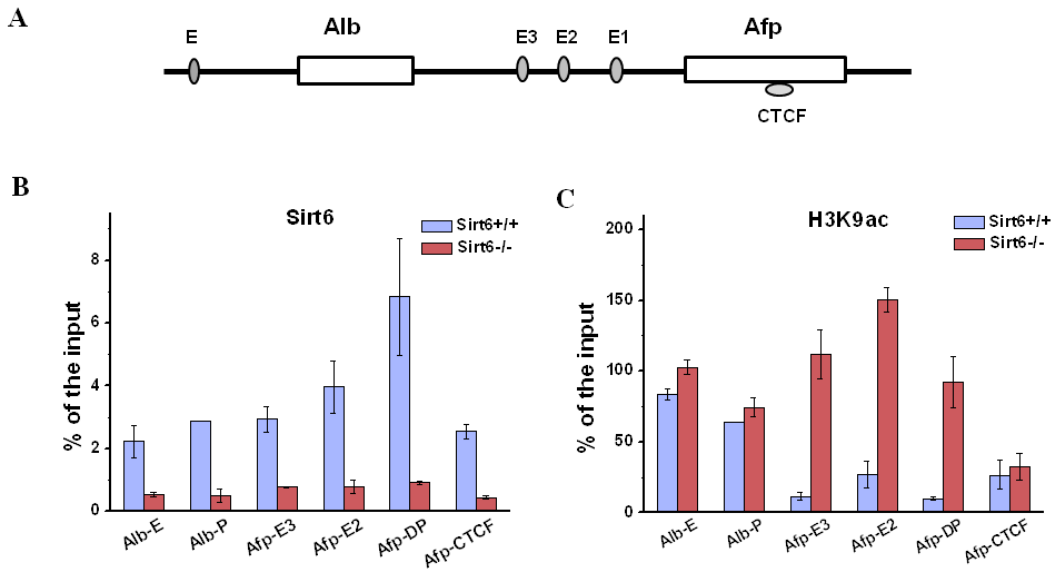

Figure 3.29 ChIP analysis of recruitment of Sirt6 and H3K9ac at the *Alb/Afp* gene locus in the absence of Sirt6. (A) Schematic representation of the *Alb/Afp* gene locus. *Alb* and *Afp* genes (white boxes) are displayed together with enhancers (gray ovals) and CTCF binding at the middle of *Afp* gene. *Afp* gene has three enhancers while *Alb* has one enhancer. (B-D) ChIP of Foxa1/2 binding at the *Alb/Afp* gene locus in pmHep. Sirt6$^{+/+}$ (blue) and Sirt6$^{-/-}$ (red) pmHep were used for ChIP. The cells were cross-linked, sonicated and IP was performed using Sirt6 and H3K9ac specific antibodies. DNA was extracted from IP sample and PCR was performed using primers spanning the indicated regions. This experiment was repeated three times and a representative result was shown. Error bars indicate s.d.

3.2.3 Occupancies of histone marks at the *Alb/Afp* gene locus when Sirt6 was lost

As one of the histone mark modulators, Sirt6 may alter the epigenetics landscape at the *Alb/Afp* regulatory regions. Hence, the histone modifications at the *Alb/Afp* regulatory regions were characterized by ChIP with specific antibodies. As shown in Figure 3.30B, there was almost no difference of the enrichment of H3K4me1 at all the locus when Sirt6 was lost, but the occupancy of active enhancer marker H3K27ac exhibited a strong increase at the *Afp* enhancers and distant promoters (DP), which are also the binding site of Foxa1(Taube et al., 2010).

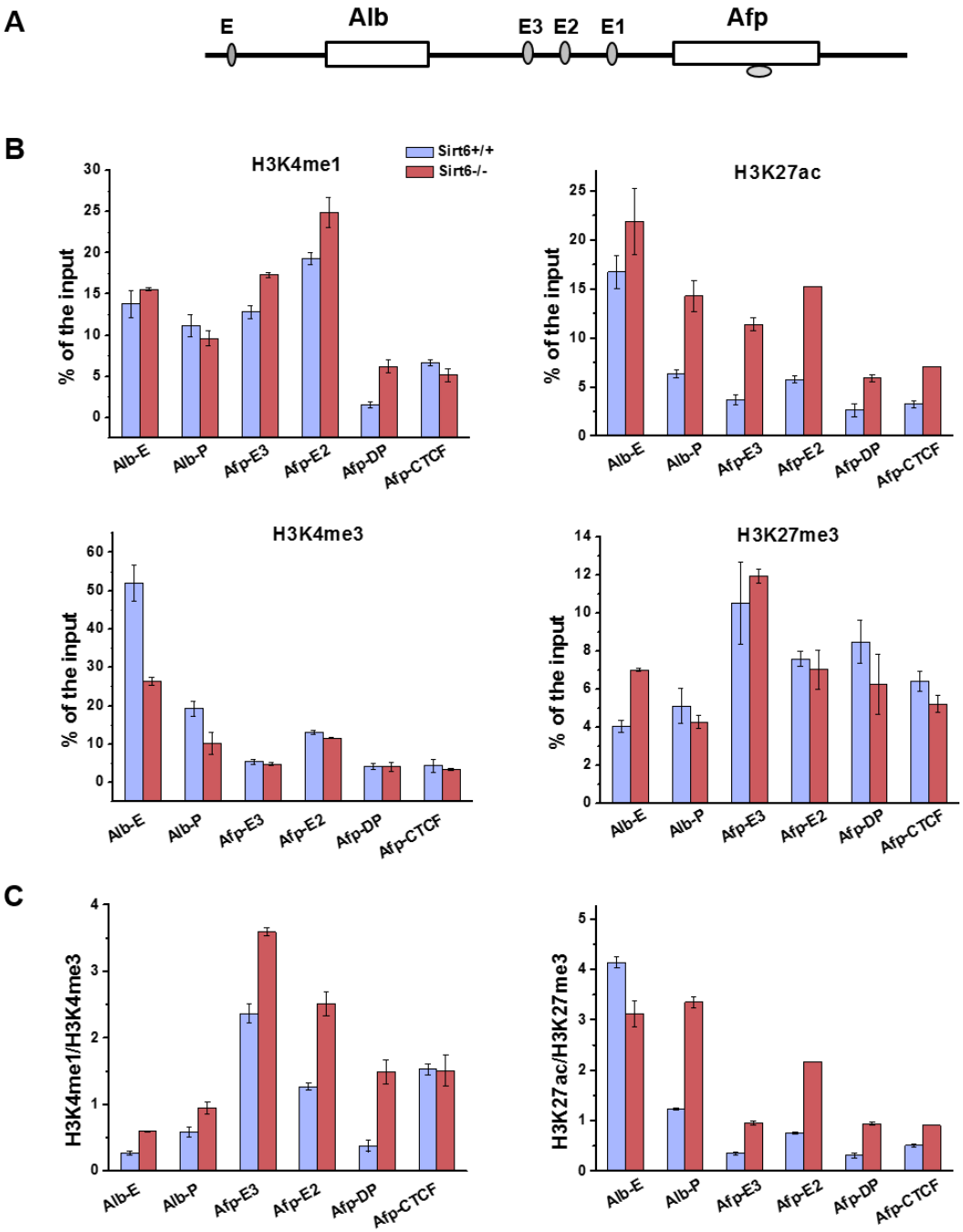

Figure 3.30 ChIP analyses of the occupancies of histone modifications at the *Alb/Afp* gene locus in Sirt6$^{+/+}$ and Sirt6$^{-/-}$ pmHep. (A) Schematic representation of the *Alb/Afp* gene locus (see also Figure 3.29 and Figure 1.3). (B) Sirt6$^{+/+}$ (blue) and Sirt6$^{-/-}$ (red) pmHep were used for ChIP. The cells were cross-linked, sonicated and IP was performed using H3K4me1, H3K4me3, H3K27ac and H3K27me3 specific antibodies. DNA was extracted from IP sample and PCR was performed using primers spanning the indicated regions of the *Alb/Afp* gene locus. ChIP profiles of qPCR data were normalized to the input. (C) Relative enrichment ratio of H3K4 and H3K27 modifications. The H3K4 ratio is the enrichment of H3K4me1 normalized with that of H3K4me3, while The H3K27 ratio is the enrichment of H3K27ac normalized with that of H3K27me3. These experiments were repeated three times and a representative result was shown. Error bars indicate s.d.

Interestingly, the bivalent marks showed alteration only specifically at the enhancer of *Alb* in Sirt6-deficent mice, namely the active mark H3K4me3 decreased 2 times while H3K27me3 increased 84% at this site. Furthermore, both the relative ration of H3K4 and H3K27 increased at the enhancers of *Afp* gene, not the *Alb* gene (Figure 3.30C). These data suggest that the bivalent marks of H3K4me3 and H3K27me3 cooperation to regulate the transcription of *Alb*, whereas the active enhancer mark H3K27ac contributes to the expression of *Afp*.

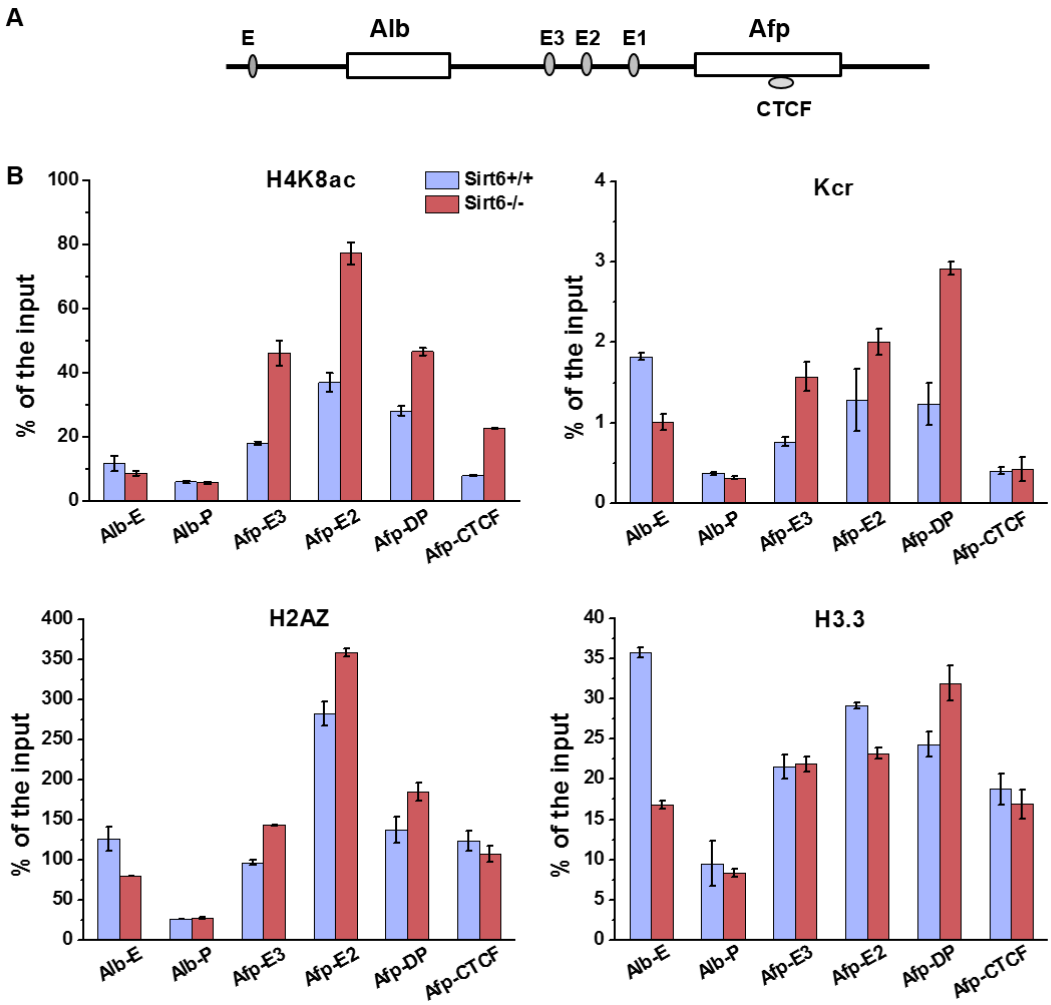

Figure 3.31 ChIP analyses of the occupancies of histone marks at the *Alb/Afp* gene locus in Sirt6$^{+/+}$ and Sirt6$^{-/-}$ pmHep. (A) Schematic representation of the *Alb/Afp* gene locus (see also Figure 3.29 and Figure 1.3). (B) Sirt6$^{+/+}$ (blue) and Sirt6$^{-/-}$ (red) pmHep were used for ChIP. The cells were cross-linked, sonicated and IP was performed using H4K8ac, H2AZ, H3.3 and Kcr specific antibodies. DNA was extracted from IP sample and PCR was performed using primers spanning the indicated regions of the *Alb/Afp* gene locus. ChIP profiles of qPCR data were normalized to the input. This experiment was repeated two times and a representative result was shown. Error bars indicate s.d.

Moreover, the other histone modifications were also analyzed by performing ChIP with the specific antibodies. As shown in Figure 3.31B, the enrichments of active marks for enhancers such as H4K8ac and Kcr showed a strong increase at the enhancers of *Afp* in Sirt6 KO mice, which is similar with that of H3K27ac. However, there was almost no difference of histone variants H3.3 and H2AZ at the locus of *Afp* gene. Interestingly, active marks at regulatory regions of *Afp/Alb* gene locus showed some conflicting data. Specifically, acetylated histones like H3K9ac, H3K27ac and H4K8ac showed no difference at the enhancer of *Alb* in Sirt6-deficient mice, but the other two histone variants H3.3 and H2AZ together with the enhancer mark Kcr drop at this site.

Taken together, loss of Sirt6 induces the active markers including H3K9ac, H3K27ac, H4K8ac and Kcr enriched at the enhancers of *Afp*, not contains H3K4me1, H3K4me3 and H2AZ, which is a bit different at the *Igf2/H19* gene locus. For *Alb* gene locus of Sirt6-deficent pmHep, the upregulated enrichment of H3K27me3 together with the decreased H3K4me3, H2AZ and H3.3 contribute to the transcription of *Alb*.

3.2.4 Bindings of Foxa1/2 at the *Alb/Afp* gene locus in the absence of Sirt6

Transcription factor-enhancer interactions are not only tissue specific but also differentiation dependent (Alder et al., 2014). Foxa1/2 acts critical in cell differentiation and cell identity (Li et al., 2012a). To better understand the mechanism, the enrichments of Foxa1 and Foxa2 at the *Alb/Afp* gene locus were characterized. As shown in Figure 3.32B and C, Foxa1/2 was prominent enriched at the enhancers region of *Afp*, and at both enhancer and promoter of *Alb* in WT. As expected, the occupancy significantly increased at *Afp* enhancers region and decreased at *Alb* enhancers when Sirt6 was lost, while no difference at promoter of both *Afp* and *Alb*. These results together with the Foxa1/2 data at the *Igf2/H19* gene locus confirmed that Sirt6 regulates these hepatic differentiation-related genes through influences Foxa1/2 switching their target enhancers. Interestingly, the acetylated Foxa2 at the *Alb/Afp* gene locus also exhibited the similar trend with that at the *Igf2/H19* gene locus, which is more enriched at enhancers of *Afp* in Sirt6-deficient mouse, especially at E2 (Figure 3.32D). Moreover, the enrichment of histone H1.4 also exhibited a downward trend at the enhancers and promoters of *Afp* gene,

even though not specifically (Figure 3.32E). Altogether, these data indicate that Sirt6 participates in expression of *Alb* and *Afp* directly by recruiting the pioneer factor-Foxa1/2, especially the acetylated Foxa2. For the oncofetal gene *Afp*, loss of Sirt6 activates its enhancers by recruiting Foxa1 and Foxa2; while for the hepatic differentiation marker *Alb*, Sirt6 knockout represses their enhancers' activity by blocking Foxa1/2 binding. This enhancer switch of Foxa1 and/or Foxa2 is Sirt6-dependent.

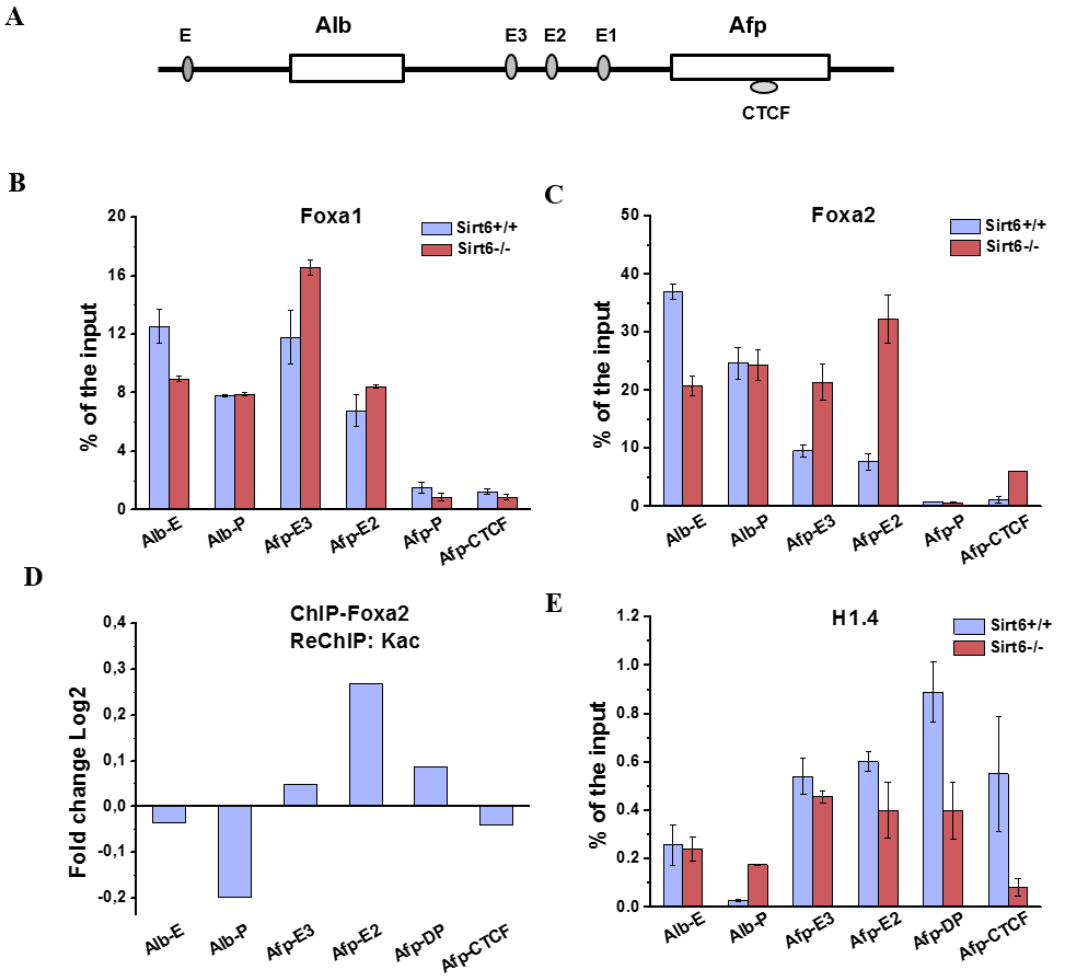

Figure 3.32 ChIP analysis of Foxa1/2 binding at the *Alb/Afp* gene locus in the absence of Sirt6. (A) Schematic representation of the *Alb/Afp* gene locus (see also Figure 3.29 and Figure 1.3). (B, C and E) ChIP of Foxa1, Foxa2 and histone H1.4 at the *Alb/Afp* gene locus in Sirt6$^{+/+}$ (blue) and Sirt6$^{-/-}$ (red) pmHep. (D) ReChip analysis of occupancy of acetylated Foxa2 at the *Alb/Afp* gene locus in pmHep. The cells were cross-linked, sonicated and IP was performed using Foxa1, Foxa2 and goat IgG antibodies. DNA was extracted from IP sample and PCR was performed using primers spanning the indicated regions of the *Alb/Afp* gene locus. For the reChIP, the 1st IP were performed using Foxa2 specific antibody. Then 2nd IP were using acetylated Lysine (Kac). ChIP and reChIP profiles of qPCR data were normalized to the input, and then that in Sirt6$^{-/-}$ by normalizing with that in Sirt6$^{+/+}$. These experiments were repeated two times and a representative result was shown. Error bars indicate s.d.

3.2.5 Recruitments of CTCF and Rad21 at the *Alb/Afp* gene locus when Sirt6 was lost

Through checking the ChIP-seq of CTCF and Rad21 at the UCSC website, both proteins are enriched at the *Alb/Afp* gene locus. To further characterize whether these two proteins are involved into the differentiation in the context of Sirt6, the recruitments of these two proteins were analyzed by ChIP in Sirt6$^{+/+}$ and Sirt6$^{-/-}$ pmHep (Figure 3.33). Interestingly, both CTCF and Rad21 only bind at the CTCF-binding locus of *Afp* (Afp-CTCF), which is similar with that at the *Igf2*/*H19* gene locus. Furthermore, Sirt6 knockout also induces the enrichment of CTCF and Rad21, especially Rad21 (about 10 times increase). These results also implicate that CTCF and cohesin maybe participate the chromatin structure of the *Alb/Afp*, and contribute to the transcription of both genes. In summary, Sirt6 regulates the expression of hepatic differentiation-related genes not only depend on the pioneer factor, Foxa1/2, but also require the architectural proteins, CTCF and cohesin.

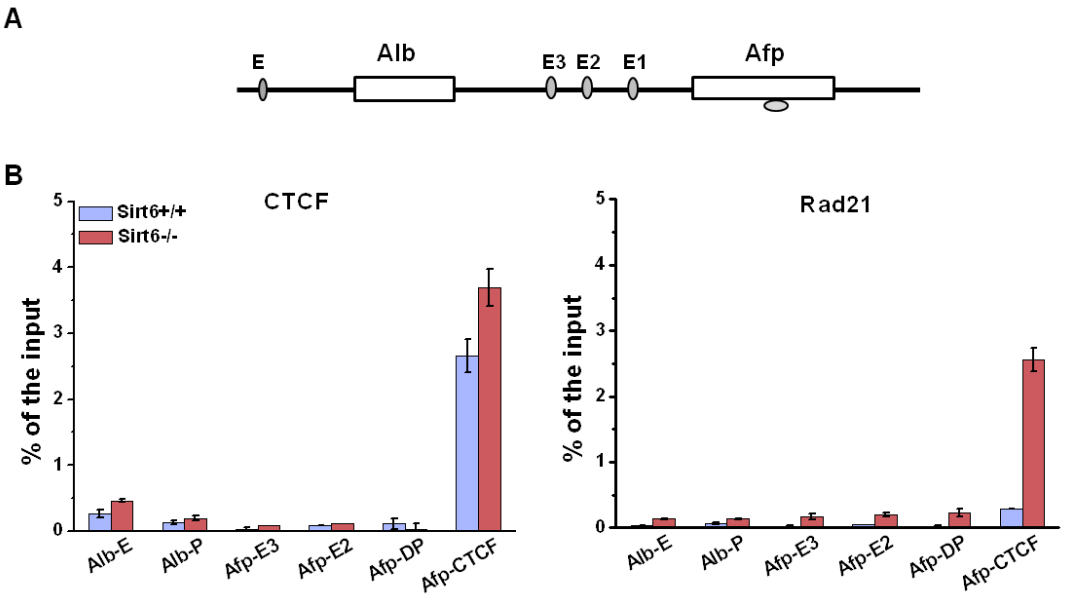

Figure 3.33 ChIP analyses of CTCF and Rad21 binding at the *Alb/Afp* gene locus in Sirt6$^{+/+}$ and Sirt6$^{-/-}$ pmHep. (A) Schematic representation of the *Alb/Afp* gene locus (see also Figure 3.29 and Figure 1.3). (B) Occupancies of CTCF and Rad21 at the *Alb/Afp* gene locus. Sirt6$^{+/+}$ (blue) and Sirt6$^{-/-}$ (red) pmHep were used for ChIP. The cells were cross-linked, sonicated and IP was performed using CTCF and Rad21 specific antibodies. DNA was extracted from IP sample and PCR was performed using primers spanning the indicated regions of the *Alb/Afp* gene locus. ChIP profiles of qPCR data were normalized to the input. This experiment was repeated three times and a representative result was shown. Error bars indicate s.d.

3.3 Sirt6 in regulation of recruitment of PRC2

3.3.1 Bindings of PRC2 proteins at the *Igf2/H19* gene locus in Sirt6-deficient mouse

PRC2 is primarily known for its role in epigenetic gene silencing. Previous reports also proved that PRC2 is required for orchestrating chromatin loop structures of the *Igf2/H19* gene locus (Li et al., 2008; Zhang et al., 2011).

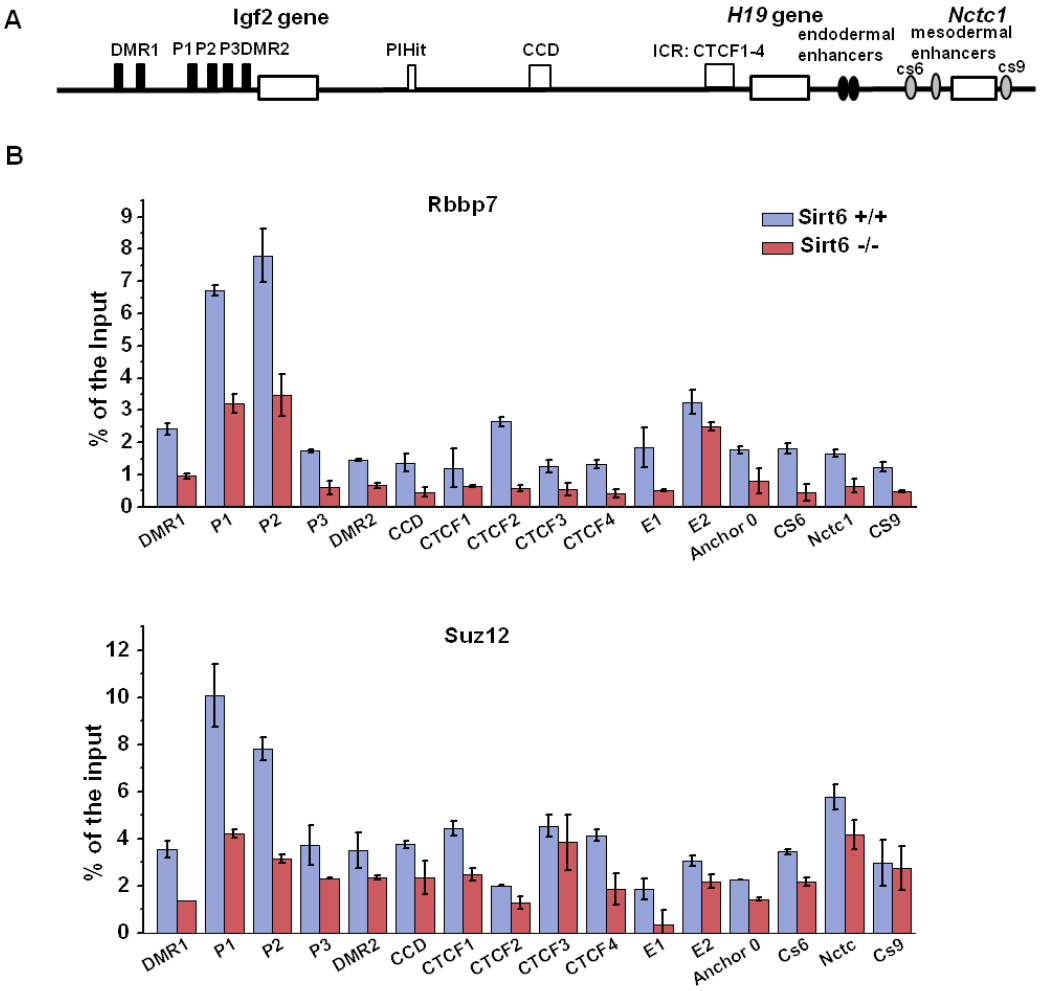

Figure 3.34 ChIP analyses of PRC2 proteins binding at the *Igf2/H19* gene locus in Sirt6-deficient mouse. (A) Schematic representation of the mouse *Igf2/H19* gene locus (see also Figure 3.4 and Figure 1.2). (B) ChIP analysis of Rbbp7 and Suz12 binding at the *Igf2/H19* gene locus in Sirt6$^{+/+}$ (blue) and Sirt6$^{-/-}$ (red) pmHep. The cells were cross-linked, sonicated and IP was performed using Rbbp7 and Suz12 specific antibodies. DNA was extracted from IP sample and PCR was performed using primers spanning the indicated regions of the *Igf2/H19* gene locus. ChIP profiles of qPCR data were normalized to the input. This experiment was repeated 3 times and a representative result was shown. Error bars indicate s.d.

To further characterize the functional mechanisms, ChIP analyses of Suz12 and Rbbp7 were performed, the two core components of PRC2, on the *Igf2/H19* gene locus. As shown in Figure 3.34, both Rbbp7 and Suz12 were enriched at the *Igf2* promoters in WT pmHep, such as P1 and P2. In Sirt6 deficient mouse, the enrichments significantly decreased at all the regions analyzed, which are consistent with the reduction of H3K27me3, the product of PRC2 enzyme activity. These data indicate that Sirt6 influences PRC2 binding on the chromosome, followed by acting at histone H3 lysine 27 trimethylation (Figure 3.5C).

3.3.2 Detection of the acetylation level of PRC2 in hepatocytes

To examine whether SIRT6 regulate target genes expression through physically interacting with PRC2, IP-cMyc was performed in SIRT6 overexpressed Hep3B cells. Indeed, IP-Myc pulled down SUZ12 and EZH2 with overexpressed SIRT6-myc in Hep3B cells, even though the interactions are weak (Figure 3.35A). This result was further confirmed by PLA assays (Figure 3.35B), which indicates that SIRT6 physically interacts with PRC2 components.

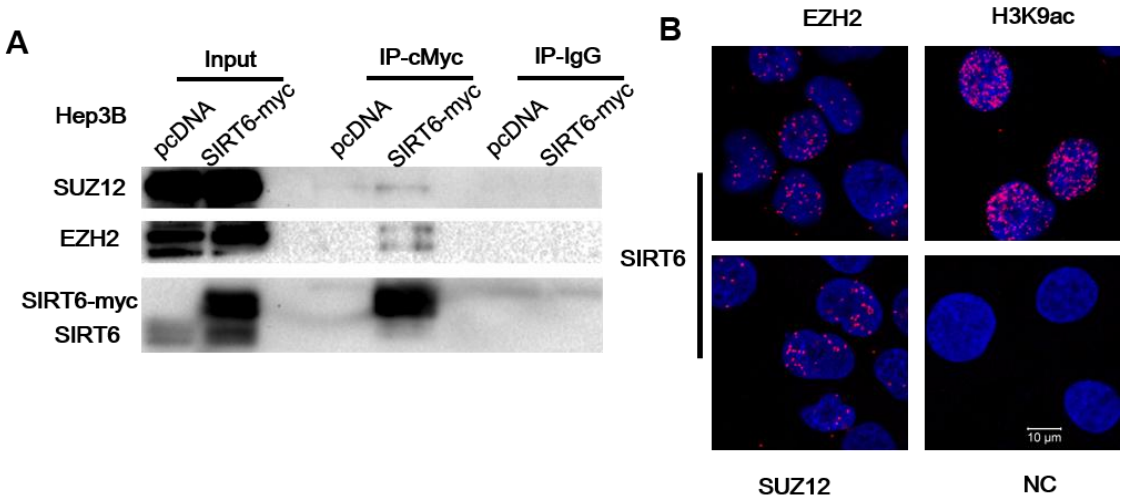

Figure 3.35 Interactions of SIRT6 and PRC2 components in Hep3B by Co-IP and PLA. (A) Co-IP of anti-c-Myc shows physical interaction between SIRT6 and SUZ12, EZH2 in Hep3B SIRT6-myc cells. The detection bands were visualized by WB with the indicated antibodies. The pcDNA was a negative control vector. (B) PLA was performed using fluorescent microscopy images to determine the relative extents of interaction (red spots) between EZH2, SUZ12 and SIRT6. Proximity ligation was performed using a rabbit anti-H3K9ac as positive controls to confirm the interactions with SIRT6. As a negative control (NC), proximity ligation was performed using PLA probes only. White scale bar is 10 μm. (PLA assays in cooperation with Henning Janssen and Dr. Dennis Strand)

In order to test whether SIRT6 influences the acetylation level of PRC2 components, an IP of Suz12 was performed in pmHep of Sirt6$^{+/+}$ and Sirt6$^{-/-}$. As shown in Figure 3.36, Suz12 was hyper-acetylated when Sirt6 was lost. Consistent with the observation, the Suz12 protein was more interacted with acetylated lysine in the nucleus and cytoplasm of Sirt6-deficient hepatocytes, whereas the interaction of Suz12 and Ezh2 showed strong signals in WT mice by PLA. Interestingly, PLA also exhibited the increased acetylated Rbbp7 in the cytoplasm of Sirt6-deficient hepatocytes (Figure 3.36B).

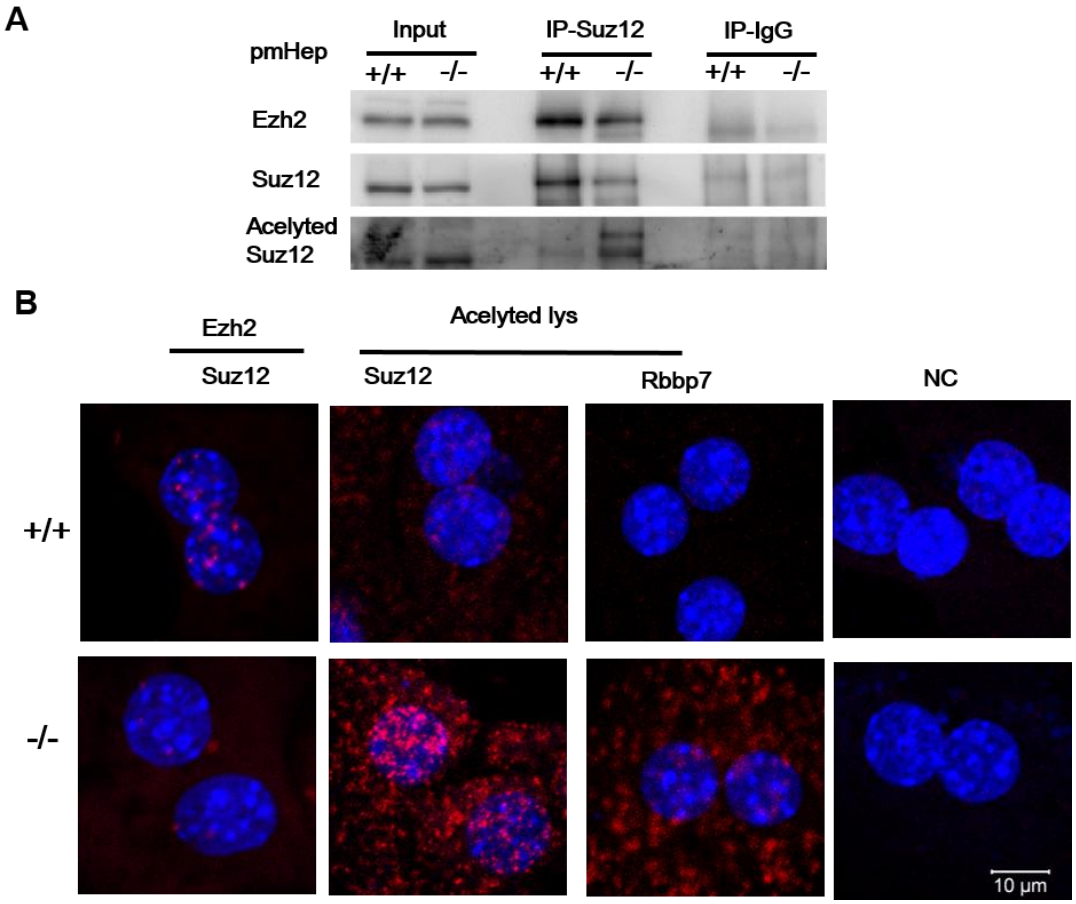

Figure 3.36 Detection of acetylated lysine in proteins of PRC2 complex in Sirt6-deficent pmHep by Co-IP and PLA. (A) The Co-IP was performed using Suz12 antibody in Sirt6$^{+/+}$ and Sirt6$^{-/-}$ pmHep. The detection bands were visualized by WB with the indicated antibodies. Rabbit IgG was used as a negative control. (B) Sirt6$^{+/+}$ and Sirt6$^{-/-}$ pmHep were plated on chamber slide and fixed with 4% PFA. PLA was performed using fluorescent microscopy images to determine the relative extents of interaction (red spots) between PRC2 components or with acetylated lysine. As a negative control of PLA, only PLA probes were used. +/+ and -/- indicate Sirt6$^{+/+}$ and Sirt6$^{-/-}$, respectively. White scale bar is 10 μm. This experiment was repeated 3 times and a representative result was shown. (PLA assays in cooperation with Henning Janssen and Dr. Dennis Strand)

3.3.3 Analysis of Suz12 location in Sirt6$^{+/+}$ and Sirt6$^{-/-}$ pmHep by IF

PLA assay showed that the acetylation of Suz12 was localized at both cytoplasm and nucleus in Sirt6 deficient primary murine hepatocytes (Figure 3.36B), therefore, whether Sirt6 influences the localization of Suz12 protein were examined. As previously reported, Suz12 was a nuclear protein in WT hepatocytes. However, Suz12 was efficiently excluded from the nucleus and largely detected in the cytoplasm after loss of Sirt6 (Figure 3.37). These data indicate that Sirt6 influences the translocation of Suz12 protein.

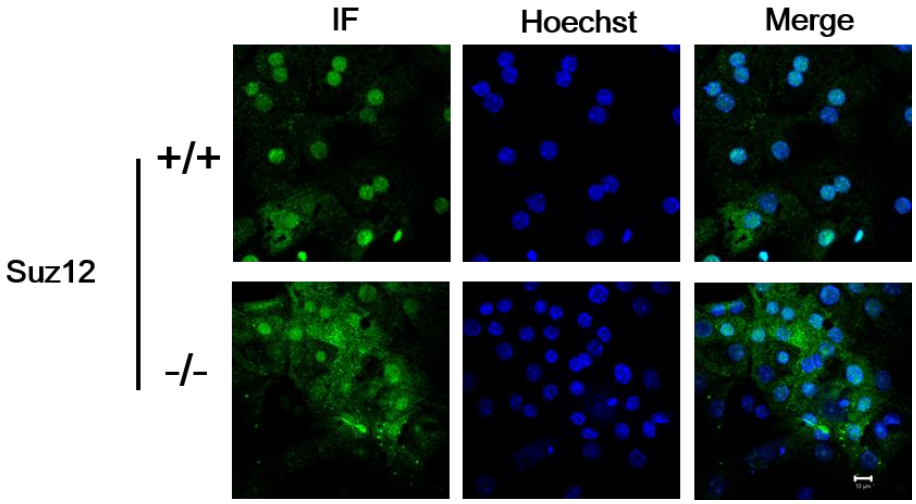

Figure 3.37 Immunofluorescence of Suz12 in Sirt6$^{+/+}$ and Sirt6$^{-/-}$ pmHep. Sirt6$^{+/+}$ and Sirt6$^{-/-}$ pmHep were plated on chamber slide and fixed with 4% PFA. Cells were stained with Suz12 specific antibody and visualized by using Alexa-488 labeled 2nd antibody. Hoechst was used to visualize the nuclear staining. +/+ and -/- indicate Sirt6$^{+/+}$ and Sirt6$^{-/-}$, respectively. White scale bar is 20 µm. This experiment was repeated 3 times and a representative result was shown.

3.3.4 Analysis of sumoylation of Suz12 in Sirt6$^{+/+}$ and Sirt6$^{-/-}$ pmHep

SUZ12 and EZH2 were previously reported to be sumoylated (Riising et al., 2008) and SUMO-regulated processes are well-defined and known for regulating gene transcription and protein localization (Stielow et al., 2008). To investigate whether SIRT6 influences the interaction between Sumo protein and PRC2 components, IP-Suz12 was performed in mouse hepatocytes. As shown in Figure 3.38, Suz12 interacted with Sumo1 and Sumo2/3, and the interaction was reduced with Sirt6 deletion, especially the interaction with Sumo2/3. Consequently, Sirt6 facilities Suz12 interacting with Sumo proteins.

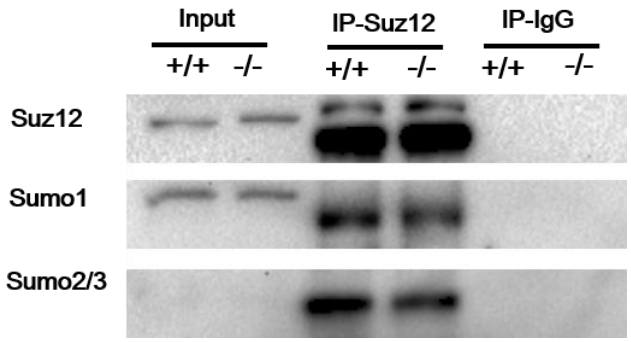

Figure 3.38 Detection of the interaction of Suz12 and Sumo proteins in Sirt6$^{+/+}$ and Sirt6$^{-/-}$ pmHep by Co-IP. The Co-IP was performed using Suz12 specific antibody in Sirt6$^{+/+}$ and Sirt6$^{-/-}$ pmHep. The detection bands were visualized by WB with the indicated antibodies. Rabbit IgG was used as a negative control. +/+ and -/- indicate Sirt6$^{+/+}$ and Sirt6$^{-/-}$, respectively.

3.3.5 Analysis of the occupancy of PRC2-mediated H1K25me3

PRC2 mediated gene silencing, in addition to target methylation of histone H3K27, also acts at histone H1.4 lysine 25 to compact nucleosome (Daujat et al., 2005; Kuzmichev et al., 2005). Thus, immunoprecipitation assays were applied to check the relation between PRC2 and histone H1.4. As expected, loss of Sirt6 eliminated the interaction between Suz12, Ezh2 and histone H1.4 (Figure 3.39).

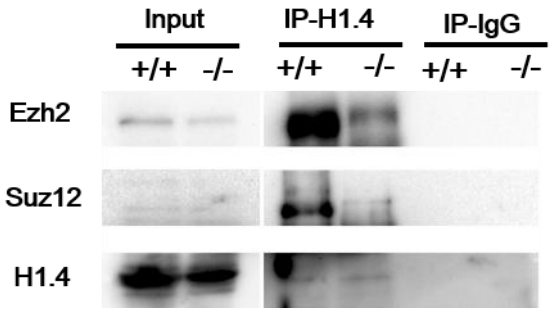

Figure 3.39 Detection of the interactions of PRC2 proteins and histone H1.4 Sirt6$^{+/+}$ and Sirt6$^{-/-}$ pmHep by Co-IP. IP was performed with histone H1.4 specific antibody and IP complexes were detected using western blotting with specific antibodies against Suz12, Ezh2 and histone H1.4. Anti-IgG antibody was used as a negative IP control. +/+ and -/- indicate Sirt6$^{+/+}$ and Sirt6$^{-/-}$, respectively.

To better understand the relationship of PRC2 and histone H1 in the context of Sirt6, ChIP-H1K25me3 analysis at the locus of *Alb/Afp* and *Igf2/H19* were performed. Strikingly, the occupancy of H1K25me3 mainly focused at the ICR region and promoters of *Igf2*, and exhibited a down trend in Sirt6-deficient pmHep (Figure 3.40A). The reduced occupancy at

ICR showed an opposite trend compared with that of CTCF and Rad21 (Figure 3.17). Thus, Sirt6 regulates *H19* and *Igf2* expression through recruiting H1K25me3, not only through H3K27me3, the classic modification by PRC2.

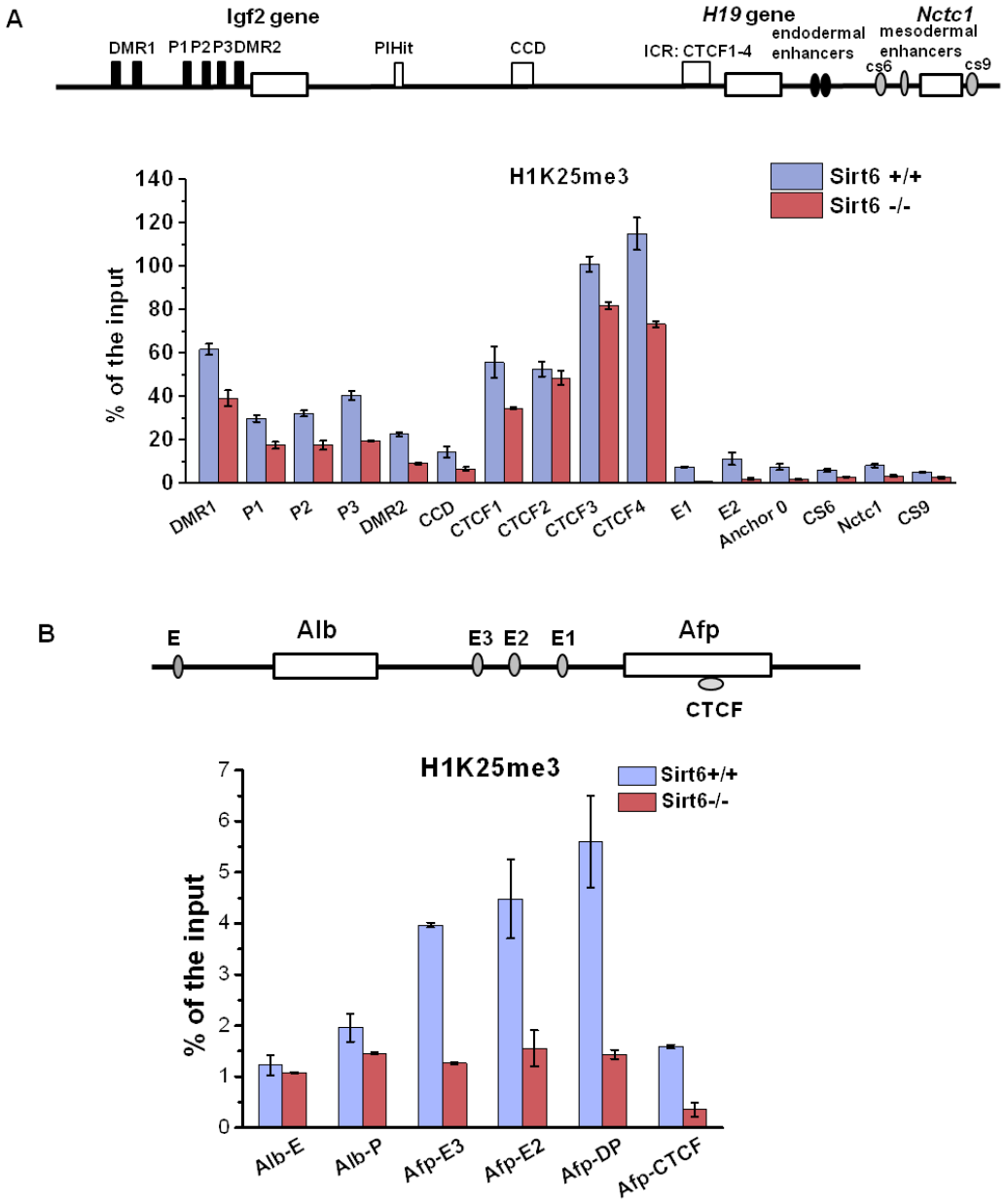

Figure 3.40 ChIP analysis of the occupancy of H1K25me3 at the *Igf2/H19* and *Alb/Afp* gene locus in Sirt6-deficient pmHep. (A-B) Schematic representation of the mouse *Igf2/H19* (see also Figure 3.4) and *Alb/Afp* gene locus (see also Figure 3.29). ChIP analysis of H1K25me3 at the *Igf2/H1*9 (A) and *Alb/Afp* (B) gene locus. Sirt6$^{+/+}$ (blue) and Sirt6$^{-/-}$ (red) pmHep were used for ChIP. The cells were cross-linked, sonicated and IP was performed using H1K25me3 specific antibody. DNA was extracted and PCR was performed using primers spanning the indicated regions of the *Igf2/H19* gene locus. ChIP profiles of qPCR data were normalized to the input. This experiment was repeated 3 times and a representative result was shown. Error bars indicate s.d.

For *Alb/Afp* locus, the enrichment of H1K25me3 was prominent at the enhancers and promoters of *Afp* gene and showed significantly decrease when knockout Sirt6. However, the enrichment of H1K25me3 did not exhibit strong difference at the locus of the *Alb* gene (Figure 3.40B). These data indicate that the occupancy of H1K25me3 at *Afp/Alb* gene locus is also altered by Sirt6 deletion.

4 Discussion

4.1 Loss of Sirt6 activates oncofetal genes expression in hepatocytes

4.1.1 Loss of Sirt6 activates oncofetal genes expression in Foxa1/2-dependent manner

Previous study has identified up-regulation of the known HCC biomarkers including *Afp, Igf2, H19*, and *GPC3* in Sirt6 deficient hepatocytes (Marquardt et al., 2013). These up-regulated genes belong to the hepatic oncofetal gene class. This class of genes are expressed abundantly in the fetal liver and inactive in the normal adult liver, but are frequently reactivated in HCC (Morford et al., 2007). Interestingly, decreased SIRT6 expression is also an early event in tumor development (Lai et al., 2013). These findings indicate that SIRT6 regulates the expression of hepatic oncofetal genes in early stage of development. Activation of genes is associated with tissue-specific transactivation factors. Foxa family members, including Foxa1 and Foxa2, are known to be involved in fetal liver development, and livers fail to form in mice when both Foxa1 and Foxa2 are deleted in foregut endoderm after gastrulation (Lee et al., 2005). More important, HCC is completely reversed in Foxa1 and Foxa2-deficient mice after diethylnitrosamine-induced hepatocarcinogenesis (Li et al., 2012b). Recent studies have already shown that Foxa, belonging to the group of liver-enriched factors, drive embryonic gene expression, such as *H19*, *Igf2*, *Gpc3* and *Afp* (Alder et al., 2014; Long and Spear, 2004). These findings suggest that Sirt6 might function as a negative regulator of Foxa1/2. Indeed, these ChIP data generated from primary murine and human hepatocytes and Hep3B cells, could demonstrate that loss of Sirt6 induces Foxa1/2 to bind specifically at the enhancers of oncofetal genes including *H19*, *Igf2* and *Afp*. In order to characterize the relationship between Foxa and SIRT6, Co-IP and PLA assays were performed in primary mouse hepatocytes. These experiments showed that Sirt6 maybe deacetylate Foxa2 *in vivo.* ReChIP also identified the dramatically enhanced acetylation of Foxa2 specifically at E1 of *H19* after loss of Sirt6. Like the increased occupancy at E1 of the *Igf2/H19* gene locus, the recruitments of Foxa1/2 also significantly up-regulated at the enhancers of *Afp* like E3 in

Sirt6-deficient mouse. Given the fact that Foxa2 acetylation facilities its localization in the nucleus and promotes transcriptional activity (von Meyenn et al., 2013), multiple hepatic oncofetal genes are induced by Foxa1/2 in the absence of Sirt6.

4.1.2 Sirt6 influences epigenetic landscapes and the enhancer activity

4.1.2.1 Switch poised enhancer to active enhancer at the Igf2/H19 gene locus in the absence of Sirt6

Large-scale studies recently have demonstrated cancer cells could disrupt enhancer activity at oncogenes or other genes important in tumor pathogenesis (Hnisz et al., 2013). Although TFs play a major instructive role in guiding genomic position of active enhancers in a given cell type, emerging evidence shows that high mobility of enhancer-associated nucleosomes is not merely a consequence of the competition with TFs, but represents an inherent and important feature of enhancer chromatin (Calo and Wysocka, 2013). Nucleosomes containing H2AZ are biochemically less stable and therefore easier to displace from DNA than canonical nucleosomes (Jin and Felsenfeld, 2007). This initial binding of H2AZ can in turn induce the binding of the pioneer factor Foxa2, driving the action of chromatin remodeling complexes such as SWI/SNF in subsequent steps that finally leads the removal of nucleosomes from the enhancers (Li et al., 2012a). As shown in this study, ChIP analyses of Foxa1/2 and histone H2AZ fully demonstrate this theory when Sirt6 is deleted. Moreover, pioneer factor Foxa could open compacted chromatin and displaces the linker histone H1 to activate target gene expression (Cirillo et al., 2002a; Cirillo et al., 1998). ChIP assays of proteins of histone H1 demonstrate that Sirt6 deletion causes a strongly specific displacement of histone H1.4 and H1.2 at E1 of *Igf2/H19* locus, the only binding site of Foxa1/2.

In addition to nucleosome deposition and attracting pioneer factors for displacement, the enhancer chromatin also requires being active through histone modification. Enhancers are classified into poised and active states according to the status of the H3K27 residue. Thereby H3K27me3 together with H3K4me1 marks the poised enhancers and H3K27ac with H3K4me1 means the active enhancers (Creyghton et al., 2010; Zentner et al., 2011). The data of these histone marks suggest that the poised enhancer switches into active enhancer after loss of Sirt6. During the process, other histone markers also play important

roles, such as H3K4me3, that was prominent enriched at the promoter regions, showing a sharply increased level after loss of Sirt6. It is known that H3K4me3 is able to regulate the preinitiation complex assembly, that leads to selective gene activation (Lauberth et al., 2013). The enriched H4K8ac and H3K9ac contribute for the recruitment of SWI/SNF and TFIID (Agalioti et al., 2002). Therefore, Sirt6 mediates epigenetic landscape alterations that influence the switch of the enhancer statement.

4.1.2.2 The IGF2/H19 enhancers region belongs to the class of super-enhancer

Analyses of ChIP profiles showed that the ratios of enhancer markers like H3K27 and H3K4 both exhibit highly increased enrichment in the absence of Sirt6. This observation together with the data of ChIP and 3C indicate that the enhancers region of the *Igf2/H19* is more than a typical enhancer, which is already validated as a stretch enhancer (Parker et al., 2013). Because both *H19* and *IGF2* serve as bio-markers of HCC, the enhancers region may be belong to the class of super-enhancers, a subset of stretch enhancers, which are generated at oncogenes and other genes important in tumor pathogenesis of cancer cells (Loven et al., 2013). The CRISPR-Cas technology indicates that the endodermal enhancers are the master regulators for transcriptions of *H19* and *IGF2*, which is consistent with previous studies (Arney, 2003; Leighton et al., 1995; Vernucci et al., 2000). In addition, the reduced expression of both genes are more than 60% and 90% in ME mono-deletion and bivalent-deletion clone, respectively. These data proves the important of mesodermal enhancers, which was confirmed by knockout the whole enhancers region. For instance, *H19* decreased another 12% in comparison with the EE deletion in mono-deletion. Thus, these data and the size of the region, together with the more than a hundred folds higher expression of *H19* and *IGF2* in the absence of Sirt6, as well as the ChIP-seq of H3K27ac data (data not show), indicates that the whole enhancers region of the *Igf2/H19* acts as a super-enhancer. Moreover, FOXA1 was proved to be one of super-enhancer-associated transcription factor in HepG2 cell (Hnisz et al., 2013), a human hepatocellular liver carcinoma cell line. Consequently, Sirt6 knockout dramatically enhances the tissue-specific enhancers' activity not only via switching poised enhancer to

active enhancer, but also through establishment of the super-enhancer to augment hepatic carcinogenic genes expression program in hepatocytes (Figure 4.1 B).

4.1.2.3 Sirt6 influences DNA methylation

Enrichment of histone markers that mark active enhancers is inversely correlated with DNA methylation density (Calo and Wysocka, 2013). Previous studies have shown that Sirt6 deficiency caused a global DNA hypomethylation of liver tissue (Marquardt et al., 2013) and loss of methylation uncovers intronic enhancer to drive *Igf2* and *H19* expression (Blattler et al., 2014). The bisulphite pyrosequencing assays in Sirt6-knockout hepatocytes demonstrate that DNA methylation is significantly reduced only at the ICR and E1 of the *Igf2/H19* gene locus, which represent CTCF/cohesin and Foxa specific binding site, respectively. Supporting the findings, earlier studies identified that DNA hypomethylation contributes to a stabilization of Foxa (Serandour et al., 2011) and CTCF binding (Nativio et al., 2009; Stedman et al., 2008). Consistent with another report (Fernandez et al., 2015), H3K4me1 is enriched at hypomethylated DNA regions. More recently, up-regulation of 5hmC (5-hydroxymethylcytosine), the oxidized form of 5-mC (5-methylcytosine) catalyzed by TET (the ten-eleven translocation enzymes), is more abundant in Sirt6-deficient ESC cells (Etchegaray et al., 2015). Unlike 5mC, 5hmC coincides with H3K4me1 as well as H3K27ac and follows active enhancer markers during differentiation (Serandour et al., 2011; Stroud et al., 2011). PRC2 directly controls DNA methylation through serving as a recruitment platform (Vire et al., 2006).These data indicates that loss of Sirt6 may facility the release of the PRC2-mediated methylation machinery, which subsequently promotes the oxidation of DNA methylation by TET and provides a platform for pioneer factor as well as TFs binding.

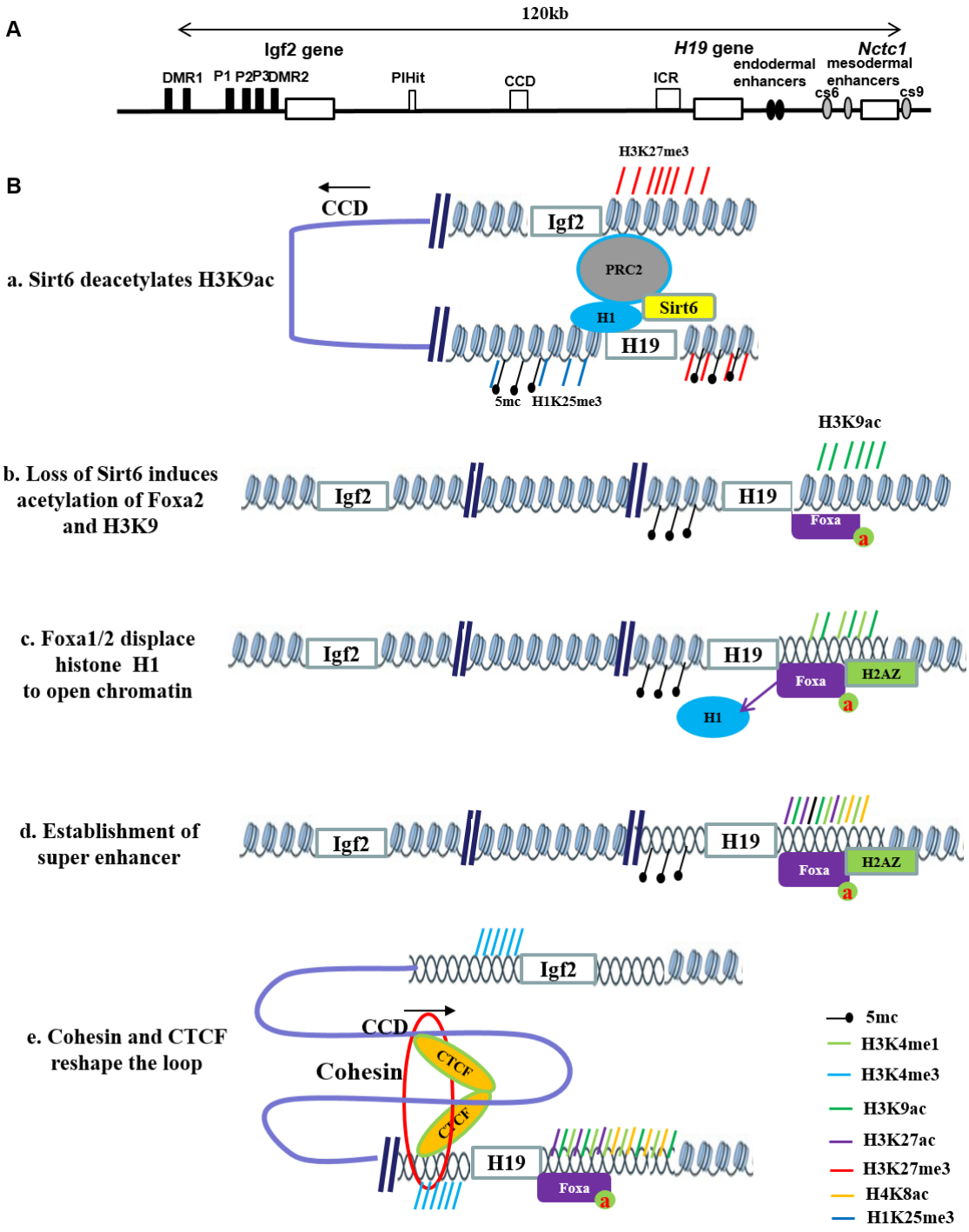

Figure 4.1 Sirt6 regulates an epigenetic switch from PRC2-dependent repression to enhancer-driven oncofetal gene expression. (A) Schematic representation of the mouse *Igf2/H19* locus. (B) Model of PRC2-dependent repression switch to Foxa-mediated activation when Sirt6 was lost. **a.** Genes of *H19* and *Igf2* are silent; all enhancers are inactive or poised and contain ‘‘repressive markers’’—H3K27me3—mediated by polycomb silencers, together with 5mc. Sirt6 deacetylates H3K9ac and enhances the interaction between PRC2 with histone H1.4. **b.** When Sirt6 was lost, H3K9 is more acetylated and enriched at enhancers region, which guides the acetylated pioneer factors (Foxa1 and Foxa2) to bind to specific sites at E1. **c.** The incorporation of H2AZ promoted by H3K4me1 binding, facilitate Foxa1/2 displacement for an open chromatin state.

d. This also leads to the appearance of other histone active marks like H3K27ac and H4K8ac. Thus, the poised enhancer switches into active enhancer due to the enrichments of H3K27ac. **e.** Following changes in chromatin state, the regulatory region becomes condensed, thereby bringing enhancers into proximity with the gene *Igf2* promoter. Cohesin, which is recruited by CTCF at ICR and CCD, has been implicated in stabilizing enhancer-promoter interactions. The orientation of CTCF binding sites determines the direction of topological DNA (Guo et al., 2015). The color lines refer to different histone markers as indicated, and the black lollipops indicate 5mC. The red circle indicates cohesion complex. The proteins are involved in the model as indicated in the picture, e.g. the gray PRC2 complex and the yellow Sirt6. The black arrow indicates the direction of CTCF-binding site at CCD.

4.1.3 Sirt6 is involved in chromatin organization

Proper efficient enhancer-promoter interactions are crucial for the switch from a poised enhancer to active enhancer sate and mediate the cell-type specific expression pattern (Calo and Wysocka, 2013; Wamstad et al., 2014). Based on these aspects, 3C was used to assess the spatial proximity and physical interactions between enhancers and promoters of the *Igf2/H19* gene locus. Three anchors including ICR, DMR1 and E1 were selected, in order to better understand these interactions. Analysis of the 3C data indicates that Sirt6 knockout causes increased reciprocal associations between DMR1, ICR and E1. These associations were also enhanced between these anchors and the enhancer-related elements like *PIHit*, CCD, *Nctc1* and DMR2. For instance, DMR2 is an *Igf2* enhancer which augments *Igf2* transcription (Murrell et al., 2001) and the CCD also has enhancer activity which is independent of its imprinting status (Ainscough et al., 2000; Koide et al., 1994). Hence, loss of Sirt6 increases the interactions among enhancers, promoters and enhancer-promoter, which can act cooperatively to strengthen the enhancement function for *H19* and *Igf2* expression.

The higher-order chromatin conformation always reflects the activities of cohesin and CTCF, since both cohesin and CTCF have been shown to be involved in bringing enhancers and promoters among one another (Dowen et al., 2014; Garrick et al., 2009; Guo et al., 2012; Zuin et al., 2014). ChIP analyses of CTCF and Rad21 in primary murine hepatocytes demonstrated that both were recruited specifically at the ICR and CCD locus and their binding doubled in the absence of Sirt6. Moreover, Co-IP and PLA of these proteins in Hep3B cell demonstrated that SIRT6 physically interacted with cohesin and

CTCF in a reciprocal manner. The 3C data further proved the increased associations between CTCF binding locus (e.g. ICR and CCD) and enhancers like E1 and promoters like DMR1 in Sirt6-deficient mouse. Consequently, it seems likely that Sirt6 is important to reshape CTCF–cohesion-mediated chromatin conformation. However, recent reports suggest that CTCF and cohesin have distinct roles in modulating the higher order structure and gene expression (Gosalia et al., 2014). Specifically, CTCF mediates the interactions between CTCF/cohesin binding sites, some of which have enhancer-blocking insulator activity. Cohesin shares this tethering role, but in addition stabilizes interactions between the promoter and enhancers. Apart from that, cohesion functionally behaves as a tissue-specific transcriptional regulator, colocalize with liver-specific transcription factors at liver-specific targets like Foxa1/2, which is independent of CTCF binding (Gosalia et al., 2014; Schmidt et al., 2010). These suggest cohesion might contribute to tissue-specific transcription, and help to explain why the CTCF-mediated insulator activity is disrupted at the *Igf2/H19* gene locus when Sirt6 was lost. More interestingly, cohesin is highly enriched at ER-bound regions in ER-positive breast cancer cells (Schmidt et al., 2010), however, it is possible that cohesin also stabilizes AR-mediated chromatin associations (Rhodes et al., 2011). Since HCC is sexually dimorphic in humans, with significantly higher incidence in males, and ER recruitment by FOXA1/2 protects against HCC while AR recruitment promotes HCC (Li et al., 2012b). Therefore, cohesion plays a functional role in Foxa1/2-regulated transcription, and may help to mediate tissue-specific transcriptional responses via long-range chromosomal interactions. Most recently, Guo et al. show that the relative orientation of CTCF binding sites in enhancers and promoters determine the direction of topological DNA looping and regulation of gene expression (Guo et al., 2015). The study facilitates us to understand why the stronger association between CCD and all the three anchors (DMR1, ICR and E1), and the enhanced occupancy at CCD of the *Igf2/H19* gene locus in Sirt6-deficient mouse. Generally, loss of Sirt6 alters chromosome architecture via CTCF/cohesion-mediated directional DNA-looping (Figure 4.1B).

4.1.4 Sirt6 regulates PRC2-mediated repression

Interestingly, PRC2 also have been reported to mediate chromatin loops of the *IGF2/H19*

by orchestrating CTCF, in addition to its repressive function on gene expression (Li et al., 2008; Zhang et al., 2011). In pluripotent cells, PRC2 is required for establishing the looping of poised enhancers (Calo and Wysocka, 2013). Consistent with previous studies, Suz12 and Rbbp7, two core components of PRC2, are enriched at the promoters of *Igf2*, and significantly decrease when Sirt6 is lost. PLA and Co-IP assays also demonstrate that Sirt6 could interact with PRC2 proteins. However, ChIP of H3K27me3 at the *Igf2/H19* gene locus exhibits the alteration not only in promoters, but also at enhancers. This is may be due to the altered loop structure, leading to enhanced recruitment of CTCF, which erases the H3K27me3 (Weth et al., 2014). Thus, Sirt6 also participates in reshaping chromatin structure via PRC2 complex. The incorporation of PRC2 contributes to establish the poised enhancer at the *Igf2/H19* gene locus in Sirt6 normal hepatocytes. In summary, all these data demonstrate that Sirt6 reshapes the loop not only through CTCF and cohesin but also via associating with PRC2.

Recent reports have shown that PRC2's role as a gene silencing complex could also performed by catalyzing the trimethylation of lysine 25 on histone H1.4 to compact the nucleosome (Daujat et al., 2005; Kuzmichev et al., 2005). Through characterizing the occupancy profiles of H1K25me3 on *Igf2/H19* gene locus, the substrate of PRC2 exhibits dramatically reduce at ICR in the absence of Sirt6, which suggest that Sirt6-dependent PRC2 regulates the gene expression via H3K27me3 and H1K25me3. Surprisingly, the occupancy of H1K25me3 mainly focused at the ICR of the *Igf2/H19* gene locus, overlapping with that of CTCF, which orchestrates chromatin loop structures together with PRC2 (Li et al., 2008). Next, testing the interaction between PRC2 and histone H1.4 seems to be necessary. Co-IP assays demonstrated that loss of Sirt6 erases the association between Suz12 and histone H1.4. Supporting the data, in the histone H1-depleted (H1.3 and H1.4) mouse embryonic stem cells, expression of H19 is 7-fold upregulated (Fan et al., 2005; Popova et al., 2013). Next step, exploring the relationship between Sirt6 and PRC2 was performed by Co-IP and PLA in primary mouse hepatocytes and Hep3B cells. As expected, SIRT6 physically interacts with PRC2 components and deacetylates Suz12 *in vivo*. In addition to cause the hyperacetylation of Suz12, loss of

Sirt6 leads to its cytoplasmic translocation and dissociation of the PRC2 complex with genome wide depletion of the repressive marker H3K27me3 (data not show). Consistent with the translocation of Suz12, histone H1.4 protein exhibits a cytoplasmic translocation and eventually secrets into serum. Based on these findings, it seems that PRC2 tightly binds histone H1 in normal pmHep, which influences the displacement of Foxa ultimately leading to transcriptional repression. Hence, loss of Sirt6 induces Foxa1/2 displacement of PRC2-interacted histone H1.4.

Strikingly, the sumoylation level of Suz12 reduces after the loss of Sirt6 in pmHep. As previous report, SUMO-regulated processes are well-defined for repression of gene expression (Stielow et al., 2008). SUMO modified sites prevent acetylation of adjacent lysine residues by sterical issues (Wu and Chiang, 2009) or masks as an interaction surface by preventing interaction with TFs (Flotho and Melchior, 2013) as well as promoting recruitment of transcriptional co-repressors (Gill, 2005). Furthermore, SIRT6 was shown to bind PIAS1 (protein inhibitor of activated STAT1), a SUMO E3 ligase (Polyakova et al., 2012), which promote Foxa1 or Foxa2 sumoylation and subsequently regulates the target gene expression (Belaguli et al., 2012; Sutinen et al., 2014; Toropainen et al., 2015). Since covalent attachment of SUMO to PIAS1 also associates to epigenetic repression, such as Pias1 deletion leads to decreased H3K9 methylation and enhanced promoter accessibility (Liu et al., 2010), coincidentally it is the same histone residue that Sirt6 modifies. However, whether Sirt6 interacts with PIAS1 to enhance the sumoylation of PRC2 and/or FOXA to inhibit target gene expression is not known so far.

Taken together, Sirt6 regulates the switch between PRC2 and Foxa2 in three ways (Figure 4.1). Firstly, Sirt6 might enhance the sumoylation of PRC2 and/or Foxa by deacetylating the lysine and operates as a co-repressor to strengthen the repressive ability. Furthermore, the alterations of modification are always associated with changes in subcellular localization that influence their stability. Secondly, Sirt6 regulates PRC2 to influence the nucleosome stability. On the one hand, Sirt6 facilities PRC2 to tightly bind the histone H1, a repressor involved in the formation and stabilization of a condensed chromatin structure. The release of PRC2 from histone H1 contributes to displacement of

pioneer factors. On the other hand, H2AZ incorporation in turn induces the pioneer factor Foxa1/2 to bind, leading to nucleosome deletion (Li et al., 2012a). Although H2AZ is enriched at PRC2 target genes in ES cells, it binds a different subset of genes in lineage-specifying cells (Creyghton et al., 2008). Finally, the switch is connected with methylation alterations. Sirt6 is required for PRC2-dependent DNA methylation maintenance. In contrast, loss of Sirt6 induces the de-methylation of Foxa enriched enhancers, which is beneficial for the recruitment of pioneer factors and other transcriptional factors or remodeler.

4.2 Sirt6 affects hepatocytes differentiation via influencing Foxa2 interactions with enhancers

It is well established that tissue-specific TFs determine cell fate by association with lineage-committed enhancers. Foxa1 and Foxa2, liver-specific TFs, have been suggested to play a critical role in hepatic differentiation and liver development. In consequence of a Foxa1 and Foxa2 knockout, no liver could form in mice in the foregut endoderm following gastrulation (Lee et al., 2005), although no effect on chromatin structure and hepatocyte development could be observed when the deletion after liver specification (Li et al., 2011). Previously publication suggested that cell differentiation is one of the pathways showing the most dramatic effects following Sirt6 knockout as determined by GeneGo analysis (Marquardt et al., 2013). A very recent study also proved that SIRT6 acts as a chromatin regulator safeguarding the balance between pluripotency and differentiation (Etchegaray et al., 2015). Then the expression of Foxa2-mediated hepatic differentiation genes in the microarray was analyzed, which was carried out with total RNA isolated from Sirt6$^{-/-}$ and wild type primary murine hepatocytes. As expected, Sirt6 regulates Foxa2-mediated hepatic differentiation through up-regulation of the embryonic genes and repressing genes involved in differentiation. Next, qRT-PCR was performed and confirmed the microarray data: the differentiation markers including *Alb* and *Cyp3a41* were significantly downregulated, whereas oncofetal makers (*H19, Igf2* and *Af*p) were dramatically elevated in Sirt6-mutant mice. Meantime, this trend was reversed when an over-expression of

SIRT6 in Hep3B cells was induced. Functional analysis of this regulatory mechanism at the *Alb/Afp* gene locus, the classic hepatic differentiation model, demonstrates that Sirt6-deficiency causes the recruitment of Foxa1/2 showing an increased incidence at enhancers of hepatoblast gene *Afp* and a reduced appearance at enhancers of differentiation marker *Alb*.

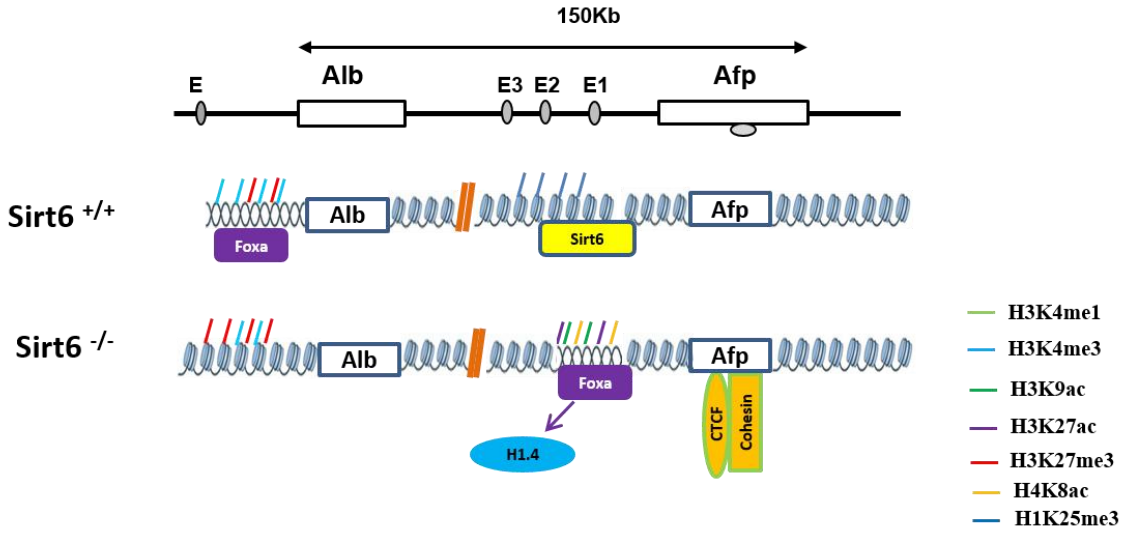

Figure 4.2 Sirt6 affects hepatic differentiation via influencing Foxa2 interactions with enhancers. Schematic representation of the mouse *Alb/Afp* gene locus (see also Figure 3.29). In normal adult hepatocytes, Sirt6 deacetylates H3K9ac and binds at the enhancers region of *Afp* and suppress *Afp* expression, while Foxa2 is recruited to enhancer of *Alb* and induces the activation of *Alb*. When loss of Sirt6, Foxa2 is recruited to enhancers region of *Afp* and displaces histone H1.4, subsequently actives transcription of *Afp*, whereas the expression of differentiation gene *Alb* is blocked. Moreover, CTCF and cohesin are recruited to the CTCF-binding site at *Afp* gene. The color lines refer to different histone markers as indicated.

Furthermore, epigenetics landscape also contributes to the expression of *Alb* and *Afp*. Specifically, loss of Sirt6 induces the active markers including H3K9ac, H3K27ac, H4K8ac and Kcr enriched at the enhancers of *Afp*, not contains H3K4me1, H3K4me3 and H2AZ, which is a bit different at the *Igf2/H19* gene locus; the upregulated enrichment of H3K27me3 together with the decreased H3K4me3, H2AZ and H3.3 contribute to the transcription of *Alb*, which is consistent with the previous study (Kim et al., 2011). Interestingly, the enrichments of the architectural proteins (CTCF and cohesion), especially Rad21 enhanced at the CTCF-binding sites of *Afp* when Sirt6 is lost. Moreover, PRC2 has also been linked to regulate pluripotency and differentiation in ESCs and

hepatic progenitor cells (Koike et al., 2014; Margueron and Reinberg, 2011; Obier et al., 2015; Pasini et al., 2007). However, ChIP assays of Suz12 (data not show), H3K27me3 and H1K25me3 at *Afp/Alb* gene locus suggest that PRC2-mediated repression is not evident at the regions of differentiation gene *Alb*. By contrast, there is no difference of the methylation level at the locus when Sirt6 is deleted (data not show). Consequently, loss of Sirt6 induces Foxa2 enhancer switch in a differentiation-dependent manner.

4.3 Perspective

Reversible post-translational modification (PTM) of proteins is a common and efficient cellular strategy used for rapid modulation of protein activities and protein expression levels (Belaguli et al., 2012). Efforts made in the present study revealed that Sirt6 is important to participate in acetylation and sumoylation modification of Suz12/Foxa2. To this end, the study determined that the modification alteration caused by loss of Sirt6, not only change the subcellular localization, but also influence their transcriptional activities. Conceivably, deciphering the complex interplay between different modifications and their impudence on the recruitment of activation or repression complexes will be necessary to better understand the mechanisms brought about by Sirt6 and hence its tumor-suppressive properties. Thus, further experiments in this direction will be needed to reveal how Sirt6 can balance the different modifications. A possible mechanism may be that Sirt6 interacts with PIAS1 to enhance the sumoylation of PRC2 and/or FOXA, which sterically hinders acetylation of adjacent K residues, resulting in repression of their target genes expression. In contrast, loss of Sirt6 impairs the activity of sumoylation but enhances that of acetylation, resulting in the dissociation of the PRC2 complex and enhances the FOXA transcription functions, respectively. These possibilities remain to be investigated in the future.

This study already demonstrates that Sirt6 regulates the subcellular localization of the Suz12 component and enhances the repressive activity of PRC2, subsequently influencing its role in target gene expression. However, the global reduced occupancy and protein level of H3K27me3 in Sirt6 knockout mice maybe indicate the diverse roles of

PRC2. Therefore, it would be interesting to investigate more closely the functional enrichment of genes that are altered in ChIP-seq of H3K27me3 with regard to their role in different networks and signaling pathways. By comparing with that in microarray of Sirt6 knockout pmHep, select the high values and important subset gene to characterize the mechanism. Up to date, accumulating evidence have revealed frequent aberrant expression of PRC2 components and their downstream molecular effects in promoting hepatocarcinogenesis (Au et al., 2013). HCC represents a tumor type where a more complete understanding of the underlying genetics could have a major impact on treatment of the disease (Zender et al., 2006). A better understanding of the mechanism between Sirt6 and PRC2 may contribute to the design of novel therapeutic strategies against HCC or other different cancer.

Sirt6, the regulator of lifespan and aging-related disease, performs its multiple roles via different enzymatic reactions include deacetylation, deacylation and ADP-ribosylation, all of which use NAD^+ as a cofactor. These multitasking enzymatic activities pave the way for its pleiotropic functions in genomic stability, metabolism and differentiation. Hence, new mechanistic insights and far-reaching functions can be derived from the discovery of highly specific substrates of Sirt6. Moreover, with a better understanding of the diverse roles, improved treatment strategies can be designed against Sirt6-related disease and cancer.

5 References

Adinolfi, M., and Lessof, M.H. (1985). Cancer, oncogenes and oncofetal antigens. The Quarterly journal of medicine *54*, 193-204.

Agalioti, T., Chen, G., and Thanos, D. (2002). Deciphering the transcriptional histone acetylation code for a human gene. Cell *111*, 381-392.

Ainscough, J.F., John, R.M., Barton, S.C., and Surani, M.A. (2000). A skeletal muscle-specific mouse Igf2 repressor lies 40 kb downstream of the gene. Development *127*, 3923-3930.

Akhtar-Zaidi, B., Cowper-Sal-lari, R., Corradin, O., Saiakhova, A., Bartels, C.F., Balasubramanian, D., Myeroff, L., Lutterbaugh, J., Jarrar, A., Kalady, M.F*., et al.* (2012). Epigenomic enhancer profiling defines a signature of colon cancer. Science *336*, 736-739.

Alder, O., Cullum, R., Lee, S., Kan, A.C., Wei, W., Yi, Y., Garside, V.C., Bilenky, M., Griffith, M., Morrissy, A.S*., et al.* (2014). Hippo signaling influences HNF4A and FOXA2 enhancer switching during hepatocyte differentiation. Cell reports *9*, 261-271.

Ariel, I., Ayesh, S., Perlman, E.J., Pizov, G., Tanos, V., Schneider, T., Erdmann, V.A., Podeh, D., Komitowski, D., Quasem, A.S*., et al.* (1997). The product of the imprinted H19 gene is an oncofetal RNA. Molecular pathology : MP *50*, 34-44.

Ariel, I., Miao, H.Q., Ji, X.R., Schneider, T., Roll, D., de Groot, N., Hochberg, A., and Ayesh, S. (1998). Imprinted H19 oncofetal RNA is a candidate tumour marker for hepatocellular carcinoma. Molecular pathology : MP *51*, 21-25.

Arney, K.L. (2003). H19 and Igf2--enhancing the confusion? Trends in genetics : TIG *19*, 17-23.

Au, S.L., Ng, I.O., and Wong, C.M. (2013). Epigenetic dysregulation in hepatocellular carcinoma: focus on polycomb group proteins. Frontiers of medicine *7*, 231-241.

Au, S.L., Wong, C.C., Lee, J.M., Fan, D.N., Tsang, F.H., Ng, I.O., and Wong, C.M. (2012). Enhancer of zeste homolog 2 epigenetically silences multiple tumor suppressor microRNAs to promote liver cancer metastasis. Hepatology *56*, 622-631.

Belaguli, N.S., Zhang, M., Brunicardi, F.C., and Berger, D.H. (2012). Forkhead box protein A2 (FOXA2) protein stability and activity are regulated by sumoylation. PloS one *7*, e48019.

Blattler, A., Yao, L., Witt, H., Guo, Y., Nicolet, C.M., Berman, B.P., and Farnham, P.J. (2014). Global loss of DNA methylation uncovers intronic enhancers in genes showing expression changes. Genome biology *15*, 469.

Borensztein, M., Monnier, P., Court, F., Louault, Y., Ripoche, M.A., Tiret, L., Yao, Z., Tapscott, S.J., Forne, T., Montarras, D*., et al.* (2013). Myod and H19-Igf2 locus interactions are required for diaphragm formation in the mouse. Development *140*, 1231-1239.

Boyer, L.A., Plath, K., Zeitlinger, J., Brambrink, T., Medeiros, L.A., Lee, T.I., Levine, S.S., Wernig, M., Tajonar, A., Ray, M.K*., et al.* (2006). Polycomb complexes repress developmental regulators in murine embryonic stem cells. Nature *441*, 349-353.

Cai, M.Y., Hou, J.H., Rao, H.L., Luo, R.Z., Li, M., Pei, X.Q., Lin, M.C., Guan, X.Y., Kung, H.F., Zeng, Y.X*., et al.* (2011a). High expression of H3K27me3 in human hepatocellular carcinomas correlates closely with vascular invasion and predicts worse prognosis in patients. Molecular medicine *17*, 12-20.

Cai, M.Y., Tong, Z.T., Zheng, F., Liao, Y.J., Wang, Y., Rao, H.L., Chen, Y.C., Wu, Q.L., Liu, Y.H., Guan, X.Y*., et al.* (2011b). EZH2 protein: a promising immunomarker for the detection of hepatocellular carcinomas in liver needle biopsies. Gut *60*, 967-976.

Calo, E., and Wysocka, J. (2013). Modification of Enhancer Chromatin: What, How, and Why?

Molecular cell *49*, 825-837.

Canver, M.C., Bauer, D.E., Dass, A., Yien, Y.Y., Chung, J., Masuda, T., Maeda, T., Paw, B.H., and Orkin, S.H. (2014). Characterization of Genomic Deletion Efficiency Mediated by Clustered Regularly Interspaced Palindromic Repeats (CRISPR)/Cas9 Nuclease System in Mammalian Cells. J Biol Chem *289*, 21312-21324.

Cao, R., Wang, L., Wang, H., Xia, L., Erdjument-Bromage, H., Tempst, P., Jones, R.S., and Zhang, Y. (2002). Role of histone H3 lysine 27 methylation in Polycomb-group silencing. Science *298*, 1039-1043.

Caravaca, J.M., Donahue, G., Becker, J.S., He, X., Vinson, C., and Zaret, K.S. (2013). Bookmarking by specific and nonspecific binding of FoxA1 pioneer factor to mitotic chromosomes. Genes & development *27*, 251-260.

Caretti, G., Di Padova, M., Micales, B., Lyons, G.E., and Sartorelli, V. (2004). The Polycomb Ezh2 methyltransferase regulates muscle gene expression and skeletal muscle differentiation. Genes & development *18*, 2627-2638.

Carroll, J.S., Liu, X.S., Brodsky, A.S., Li, W., Meyer, C.A., Szary, A.J., Eeckhoute, J., Shao, W., Hestermann, E.V., Geistlinger, T.R*., et al.* (2005). Chromosome-wide mapping of estrogen receptor binding reveals long-range regulation requiring the forkhead protein FoxA1. Cell *122*, 33-43.

Cha, T.L., Zhou, B.P., Xia, W., Wu, Y., Yang, C.C., Chen, C.T., Ping, B., Otte, A.P., and Hung, M.C. (2005). Akt-mediated phosphorylation of EZH2 suppresses methylation of lysine 27 in histone H3. Science *310*, 306-310.

Chen, Y., Lin, M.C., Yao, H., Wang, H., Zhang, A.Q., Yu, J., Hui, C.K., Lau, G.K., He, M.L., Sung, J*., et al.* (2007). Lentivirus-mediated RNA interference targeting enhancer of zeste homolog 2 inhibits hepatocellular carcinoma growth through down-regulation of stathmin. Hepatology *46*, 200-208.

Cheng, A.S., Lau, S.S., Chen, Y., Kondo, Y., Li, M.S., Feng, H., Ching, A.K., Cheung, K.F., Wong, H.K., Tong, J.H*., et al.* (2011). EZH2-mediated concordant repression of Wnt antagonists promotes beta-catenin-dependent hepatocarcinogenesis. Cancer research *71*, 4028-4039.

Chien, R., Zeng, W., Ball, A.R., and Yokomori, K. (2011). Cohesin: a critical chromatin organizer in mammalian gene regulation. Biochemistry and cell biology = Biochimie et biologie cellulaire *89*, 445-458.

Cirillo, L.A., Lin, F.R., Cuesta, I., Friedman, D., Jarnik, M., and Zaret, K.S. (2002a). Opening of compacted chromatin by early developmental transcription factors HNF3 (FoxA) and GATA-4. Molecular cell *9*, 279-289.

Cirillo, L.A., Lin, F.R., Cuesta, I., Friedman, D., Jarnik, M., and Zaret, K.S. (2002b). Opening of compacted chromatin by early developmental transcription factors HNF3 (FoxA) and GATA-4. Molecular cell *9*, 279-289.

Cirillo, L.A., McPherson, C.E., Bossard, P., Stevens, K., Cherian, S., Shim, E.Y., Clark, K.L., Burley, S.K., and Zaret, K.S. (1998). Binding of the winged-helix transcription factor HNF3 to a linker histone site on the nucleosome. Embo Journal *17*, 244-254.

Clark, K.L., Halay, E.D., Lai, E., and Burley, S.K. (1993). Co-crystal structure of the HNF-3/fork head DNA-recognition motif resembles histone H5. Nature *364*, 412-420.

Clark, T., Maximin, S., Meier, J., Pokharel, S., and Bhargava, P. (2015). Hepatocellular Carcinoma: Review of Epidemiology, Screening, Imaging Diagnosis, Response Assessment, and Treatment. Current problems in diagnostic radiology *44*, 479-486.

Cong, L., Ran, F.A., Cox, D., Lin, S., Barretto, R., Habib, N., Hsu, P.D., Wu, X., Jiang, W., Marraffini, L.A*., et al.* (2013). Multiplex genome engineering using CRISPR/Cas systems. Science *339*, 819-823.

Court, F., Baniol, M., Hagege, H., Petit, J.S., Lelay-Taha, M.N., Carbonell, F., Weber, M., Cathala, G., and Forne, T. (2011). Long-range chromatin interactions at the mouse Igf2/H19 locus reveal a novel paternally

expressed long non-coding RNA. Nucleic acids research *39*, 5893-5906.

Couvert, P., Carrie, A., Tezenas du Montcel, S., Vaysse, J., Sutton, A., Barget, N., Trinchet, J.C., Beaugrand, M., Ganne, N., Giral, P.*, et al.* (2012). Insulin-like growth factor 2 gene methylation in peripheral blood mononuclear cells of patients with hepatitis C related cirrhosis or hepatocellular carcinoma. Clinics and research in hepatology and gastroenterology *36*, 345-351.

Creyghton, M.P., Cheng, A.W., Welstead, G.G., Kooistra, T., Carey, B.W., Steine, E.J., Hanna, J., Lodato, M.A., Frampton, G.M., Sharp, P.A.*, et al.* (2010). Histone H3K27ac separates active from poised enhancers and predicts developmental state. Proceedings of the National Academy of Sciences of the United States of America *107*, 21931-21936.

Creyghton, M.P., Markoulaki, S., Levine, S.S., Hanna, J., Lodato, M.A., Sha, K., Young, R.A., Jaenisch, R., and Boyer, L.A. (2008). H2AZ Is Enriched at Polycomb Complex Target Genes in ES Cells and Is Necessary for Lineage Commitment. Cell *135*, 649-661.

Daujat, S., Zeissler, U., Waldmann, T., Happel, N., and Schneider, R. (2005). HP1 binds specifically to Lys(26)-methylated histone H1.4, whereas simultaneous Ser(27) phosphorylation blocks HP1 binding. Journal of Biological Chemistry *280*, 38090-38095.

Dominy, J.E., Jr., Lee, Y., Jedrychowski, M.P., Chim, H., Jurczak, M.J., Camporez, J.P., Ruan, H.B., Feldman, J., Pierce, K., Mostoslavsky, R.*, et al.* (2012). The deacetylase Sirt6 activates the acetyltransferase GCN5 and suppresses hepatic gluconeogenesis. Molecular cell *48*, 900-913.

Dowen, J.M., Fan, Z.P., Hnisz, D., Ren, G., Abraham, B.J., Zhang, L.N., Weintraub, A.S., Schuijers, J., Lee, T.I., Zhao, K.*, et al.* (2014). Control of cell identity genes occurs in insulated neighborhoods in mammalian chromosomes. Cell *159*, 374-387.

Elson, D.A., and Bartolomei, M.S. (1997). A 5' differentially methylated sequence and the 3'-flanking region are necessary for H19 transgene imprinting. Molecular and cellular biology *17*, 309-317.

Ernst, J., Kheradpour, P., Mikkelsen, T.S., Shoresh, N., Ward, L.D., Epstein, C.B., Zhang, X., Wang, L., Issner, R., Coyne, M.*, et al.* (2011). Mapping and analysis of chromatin state dynamics in nine human cell types. Nature *473*, 43-49.

Etchegaray, J.P., Chavez, L., Huang, Y., Ross, K.N., Choi, J., Martinez-Pastor, B., Walsh, R.M., Sommer, C.A., Lienhard, M., Gladden, A.*, et al.* (2015). The histone deacetylase SIRT6 controls embryonic stem cell fate via TET-mediated production of 5-hydroxymethylcytosine. Nature cell biology *17*, 545-557.

Eun, B., Sampley, M.L., Good, A.L., Gebert, C.M., and Pfeifer, K. (2013). Promoter cross-talk via a shared enhancer explains paternally biased expression of Nctc1 at the Igf2/H19/Nctc1 imprinted locus. Nucleic acids research *41*, 817-826.

Ezhkova, E., Pasolli, H.A., Parker, J.S., Stokes, N., Su, I.H., Hannon, G., Tarakhovsky, A., and Fuchs, E. (2009). Ezh2 orchestrates gene expression for the stepwise differentiation of tissue-specific stem cells. Cell *136*, 1122-1135.

Fan, Y.H., Nikitina, T., Zhao, J., Fleury, T.J., Bhattacharyya, R., Bouhassira, E.E., Stein, A., Woodcock, C.L., and Skoultchi, A.I. (2005). Histone H1 depletion in mammals alters global chromatin structure but causes specific changes in gene regulation. Cell *123*, 1199-1212.

Fernandez, A.F., Bayon, G.F., Urdinguio, R.G., Torano, E.G., Garcia, M.G., Carella, A., Petrus-Reurer, S., Ferrero, C., Martinez-Camblor, P., Cubillo, I.*, et al.* (2015). H3K4me1 marks DNA regions hypomethylated during aging in human stem and differentiated cells. Genome research *25*, 27-40.

Flotho, A., and Melchior, F. (2013). Sumoylation: a regulatory protein modification in health and disease. Annual review of biochemistry *82*, 357-385.

Franceschi, S., and Raza, S.A. (2009). Epidemiology and prevention of hepatocellular carcinoma.

Cancer letters *286*, 5-8.

Friedman, J.R., and Kaestner, K.H. (2006). The Foxa family of transcription factors in development and metabolism. Cellular and molecular life sciences : CMLS *63*, 2317-2328.

Gao, S.B., Zheng, Q.F., Xu, B., Pan, C.B., Li, K.L., Zhao, Y., Zheng, Q.L., Lin, X., Xue, L.X., and Jin, G.H. (2014). EZH2 represses target genes through H3K27-dependent and H3K27-independent mechanisms in hepatocellular carcinoma. Molecular cancer research : MCR *12*, 1388-1397.

Garrick, D., De Gobbi, M., Gibbons, R., and Higgs, D.R. (2009). CTCF, cohesin and higher-order chromatin structure. Epigenomics *1*, 232.

Gil, R., Barth, S., Kanfi, Y., and Cohen, H.Y. (2013). SIRT6 exhibits nucleosome-dependent deacetylase activity. Nucleic acids research *41*, 8537-8545.

Gill, G. (2005). Something about SUMO inhibits transcription. Current opinion in genetics & development *15*, 536-541.

Gosalia, N., Neems, D., Kerschner, J.L., Kosak, S.T., and Harris, A. (2014). Architectural proteins CTCF and cohesin have distinct roles in modulating the higher order structure and expression of the CFTR locus. Nucleic acids research *42*, 9612-9622.

Guo, Y., Monahan, K., Wu, H., Gertz, J., Varley, K.E., Li, W., Myers, R.M., Maniatis, T., and Wu, Q. (2012). CTCF/cohesin-mediated DNA looping is required for protocadherin alpha promoter choice. Proceedings of the National Academy of Sciences of the United States of America *109*, 21081-21086.

Guo, Y., Xu, Q., Canzio, D., Shou, J., Li, J., Gorkin, D.U., Jung, I., Wu, H., Zhai, Y., Tang, Y.*, et al.* (2015). CRISPR Inversion of CTCF Sites Alters Genome Topology and Enhancer/Promoter Function. Cell *162*, 900-910.

Han, L., Lee, D.H., and Szabo, P.E. (2008). CTCF is the master organizer of domain-wide allele-specific chromatin at the H19/Igf2 imprinted region. Molecular and cellular biology *28*, 1124-1135.

Han, Z., Liu, L., Liu, Y., and Li, S. (2014). Sirtuin SIRT6 suppresses cell proliferation through inhibition of Twist1 expression in non-small cell lung cancer. International journal of clinical and experimental pathology *7*, 4774-4781.

Hannan, N.R.F., Segeritz, C.P., Touboul, T., and Vallier, L. (2013). Production of hepatocyte-like cells from human pluripotent stem cells. Nat Protoc *8*, 430-437.

Hayashi, A., Yamauchi, N., Shibahara, J., Kimura, H., Morikawa, T., Ishikawa, S., Nagae, G., Nishi, A., Sakamoto, Y., Kokudo, N.*, et al.* (2014). Concurrent activation of acetylation and tri-methylation of H3K27 in a subset of hepatocellular carcinoma with aggressive behavior. PloS one *9*, e91330.

Heintzman, N.D., Stuart, R.K., Hon, G., Fu, Y., Ching, C.W., Hawkins, R.D., Barrera, L.O., Van Calcar, S., Qu, C., Ching, K.A.*, et al.* (2007). Distinct and predictive chromatin signatures of transcriptional promoters and enhancers in the human genome. Nat Genet *39*, 311-318.

Herz, H.M., Hu, D., and Shilatifard, A. (2014). Enhancer malfunction in cancer. Molecular cell *53*, 859-866.

Hnisz, D., Abraham, B.J., Lee, T.I., Lau, A., Saint-Andre, V., Sigova, A.A., Hoke, H.A., and Young, R.A. (2013). Super-Enhancers in the Control of Cell Identity and Disease. Cell *155*, 934-947.

Hoffman, B.G., Robertson, G., Zavaglia, B., Beach, M., Cullum, R., Lee, S., Soukhatcheva, G., Li, L., Wederell, E.D., Thiessen, N.*, et al.* (2010). Locus co-occupancy, nucleosome positioning, and H3K4me1 regulate the functionality of FOXA2-, HNF4A-, and PDX1-bound loci in islets and liver. Genome research *20*, 1037-1051.

Hu, G., Cui, K., Northrup, D., Liu, C., Wang, C., Tang, Q., Ge, K., Levens, D., Crane-Robinson, C., and Zhao, K. (2013). H2A.Z facilitates access of active and repressive complexes to chromatin in embryonic

stem cell self-renewal and differentiation. Cell stem cell *12*, 180-192.

Iizuka, N., Oka, M., Tamesa, T., Hamamoto, Y., and Yamada-Okabe, H. (2004). Imbalance in expression levels of insulin-like growth factor 2 and H19 transcripts linked to progression of hepatocellular carcinoma. Anticancer research *24*, 4085-4089.

Imai, S., Armstrong, C.M., Kaeberlein, M., and Guarente, L. (2000). Transcriptional silencing and longevity protein Sir2 is an NAD-dependent histone deacetylase. Nature *403*, 795-800.

Ishihara, K., Hatano, N., Furuumi, H., Kato, R., Iwaki, T., Miura, K., Jinno, Y., and Sasaki, H. (2000). Comparative genomic sequencing identifies novel tissue-specific enhancers and sequence elements for methylation-sensitive factors implicated in Igf2/H19 imprinting. Genome research *10*, 664-671.

Jiang, H., Khan, S., Wang, Y., Charron, G., He, B., Sebastian, C., Du, J., Kim, R., Ge, E., Mostoslavsky, R.*, et al.* (2013). SIRT6 regulates TNF-alpha secretion through hydrolysis of long-chain fatty acyl lysine. Nature *496*, 110-113.

Jin, C.Y., and Felsenfeld, G. (2007). Nucleosome stability mediated by histone variants H3.3 and H2A.Z. Genes & development *21*, 1519-1529.

Kaidi, A., Weinert, B.T., Choudhary, C., and Jackson, S.P. (2010). Human SIRT6 Promotes DNA End Resection Through CtIP Deacetylation. Science *329*, 1348-1353.

Kajiyama, Y., Tian, J., and Locker, J. (2006). Characterization of distant enhancers and promoters in the albumin-alpha-fetoprotein locus during active and silenced expression. The Journal of biological chemistry *281*, 30122-30131.

Kashyap, A., Zimmerman, T., Ergul, N., Bosserhoff, A., Hartman, U., Alla, V., Bataille, F., Galle, P.R., Strand, S., and Strand, D. (2013). The human Lgl polarity gene, Hugl-2, induces MET and suppresses Snail tumorigenesis. Oncogene *32*, 1396-1407.

Kim, H., Jang, M.J., Kang, M.J., and Han, Y.M. (2011). Epigenetic signatures and temporal expression of lineage-specific genes in hESCs during differentiation to hepatocytes in vitro. Human molecular genetics *20*, 401-412.

Kim, H.S., Xiao, C., Wang, R.H., Lahusen, T., Xu, X., Vassilopoulos, A., Vazquez-Ortiz, G., Jeong, W.I., Park, O., Ki, S.H.*, et al.* (2010). Hepatic-specific disruption of SIRT6 in mice results in fatty liver formation due to enhanced glycolysis and triglyceride synthesis. Cell metabolism *12*, 224-236.

Kim, K.S., and Lee, Y.I. (1997). Biallelic expression of the H19 and IGF2 genes in hepatocellular carcinoma. Cancer letters *119*, 143-148.

Kirmizis, A., Bartley, S.M., and Farnham, P.J. (2003). Identification of the polycomb group protein SU(Z)12 as a potential molecular target for human cancer therapy. Molecular cancer therapeutics *2*, 113-121.

Koide, T., Ainscough, J., Wijgerde, M., and Surani, M.A. (1994). Comparative analysis of Igf-2/H19 imprinted domain: identification of a highly conserved intergenic DNase I hypersensitive region. Genomics *24*, 1-8.

Koike, H., Ouchi, R., Ueno, Y., Nakata, S., Obana, Y., Sekine, K., Zheng, Y.W., Takebe, T., Isono, K., Koseki, H.*, et al.* (2014). Polycomb group protein Ezh2 regulates hepatic progenitor cell proliferation and differentiation in murine embryonic liver. PloS one *9*, e104776.

Kron, K.J., Bailey, S.D., and Lupien, M. (2014). Enhancer alterations in cancer: a source for a cell identity crisis. Genome medicine *6*, 77.

Kugel, S., and Mostoslavsky, R. (2014). Chromatin and beyond: the multitasking roles for SIRT6. Trends in biochemical sciences *39*, 72-81.

Kuzmichev, A., Jenuwein, T., Tempst, P., and Reinberg, D. (2004). Different EZH2-containing complexes

target methylation of histone H1 or nucleosomal histone H3. Molecular cell *14*, 183-193.

Kuzmichev, A., Margueron, R., Vaquero, A., Preissner, T.S., Scher, M., Kirmizis, A., Ouyang, X., Brockdorff, N., Abate-Shen, C., Farnham, P.*, et al.* (2005). Composition and histone substrates of polycomb repressive group complexes change during cellular differentiation. Proceedings of the National Academy of Sciences of the United States of America *102*, 1859-1864.

Lai, C.C., Lin, P.M., Lin, S.F., Hsu, C.H., Lin, H.C., Hu, M.L., Hsu, C.M., and Yang, M.Y. (2013). Altered expression of SIRT gene family in head and neck squamous cell carcinoma. Tumour biology : the journal of the International Society for Oncodevelopmental Biology and Medicine *34*, 1847-1854.

Lauberth, S.M., Nakayama, T., Wu, X., Ferris, A.L., Tang, Z., Hughes, S.H., and Roeder, R.G. (2013). H3K4me3 interactions with TAF3 regulate preinitiation complex assembly and selective gene activation. Cell *152*, 1021-1036.

Lazarevich, N.L. (2000). Molecular mechanisms of alpha-fetoprotein gene expression. Biochemistry Biokhimiia *65*, 117-133.

Le Lay, J., and Kaestner, K.H. (2010). The Fox genes in the liver: from organogenesis to functional integration. Physiological reviews *90*, 1-22.

Lee, C.S., Friedman, J.R., Fulmer, J.T., and Kaestner, K.H. (2005). The initiation of liver development is dependent on Foxa transcription factors. Nature *435*, 944-947.

Lee, T.I., Jenner, R.G., Boyer, L.A., Guenther, M.G., Levine, S.S., Kumar, R.M., Chevalier, B., Johnstone, S.E., Cole, M.F., Isono, K.*, et al.* (2006). Control of developmental regulators by Polycomb in human embryonic stem cells. Cell *125*, 301-313.

Lehnertz, B., Ueda, Y., Derijck, A.A., Braunschweig, U., Perez-Burgos, L., Kubicek, S., Chen, T., Li, E., Jenuwein, T., and Peters, A.H. (2003). Suv39h-mediated histone H3 lysine 9 methylation directs DNA methylation to major satellite repeats at pericentric heterochromatin. Current biology : CB *13*, 1192-1200.

Leighton, P.A., Saam, J.R., Ingram, R.S., Stewart, C.L., and Tilghman, S.M. (1995). An enhancer deletion affects both H19 and Igf2 expression. Genes & development *9*, 2079-2089.

LeRoith, D., and Roberts, C.T., Jr. (2003). The insulin-like growth factor system and cancer. Cancer letters *195*, 127-137.

Levine, M., Cattoglio, C., and Tjian, R. (2014). Looping back to leap forward: transcription enters a new era. Cell *157*, 13-25.

Lewis, E.B. (1978). A gene complex controlling segmentation in Drosophila. Nature *276*, 565-570.

Li, T., Hu, J.F., Qiu, X., Ling, J., Chen, H., Wang, S., Hou, A., Vu, T.H., and Hoffman, A.R. (2008). CTCF regulates allelic expression of Igf2 by orchestrating a promoter-polycomb repressive complex 2 intrachromosomal loop. Molecular and cellular biology *28*, 6473-6482.

Li, X., Nong, Z., Ekstrom, C., Larsson, E., Nordlinder, H., Hofmann, W.J., Trautwein, C., Odenthal, M., Dienes, H.P., Ekstrom, T.J.*, et al.* (1997). Disrupted IGF2 promoter control by silencing of promoter P1 in human hepatocellular carcinoma. Cancer research *57*, 2048-2054.

Li, Z., Gadue, P., Chen, K., Jiao, Y., Tuteja, G., Schug, J., Li, W., and Kaestner, K.H. (2012a). Foxa2 and H2A.Z mediate nucleosome depletion during embryonic stem cell differentiation. Cell *151*, 1608-1616.

Li, Z., Tuteja, G., Schug, J., and Kaestner, K.H. (2012b). Foxa1 and Foxa2 are essential for sexual dimorphism in liver cancer. Cell *148*, 72-83.

Li, Z.Y., Schug, J., Tuteja, G., White, P., and Kaestner, K.H. (2011). The nucleosome map of the mammalian liver. Nature structural & molecular biology *18*, 742-U145.

Lin, X., Tirichine, L., and Bowler, C. (2012). Protocol: Chromatin immunoprecipitation (ChIP) methodology to investigate histone modifications in two model diatom species. Plant methods *8*, 48.

Lin, Z., Yang, H., Tan, C., Li, J., Liu, Z., Quan, Q., Kong, S., Ye, J., Gao, B., and Fang, D. (2013). USP10 antagonizes c-Myc transcriptional activation through SIRT6 stabilization to suppress tumor formation. Cell reports *5*, 1639-1649.

Liszt, G., Ford, E., Kurtev, M., and Guarente, L. (2005). Mouse Sir2 homolog SIRT6 is a nuclear ADP-ribosyltransferase. The Journal of biological chemistry *280*, 21313-21320.

Liu, B., Tahk, S., Yee, K.M., Fan, G., and Shuai, K. (2010). The ligase PIAS1 restricts natural regulatory T cell differentiation by epigenetic repression. Science *330*, 521-525.

Lloret-Llinares, M., Perez-Lluch, S., Rossell, D., Moran, T., Ponsa-Cobas, J., Auer, H., Corominas, M., and Azorin, F. (2012). dKDM5/LID regulates H3K4me3 dynamics at the transcription-start site (TSS) of actively transcribed developmental genes. Nucleic acids research *40*, 9493-9505.

Llovet, J.M., Burroughs, A., and Bruix, J. (2003). Hepatocellular carcinoma. Lancet *362*, 1907-1917.

Long, L., and Spear, B.T. (2004). FoxA proteins regulate H19 endoderm enhancer E1 and exhibit developmental changes in enhancer binding in vivo. Molecular and cellular biology *24*, 9601-9609.

Loven, J., Hoke, H.A., Lin, C.Y., Lau, A., Orlando, D.A., Vakoc, C.R., Bradner, J.E., Lee, T.I., and Young, R.A. (2013). Selective Inhibition of Tumor Oncogenes by Disruption of Super-Enhancers. Cell *153*, 320-334.

Lu, C.T., Hsu, C.M., Lin, P.M., Lai, C.C., Lin, H.C., Yang, C.H., Hsiao, H.H., Liu, Y.C., Lin, H.Y., Lin, S.F.*, et al.* (2014). The potential of SIRT6 and SIRT7 as circulating markers for head and neck squamous cell carcinoma. Anticancer research *34*, 7137-7143.

Lupien, M., Eeckhoute, J., Meyer, C.A., Wang, Q., Zhang, Y., Li, W., Carroll, J.S., Liu, X.S., and Brown, M. (2008). FoxA1 translates epigenetic signatures into enhancer-driven lineage-specific transcription. Cell *132*, 958-970.

Mao, Z., Hine, C., Tian, X., Van Meter, M., Au, M., Vaidya, A., Seluanov, A., and Gorbunova, V. (2011). SIRT6 promotes DNA repair under stress by activating PARP1. Science *332*, 1443-1446.

Marenduzzo, D., Faro-Trindade, I., and Cook, P.R. (2007). What are the molecular ties that maintain genomic loops? Trends in Genetics *23*, 126-133.

Margueron, R., and Reinberg, D. (2011). The Polycomb complex PRC2 and its mark in life. Nature *469*, 343-349.

Marquardt, J.U., Fischer, K., Baus, K., Kashyap, A., Ma, S., Krupp, M., Linke, M., Teufel, A., Zechner, U., Strand, D.*, et al.* (2013). Sirtuin-6-dependent genetic and epigenetic alterations are associated with poor clinical outcome in hepatocellular carcinoma patients. Hepatology *58*, 1054-1064.

Martin, C., Cao, R., and Zhang, Y. (2006). Substrate preferences of the EZH2 histone methyltransferase complex. The Journal of biological chemistry *281*, 8365-8370.

Matouk, I., Raveh, E., Ohana, P., Lail, R.A., Gershtain, E., Gilon, M., De Groot, N., Czerniak, A., and Hochberg, A. (2013). The increasing complexity of the oncofetal h19 gene locus: functional dissection and therapeutic intervention. International journal of molecular sciences *14*, 4298-4316.

Matouk, I.J., DeGroot, N., Mezan, S., Ayesh, S., Abu-lail, R., Hochberg, A., and Galun, E. (2007). The H19 non-coding RNA is essential for human tumor growth. PloS one *2*, e845.

McCord, R.A., Michishita, E., Hong, T., Berber, E., Boxer, L.D., Kusumoto, R., Guan, S., Shi, X., Gozani, O., Burlingame, A.L.*, et al.* (2009). SIRT6 stabilizes DNA-dependent protein kinase at chromatin for DNA double-strand break repair. Aging *1*, 109-121.

Michishita, E., McCord, R.A., Berber, E., Kioi, M., Padilla-Nash, H., Damian, M., Cheung, P., Kusumoto, R., Kawahara, T.L., Barrett, J.C.*, et al.* (2008). SIRT6 is a histone H3 lysine 9 deacetylase that modulates telomeric chromatin. Nature *452*, 492-496.

Michishita, E., McCord, R.A., Boxer, L.D., Barber, M.F., Hong, T., Gozani, O., and Chua, K.F. (2009). Cell

cycle-dependent deacetylation of telomeric histone H3 lysine K56 by human SIRT6. Cell Cycle *8*, 2664-2666.

Michishita, E., Park, J.Y., Burneskis, J.M., Barrett, J.C., and Horikawa, I. (2005). Evolutionarily conserved and nonconserved cellular localizations and functions of human SIRT proteins. Molecular biology of the cell *16*, 4623-4635.

Min, L., Ji, Y., Bakiri, L., Qiu, Z., Cen, J., Chen, X., Chen, L., Scheuch, H., Zheng, H., Qin, L.*, et al.* (2012). Liver cancer initiation is controlled by AP-1 through SIRT6-dependent inhibition of survivin. Nature cell biology *14*, 1203-1211.

Ming, M., Han, W., Zhao, B., Sundaresan, N.R., Deng, C.X., Gupta, M.P., and He, Y.Y. (2014). SIRT6 promotes COX-2 expression and acts as an oncogene in skin cancer. Cancer research *74*, 5925-5933.

Morace, C., Cucunato, M., Bellerone, R., De Caro, G., Crino, S., Fortiguerra, A., Spadaro, F., Zirilli, A., Alibrandi, A., Consolo, P.*, et al.* (2012). Insulin-like growth factor-II is a useful marker to detect hepatocellular carcinoma? European journal of internal medicine *23*, e157-161.

Morford, L.A., Davis, C., Jin, L., Dobierzewska, A., Peterson, M.L., and Spear, B.T. (2007). The oncofetal gene glypican 3 is regulated in the postnatal liver by zinc fingers and homeoboxes 2 and in the regenerating liver by alpha-fetoprotein regulator 2. Hepatology *46*, 1541-1547.

Mostoslavsky, R., Chua, K.F., Lombard, D.B., Pang, W.W., Fischer, M.R., Gellon, L., Liu, P., Mostoslavsky, G., Franco, S., Murphy, M.M.*, et al.* (2006). Genomic instability and aging-like phenotype in the absence of mammalian SIRT6. Cell *124*, 315-329.

Murrell, A., Heeson, S., Bowden, L., Constancia, M., Dean, W., Kelsey, G., and Reik, W. (2001). An intragenic methylated region in the imprinted Igf2 gene augments transcription. EMBO reports *2*, 1101-1106.

Nakshatri, H., and Badve, S. (2007). FOXA1 as a therapeutic target for breast cancer. Expert opinion on therapeutic targets *11*, 507-514.

Nativio, R., Wendt, K.S., Ito, Y., Huddleston, J.E., Uribe-Lewis, S., Woodfine, K., Krueger, C., Reik, W., Peters, J.M., and Murrell, A. (2009). Cohesin is required for higher-order chromatin conformation at the imprinted IGF2-H19 locus. PLoS genetics *5*, e1000739.

Niessen, H.E., Demmers, J.A., and Voncken, J.W. (2009). Talking to chromatin: post-translational modulation of polycomb group function. Epigenetics & chromatin *2*, 10.

Obier, N., Lin, Q., Cauchy, P., Hornich, V., Zenke, M., Becker, M., and Muller, A.M. (2015). Polycomb protein EED is required for silencing of pluripotency genes upon ESC differentiation. Stem cell reviews *11*, 50-61.

Ohlsson, R. (2004). Loss of IGF2 imprinting: mechanisms and consequences. Novartis Foundation symposium *262*, 108-121; discussion 121-104, 265-108.

Palmer, N.O., Fullston, T., Mitchell, M., Setchell, B.P., and Lane, M. (2011). SIRT6 in mouse spermatogenesis is modulated by diet-induced obesity. Reproduction, fertility, and development *23*, 929-939.

Parker, S.C., Stitzel, M.L., Taylor, D.L., Orozco, J.M., Erdos, M.R., Akiyama, J.A., van Bueren, K.L., Chines, P.S., Narisu, N., Program, N.C.S.*, et al.* (2013). Chromatin stretch enhancer states drive cell-specific gene regulation and harbor human disease risk variants. Proceedings of the National Academy of Sciences of the United States of America *110*, 17921-17926.

Pasini, D., Bracken, A.P., Hansen, J.B., Capillo, M., and Helin, K. (2007). The polycomb group protein Suz12 is required for embryonic stem cell differentiation. Molecular and cellular biology *27*, 3769-3779.

Pedone, P.V., Pikaart, M.J., Cerrato, F., Vernucci, M., Ungaro, P., Bruni, C.B., and Riccio, A. (1999). Role

of histone acetylation and DNA methylation in the maintenance of the imprinted expression of the H19 and Igf2 genes. FEBS letters *458*, 45-50.

Pellicoro, A., Ramachandran, P., Iredale, J.P., and Fallowfield, J.A. (2014). Liver fibrosis and repair: immune regulation of wound healing in a solid organ. Nature reviews Immunology *14*, 181-194.

Peters, A.H., Mermoud, J.E., O'Carroll, D., Pagani, M., Schweizer, D., Brockdorff, N., and Jenuwein, T. (2002). Histone H3 lysine 9 methylation is an epigenetic imprint of facultative heterochromatin. Nat Genet *30*, 77-80.

Plath, K., Fang, J., Mlynarczyk-Evans, S.K., Cao, R., Worringer, K.A., Wang, H., de la Cruz, C.C., Otte, A.P., Panning, B., and Zhang, Y. (2003). Role of histone H3 lysine 27 methylation in X inactivation. Science *300*, 131-135.

Polyakova, O., Borman, S., Grimley, R., Vamathevan, J., Hayes, B., and Solari, R. (2012). Identification of novel interacting partners of Sirtuin6. PloS one *7*, e51555.

Popova, E.Y., Grigoryev, S.A., Fan, Y.H., Skoultchi, A.I., Zhang, S.S., and Barnstable, C.J. (2013). Developmentally Regulated Linker Histone H1c Promotes Heterochromatin Condensation and Mediates Structural Integrity of Rod Photoreceptors in Mouse Retina. Journal of Biological Chemistry *288*, 17895-17907.

Rada-Iglesias, A., Bajpai, R., Swigut, T., Brugmann, S.A., Flynn, R.A., and Wysocka, J. (2011). A unique chromatin signature uncovers early developmental enhancers in humans. Nature *470*, 279-283.

Rhodes, J.M., McEwan, M., and Horsfield, J.A. (2011). Gene regulation by cohesin in cancer: is the ring an unexpected party to proliferation? Molecular cancer research : MCR *9*, 1587-1607.

Riising, E.M., Boggio, R., Chiocca, S., Helin, K., and Pasini, D. (2008). The polycomb repressive complex 2 is a potential target of SUMO modifications. PloS one *3*, e2704.

Rougeulle, C., Chaumeil, J., Sarma, K., Allis, C.D., Reinberg, D., Avner, P., and Heard, E. (2004). Differential histone H3 Lys-9 and Lys-27 methylation profiles on the X chromosome. Molecular and cellular biology *24*, 5475-5484.

Sachdeva, M., Chawla, Y.K., and Arora, S.K. (2015). Immunology of hepatocellular carcinoma. World journal of hepatology *7*, 2080-2090.

Sasaki, M., Ikeda, H., Itatsu, K., Yamaguchi, J., Sawada, S., Minato, H., Ohta, T., and Nakanuma, Y. (2008). The overexpression of polycomb group proteins Bmi1 and EZH2 is associated with the progression and aggressive biological behavior of hepatocellular carcinoma. Lab Invest *88*, 873-882.

Schmidt, D., Schwalie, P.C., Ross-Innes, C.S., Hurtado, A., Brown, G.D., Carroll, J.S., Flicek, P., and Odom, D.T. (2010). A CTCF-independent role for cohesin in tissue-specific transcription. Genome research *20*, 578-588.

Schotta, G., Lachner, M., Sarma, K., Ebert, A., Sengupta, R., Reuter, G., Reinberg, D., and Jenuwein, T. (2004). A silencing pathway to induce H3-K9 and H4-K20 trimethylation at constitutive heterochromatin. Genes & development *18*, 1251-1262.

Sebastian, C., Zwaans, B.M., Silberman, D.M., Gymrek, M., Goren, A., Zhong, L., Ram, O., Truelove, J., Guimaraes, A.R., Toiber, D*., et al.* (2012). The histone deacetylase SIRT6 is a tumor suppressor that controls cancer metabolism. Cell *151*, 1185-1199.

Sell, S., and Leffert, H.L. (2008). Liver cancer stem cells. Journal of clinical oncology : official journal of the American Society of Clinical Oncology *26*, 2800-2805.

Serandour, A.A., Avner, S., Percevault, F., Demay, F., Bizot, M., Lucchetti-Miganeh, C., Barloy-Hubler, F., Brown, M., Lupien, M., Metivier, R*., et al.* (2011). Epigenetic switch involved in activation of pioneer factor FOXA1-dependent enhancers. Genome research *21*, 555-565.

Shlyueva, D., Stampfel, G., and Stark, A. (2014). Transcriptional enhancers: from properties to genome-wide predictions. Nature reviews Genetics *15*, 272-286.

Singal, A.G., and El-Serag, H.B. (2015). Hepatocellular Carcinoma From Epidemiology to Prevention: Translating Knowledge into Practice. Clinical gastroenterology and hepatology : the official clinical practice journal of the American Gastroenterological Association *13*, 2140-2151.

Singh, P., Cho, J., Tsai, S.Y., Rivas, G.E., Larson, G.P., and Szabo, P.E. (2010). Coordinated allele-specific histone acetylation at the differentially methylated regions of imprinted genes. Nucleic acids research *38*, 7974-7990.

Smith, E., and Shilatifard, A. (2014). Enhancer biology and enhanceropathies. Nature structural & molecular biology *21*, 210-219.

Sohda, T., Iwata, K., Soejima, H., Kamimura, S., Shijo, H., and Yun, K. (1998). In situ detection of insulin-like growth factor II (IGF2) and H19 gene expression in hepatocellular carcinoma. Journal of human genetics *43*, 49-53.

Stedman, W., Kang, H., Lin, S., Kissil, J.L., Bartolomei, M.S., and Lieberman, P.M. (2008). Cohesins localize with CTCF at the KSHV latency control region and at cellular c-myc and H19/Igf2 insulators. The EMBO journal *27*, 654-666.

Stielow, B., Sapetschnig, A., Kruger, I., Kunert, N., Brehm, A., Boutros, M., and Suske, G. (2008). Identification of SUMO-dependent chromatin-associated transcriptional repression components by a genome-wide RNAi screen. Molecular cell *29*, 742-754.

Stringer, J.M., Suzuki, S., Pask, A.J., Shaw, G., and Renfree, M.B. (2012). Promoter-specific expression and imprint status of marsupial IGF2. PloS one *7*, e41690.

Stroud, H., Feng, S., Morey Kinney, S., Pradhan, S., and Jacobsen, S.E. (2011). 5-Hydroxymethylcytosine is associated with enhancers and gene bodies in human embryonic stem cells. Genome biology *12*, R54.

Stuhlmuller, B., Kunisch, E., Franz, J., Martinez-Gamboa, L., Hernandez, M.M., Pruss, A., Ulbrich, N., Erdmann, V.A., Burmester, G.R., and Kinne, R.W. (2003). Detection of oncofetal h19 RNA in rheumatoid arthritis synovial tissue. The American journal of pathology *163*, 901-911.

Sundaresan, N.R., Vasudevan, P., Zhong, L., Kim, G., Samant, S., Parekh, V., Pillai, V.B., Ravindra, P.V., Gupta, M., Jeevanandam, V.*, et al.* (2012). The sirtuin SIRT6 blocks IGF-Akt signaling and development of cardiac hypertrophy by targeting c-Jun. Nature medicine *18*, 1643-1650.

Sutinen, P., Rahkama, V., Rytinki, M., and Palvimo, J.J. (2014). Nuclear mobility and activity of FOXA1 with androgen receptor are regulated by SUMOylation. Molecular endocrinology *28*, 1719-1728.

Tan, M., Luo, H., Lee, S., Jin, F., Yang, J.S., Montellier, E., Buchou, T., Cheng, Z., Rousseaux, S., Rajagopal, N.*, et al.* (2011). Identification of 67 histone marks and histone lysine crotonylation as a new type of histone modification. Cell *146*, 1016-1028.

Tao, R., Xiong, X., DePinho, R.A., Deng, C.X., and Dong, X.C. (2013). Hepatic SREBP-2 and cholesterol biosynthesis are regulated by FoxO3 and Sirt6. Journal of lipid research *54*, 2745-2753.

Taube, J.H., Allton, K., Duncan, S.A., Shen, L., and Barton, M.C. (2010). Foxa1 functions as a pioneer transcription factor at transposable elements to activate Afp during differentiation of embryonic stem cells. The Journal of biological chemistry *285*, 16135-16144.

Teufel, A., Maass, T., Strand, S., Kanzler, S., Galante, T., Becker, K., Strand, D., Biesterfeld, S., Westphal, H., and Galle, P.R. (2010). Liver-specific Ldb1 deletion results in enhanced liver cancer development. Journal of hepatology *53*, 1078-1084.

Tilghman, S.M., and Belayew, A. (1982). Transcriptional control of the murine

albumin/alpha-fetoprotein locus during development. Proceedings of the National Academy of Sciences of the United States of America *79*, 5254-5257.

Toiber, D., Erdel, F., Bouazoune, K., Silberman, D.M., Zhong, L., Mulligan, P., Sebastian, C., Cosentino, C., Martinez-Pastor, B., Giacosa, S.*, et al.* (2013). SIRT6 recruits SNF2H to DNA break sites, preventing genomic instability through chromatin remodeling. Molecular cell *51*, 454-468.

Toropainen, S., Malinen, M., Kaikkonen, S., Rytinki, M., Jaaskelainen, T., Sahu, B., Janne, O.A., and Palvimo, J.J. (2015). SUMO ligase PIAS1 functions as a target gene selective androgen receptor coregulator on prostate cancer cell chromatin. Nucleic acids research *43*, 848-861.

Valdes-Mora, F., Song, J.Z., Statham, A.L., Strbenac, D., Robinson, M.D., Nair, S.S., Patterson, K.I., Tremethick, D.J., Stirzaker, C., and Clark, S.J. (2012). Acetylation of H2A.Z is a key epigenetic modification associated with gene deregulation and epigenetic remodeling in cancer. Genome research *22*, 307-321.

Van Meter, M., Kashyap, M., Rezazadeh, S., Geneva, A.J., Morello, T.D., Seluanov, A., and Gorbunova, V. (2014). SIRT6 represses LINE1 retrotransposons by ribosylating KAP1 but this repression fails with stress and age. Nature communications *5*, 5011.

Van Meter, M., Mao, Z., Gorbunova, V., and Seluanov, A. (2011). SIRT6 overexpression induces massive apoptosis in cancer cells but not in normal cells. Cell Cycle *10*, 3153-3158.

Vaupel, P., and Mayer, A. (2007). Hypoxia in cancer: significance and impact on clinical outcome. Cancer metastasis reviews *26*, 225-239.

Vernucci, M., Cerrato, F., Besnard, N., Casola, S., Pedone, P.V., Bruni, C.B., and Riccio, A. (2000). The H19 endodermal enhancer is required for Igf2 activation and tumor formation in experimental liver carcinogenesis. Oncogene *19*, 6376-6385.

Vire, E., Brenner, C., Deplus, R., Blanchon, L., Fraga, M., Didelot, C., Morey, L., Van Eynde, A., Bernard, D., Vanderwinden, J.M.*, et al.* (2006). The Polycomb group protein EZH2 directly controls DNA methylation. Nature *439*, 871-874.

Vizan, P., Beringer, M., Ballare, C., and Di Croce, L. (2015). Role of PRC2-associated factors in stem cells and disease. The FEBS journal *282*, 1723-1735.

Volkel, P., Dupret, B., Le Bourhis, X., and Angrand, P.O. (2015). Diverse involvement of EZH2 in cancer epigenetics. American journal of translational research *7*, 175-193.

von Meyenn, F., Porstmann, T., Gasser, E., Selevsek, N., Schmidt, A., Aebersold, R., and Stoffel, M. (2013). Glucagon-induced acetylation of Foxa2 regulates hepatic lipid metabolism. Cell metabolism *17*, 436-447.

Wamstad, J.A., Wang, X., Demuren, O.O., and Boyer, L.A. (2014). Distal enhancers: new insights into heart development and disease. Trends in cell biology *24*, 294-302.

Wan, J., Zhan, J., Li, S., Ma, J., Xu, W., Liu, C., Xue, X., Xie, Y., Fang, W., Chin, Y.E.*, et al.* (2015). PCAF-primed EZH2 acetylation regulates its stability and promotes lung adenocarcinoma progression. Nucleic acids research *43*, 3591-3604.

Wang, J., Zhu, C.P., Hu, P.F., Qian, H., Ning, B.F., Zhang, Q., Chen, F., Liu, J., Shi, B., Zhang, X.*, et al.* (2014). FOXA2 suppresses the metastasis of hepatocellular carcinoma partially through matrix metalloproteinase-9 inhibition. Carcinogenesis *35*, 2576-2583.

Wang, J.C., Kafeel, M.I., Avezbakiyev, B., Chen, C., Sun, Y., Rathnasabapathy, C., Kalavar, M., He, Z., Burton, J., and Lichter, S. (2011a). Histone deacetylase in chronic lymphocytic leukemia. Oncology *81*, 325-329.

Wang, W.H., Studach, L.L., and Andrisani, O.M. (2011b). Proteins ZNF198 and SUZ12 are down-regulated in hepatitis B virus (HBV) X protein-mediated hepatocyte transformation and in HBV

replication. Hepatology *53*, 1137-1147.

Wei, Y., Chen, Y.H., Li, L.Y., Lang, J., Yeh, S.P., Shi, B., Yang, C.C., Yang, J.Y., Lin, C.Y., Lai, C.C.*, et al.* (2011). CDK1-dependent phosphorylation of EZH2 suppresses methylation of H3K27 and promotes osteogenic differentiation of human mesenchymal stem cells. Nature cell biology *13*, 87-94.

Weinstein, D.C., Ruiz i Altaba, A., Chen, W.S., Hoodless, P., Prezioso, V.R., Jessell, T.M., and Darnell, J.E., Jr. (1994). The winged-helix transcription factor HNF-3 beta is required for notochord development in the mouse embryo. Cell *78*, 575-588.

Weth, O., Paprotka, C., Gunther, K., Schulte, A., Baierl, M., Leers, J., Galjart, N., and Renkawitz, R. (2014). CTCF induces histone variant incorporation, erases the H3K27me3 histone mark and opens chromatin. Nucleic acids research *42*, 11941-11951.

Whyte, W.A., Orlando, D.A., Hnisz, D., Abraham, B.J., Lin, C.Y., Kagey, M.H., Rahl, P.B., Lee, T.I., and Young, R.A. (2013). Master Transcription Factors and Mediator Establish Super-Enhancers at Key Cell Identity Genes. Cell *153*, 307-319.

Wisniewski, J.R., Zougman, A., Kruger, S., and Mann, M. (2007). Mass spectrometric mapping of linker histone H1 variants reveals multiple acetylations, methylations, and phosphorylation as well as differences between cell culture and tissue. Molecular & Cellular Proteomics *6*, 72-87.

Wu, M., Seto, E., and Zhang, J. (2015). E2F1 enhances glycolysis through suppressing Sirt6 transcription in cancer cells. Oncotarget *6*, 11252-11263.

Wu, S.C., and Zhang, Y. (2011). Cyclin-dependent kinase 1 (CDK1)-mediated phosphorylation of enhancer of zeste 2 (Ezh2) regulates its stability. The Journal of biological chemistry *286*, 28511-28519.

Wu, S.Y., and Chiang, C.M. (2009). Crosstalk between sumoylation and acetylation regulates p53-dependent chromatin transcription and DNA binding. The EMBO journal *28*, 1246-1259.

Xiao, C., Kim, H.S., Lahusen, T., Wang, R.H., Xu, X., Gavrilova, O., Jou, W., Gius, D., and Deng, C.X. (2010). SIRT6 deficiency results in severe hypoglycemia by enhancing both basal and insulin-stimulated glucose uptake in mice. The Journal of biological chemistry *285*, 36776-36784.

Xu, C., Bian, C., Yang, W., Galka, M., Ouyang, H., Chen, C., Qiu, W., Liu, H., Jones, A.E., MacKenzie, F.*, et al.* (2010). Binding of different histone marks differentially regulates the activity and specificity of polycomb repressive complex 2 (PRC2). Proceedings of the National Academy of Sciences of the United States of America *107*, 19266-19271.

Xu, Z., Zhang, L., Zhang, W., Meng, D., Zhang, H., Jiang, Y., Xu, X., Van Meter, M., Seluanov, A., Gorbunova, V.*, et al.* (2015). SIRT6 rescues the age related decline in base excision repair in a PARP1-dependent manner. Cell Cycle *14*, 269-276.

Yamaguchi, N., Ito, E., Azuma, S., Honma, R., Yanagisawa, Y., Nishikawa, A., Kawamura, M., Imai, J., Tatsuta, K., Inoue, J.*, et al.* (2008). FoxA1 as a lineage-specific oncogene in luminal type breast cancer. Biochemical and biophysical research communications *365*, 711-717.

Yang, B., Zwaans, B.M., Eckersdorff, M., and Lombard, D.B. (2009). The sirtuin SIRT6 deacetylates H3 K56Ac in vivo to promote genomic stability. Cell Cycle *8*, 2662-2663.

Yang, S.J., Choi, J.M., Chae, S.W., Kim, W.J., Park, S.E., Rhee, E.J., Lee, W.Y., Oh, K.W., Park, S.W., Kim, S.W.*, et al.* (2011). Activation of peroxisome proliferator-activated receptor gamma by rosiglitazone increases sirt6 expression and ameliorates hepatic steatosis in rats. PloS one *6*, e17057.

Yang, S.J., Choi, J.M., Chang, E., Park, S.W., and Park, C.Y. (2014). Sirt1 and Sirt6 mediate beneficial effects of rosiglitazone on hepatic lipid accumulation. PloS one *9*, e105456.

Yao, H., Brick, K., Evrard, Y., Xiao, T., Camerini-Otero, R.D., and Felsenfeld, G. (2010). Mediation of CTCF transcriptional insulation by DEAD-box RNA-binding protein p68 and steroid receptor RNA activator

SRA. Genes & development *24*, 2543-2555.

Yoshimizu, T., Miroglio, A., Ripoche, M.A., Gabory, A., Vernucci, M., Riccio, A., Colnot, S., Godard, C., Terris, B., Jammes, H.*, et al.* (2008). The H19 locus acts in vivo as a tumor suppressor. Proceedings of the National Academy of Sciences of the United States of America *105*, 12417-12422.

Yu, X., Gupta, A., Wang, Y., Suzuki, K., Mirosevich, J., Orgebin-Crist, M.C., and Matusik, R.J. (2005). Foxa1 and Foxa2 interact with the androgen receptor to regulate prostate and epididymal genes differentially. Annals of the New York Academy of Sciences *1061*, 77-93.

Yuan, H., Su, L., and Chen, W.Y. (2013). The emerging and diverse roles of sirtuins in cancer: a clinical perspective. OncoTargets and therapy *6*, 1399-1416.

Yun, K., Jinno, Y., Sohda, T., Niikawa, N., and Ikeda, T. (1998). Promoter-specific insulin-like growth factor 2 gene imprinting in human fetal liver and hepatoblastoma. The Journal of pathology *185*, 91-98.

Zaret, K. (1999). Developmental competence of the gut endoderm: genetic potentiation by GATA and HNF3/fork head proteins. Developmental biology *209*, 1-10.

Zaret, K.S. (2008). Genetic programming of liver and pancreas progenitors: lessons for stem-cell differentiation. Nature reviews Genetics *9*, 329-340.

Zender, L., Spector, M.S., Xue, W., Flemming, P., Cordon-Cardo, C., Silke, J., Fan, S.T., Luk, J.M., Wigler, M., Hannon, G.J.*, et al.* (2006). Identification and validation of oncogenes in liver cancer using an integrative oncogenomic approach. Cell *125*, 1253-1267.

Zentner, G.E., Tesar, P.J., and Scacheri, P.C. (2011). Epigenetic signatures distinguish multiple classes of enhancers with distinct cellular functions. Genome research *21*, 1273-1283.

Zhang, H., Niu, B., Hu, J.F., Ge, S., Wang, H., Li, T., Ling, J., Steelman, B.N., Qian, G., and Hoffman, A.R. (2011). Interruption of intrachromosomal looping by CCCTC binding factor decoy proteins abrogates genomic imprinting of human insulin-like growth factor II. The Journal of cell biology *193*, 475-487.

Zhang, L., Yang, F., Yuan, J.H., Yuan, S.X., Zhou, W.P., Huo, X.S., Xu, D., Bi, H.S., Wang, F., and Sun, S.H. (2013). Epigenetic activation of the MiR-200 family contributes to H19-mediated metastasis suppression in hepatocellular carcinoma. Carcinogenesis *34*, 577-586.

Zhong, L., D'Urso, A., Toiber, D., Sebastian, C., Henry, R.E., Vadysirisack, D.D., Guimaraes, A., Marinelli, B., Wikstrom, J.D., Nir, T.*, et al.* (2010). The histone deacetylase Sirt6 regulates glucose homeostasis via Hif1alpha. Cell *140*, 280-293.

Zuin, J., Dixon, J.R., van der Reijden, M.I., Ye, Z., Kolovos, P., Brouwer, R.W., van de Corput, M.P., van de Werken, H.J., Knoch, T.A., van, I.W.F.*, et al.* (2014). Cohesin and CTCF differentially affect chromatin architecture and gene expression in human cells. Proceedings of the National Academy of Sciences of the United States of America *111*, 996-1001.

List of figures

List of tables

List of abbreviations

A	AFP	Alpha-fetoprotein
	ALB	Albumin
	acH2AZ	Acetylated H2AZ
	AR	Androgen receptor
B	BER	Base excision repair
	bp	Base pair(s)
	BSA	Bovine serum albumin
C	CCD	Centrally conserved DNase I hypersensitive domain
	cDNA	Complementary DNA
	CtIP	C-terminal binding protein interacting protein
	ChIP	Chromatin Immunoprecipitation
	ChIP-seq	Chromatin Immunoprecipitation sequence
	3C	Chromosome conformation capture
	CTCF-Ds	CTCF-downstream binding locus
	CTCF-AD	CTCF-upstream binding locus
D	DSB	Double-strand break repair
	dH_2O	Distilled water
	DMSO	Dimethyl sulfoxide
	dNTP	Deoxyribonucleotide
	DTT	Dithiothreitol
	DNA	Deoxyribonucleic acid
	DMR	Differentially methylated region
	DP	Distant promoters
E	E	Enhancer
	EZH2	Enhancer of zeste
	EED	Embryonic ectoderm development
	E. coli	Escherichia coli
	EDTA	Ethylenediaminetetraacetic acid
	EE	Endodermal enhancers
	ERα	Estrogen receptor
F	FCS	Fetal calf serum
	FOXA1/2	FOXA1 and FOXA2 (Forkhead Box A1 and A2)
G	GCN5	Acetyltransferase general control non-repressed protein 5
	GPC3	Glypican-3
H	HR	Homologous recombinant
	HCC	Hepatocellular carcinoma
	h	Hour(s)
I	Igf2	Insulin-like growth factor 2
	ICR	Imprinting control region

	IP	Immunoprecipitation
K	KO	Knockout
	KAP1	KRAB-associated protein 1
	Kac	Acetylated lysine
	Kcr	Crotonylated lysine
L	L	Litre
	LB	Luria Bertani broth
M	m	Milli
	MEF	Mouse embryonic fibroblasts
	µ	Micro
	min	Minute(s)
	M	Mole
	2-ME	2-Methoxyestradiol
	mRNA	Messenger RNA
	ME	Mesodermal enhancers
N	NFκB	Nuclear factor kappa B
	nt	Nucleotide(s)
	NAD	Nicotinamide adenine dinucleotide
O	O.N	Overnight
P	PIC	Protease inhibitor cocktail
	P	Promoter
	PRC2	Polycomb group 2
	PARP1	Poly(ADP-ribose) polymerase 1
	PTM	Post-translational modifications
	PAGE	Polyacrylamid gel electrophoresis
	PCR	Polymerase chain reaction
	PFA	Paraformaldehyde
	pmHep	Primary murine hepatocytes
	phHep	Primary human hepatocytes
	PIHit	The midstream paternally expressed *IGF2/H19* intergenic transcript
	PLA	Proximity ligation assay
Q	qPCR	Quantitative real-time PCR
R	RNA	Ribonucleic acid
	RT	Room temperature
	RPII	RNA polymerase II
S	s	Second
T	TNF α	Tumor necrosis factor-α
	TIP	Transcription initiation platforms
W	WT	Wild type

Curriculum vitae

First Name: Shengyun **Family Name:** Ma

Education

Ph.D., major in Molecular Hepatology, Medical Center of the Johannes Gutenberg University, Mainz, Germany (08.2012-present). Dissertation: Sirt6-dependent gene regulation of oncofetal gene loci in hepatocytes.

M.S., major in Genetics, Zhejiang University, Hangzhou, China (09. 2009-03.2012). Dissertation: Expression pattern and function of miR408 in seed development of rice (*Oryza sativa*).

B.S., major in Biotechnology, Henan University of Sci-Tech, Luoyang, China (09. 2005-07. 2009). Dissertation: Preliminary study of the biological effects of audible sound stimulation on the colony character of *Escherichia coli*.

Publications

Marquardt, J.U., Fischer, K., Baus, K., Kashyap, A., **Ma, S.**, Krupp, M., Linke, M., Teufel, A., Zechner, U., Strand, D., et al. (2013). Sirtuin-6-dependent genetic and epigenetic alterations are associated with poor clinical outcome in hepatocellular carcinoma patients. Hepatology *58*, 1054-1064.

Li, X., Bian, H., Song, D., **Ma, S.**, Han, N., Wang, J., and Zhu, M. (2013). Flowering time control in ornamental gloxinia (*Sinningia speciosa*) by manipulation of miR159 expression. Annals of botany *111*, 71-799.

Ma, S. Y., Bai, Y., Han, N., Wang, J. H., Weng, X. Y., Bian, H. W., and Zhu, M. Y. (2012). [Recent research progress of biogenesis and functions of miRNA*]. Yi chuan = Hereditas / Zhongguo yi chuan xue hui bian ji *34*, 383-388.

Bian, H., Xie, Y., Guo, F., Han, N., **Ma, S.**, Zeng, Z., Wang, J., Yang, Y., and Zhu, M. (2012). Distinctive expression patterns and roles of the miRNA393/TIR1 homolog module in regulating flag leaf inclination and primary and crown root growth in rice (Oryza sativa). The New phytologist *196*, 149-161.

Shaobin, G., Wu, Y., Li, K., Li, S., **Ma, S.**, Wang, Q., and Wang, R. (2010). A pilot study of the effect of audible sound on the growth of Escherichia coli. Colloids and surfaces B, Biointerfaces *78*, 367-371.

Acknowledgements

I would like to express my sincere gratitude to my supervisor, for her continuously patient guidance and encouragement on science in the past three and half years. She always has the strong sense to the correct direction according to the existing data no matter whether it is expected or not. She has been always available and cultivating my ability of divergent thinking whenever I have questions of the projects. She is extremely rigorous at science and very nice in the life.

I would like also to thank our cooperation partner, who provided me very helpful suggestions, shared valuable fresh ideas with me. Their inspiring discussions and suggestions are constructive and indispensable for my research.

I would like to thank all my colleges for creating such a friendly and pleasant working atmosphere. Besides, thanks very much for the helps of all the friends in Mainz.

I would like to express my appreciation to my parents and sisters for their love and support so many years. I would like to thank my brother-in-law, who helps me to take care of my parents and sisters. Last but not least, I would like to thank my niece, a little angel, who brings so much happiness to all the family.